ORNL-4651
UC-25 – Metals, Ceramics, and Materials
UC-4 – Chemistry

ELECTROCHEMISTRY OF URANIUM AND URANIUM-ALLOYS IN AQUEOUS SOLUTIONS

G. H. Jenks

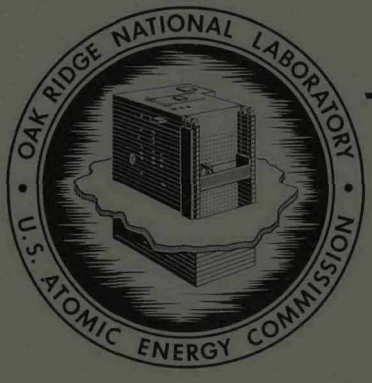

OAK RIDGE NATIONAL LABORATORY
operated by
UNION CARBIDE CORPORATION
for the
U.S. ATOMIC ENERGY COMMISSION

Printed in the United States of America. Available from
National Technical Information Service
U.S. Department of Commerce
5285 Port Royal Road, Springfield, Virginia 22151
Price: Printed Copy $3.00; Microfiche $0.95

DISCLAIMER

ORNL-4651

Contract No. W-7405-eng-26

REACTOR CHEMISTRY DIVISION

ELECTROCHEMISTRY OF URANIUM AND URANIUM-ALLOYS IN AQUEOUS SOLUTIONS

G. H. Jenks

JUNE 1971

OAK RIDGE NATIONAL LABORATORY
Oak Ridge, Tennessee
operated by
UNION CARBIDE CORPORATION
for the
U.S. ATOMIC ENERGY COMMISSION

CONTENTS

(Contents cont'd.)

(Contents cont'd.)

(Contents cont'd.)

Acknowledgement

It is a pleasure to acknowledge helpful discussions on theoretical and experimental aspects of electrochemistry of corrosion with: A. L. Bacarella, J. C. Griess, R. E. Meyer, F. A. Posey, and R. A. Strehlow.

Summary

An investigation of certain aspects of the corrosion of uranium and uranium alloys was made as part of an effort to understand and control the corrosion of these materials in aqueous solutions at normal ambient temperatures.

The principal part of this work consisted of experimental electrochemical studies of corrosion of uranium and of the alloy U-7.5Nb-2.5Zr at 25°C. These studies had the principal objective of providing an outline of the electrochemistry of these materials in the absence of aggressive anions. The solutions were primarily 0.1M K_2SO_4 at pH 5 to 10 and 0.1 and 1N H_2SO_4. A few pitting experiments were made with the alloy in solutions containing chloride in addition to 0.1M K_2SO_4 and in solutions of 0.1N HCl and 0.1N KCl, pH 8.7. Gas atmospheres employed were: $4H_2$:96Ar, Ar, 20 O_2:80Ar. The potentials investigated ranged from < -1v to 5v vs SCE. Most of the polarizations were carried out potentiostatically but some were conducted galvanostatically. In either case current or potential values were recorded when judged to be within 5 to 10% of the steady-state value. Another part of this work consisted of reviews and analyses of literature information pertaining to the electrochemistry of uranium corrosion in aqueous environments below 100°C, and pertaining to certain electrochemical aspects of pitting, crevice corrosion, and stress corrosion cracking.

The experimental work is presented in the text. The work with literature information is presented in Appendixes 1-5. Summaries of

conclusions drawn from the results of the experimental work and of notable features of the results are set forth below.

Uranium

The experimental results lead to the following general conclusions regarding the electrochemistry of uranium in the test solutions of 0.1M K_2SO_4, (pH = 5 to 6) and in 1N H_2SO_4 with different gas atmospheres.

a. A passive film of UO_2 forms on uranium above potentials near those for the equilibrium,

$$UH_3 + H_2O \rightleftharpoons UO + 5H^+ + 5e^-;\ E^0 = -.664 - 0.591\ pH \qquad (1)^*$$

b. The passive film is removed, and increasing anodic rates occur above potentials near those for the equilibrium between anhydrous UO_2 and UO_3,

$$UO_2(anh) + H_2O \rightleftharpoons UO_3(anh) + 2H^+ + 2e^-;\ E^0 = .415 - .0591\ pH \qquad (2)^*$$

The UO_3 is soluble.

c. The cathodic rate on the passive metal increases sharply below potentials near those for the equilibrium,

$$UH_3 + 2H_2O \rightleftharpoons UO_2 + 7H^+ + 7e^-;\ E^0 = -.958 - .0591\ pH \qquad (3)^*$$

This indicates that UH_3 is formed from UO_2 and/or from U by reaction with H_2O or with H^+ below these potentials.

The above conclusions are probably valid for solutions of other, intermediate, pH but this remains to be verified.

Prior information on the corrosion of uranium in aqueous solutions at temperatures of 25 to 100°C is summarized, and is correlated and

---

*Potential vs SCE

interpreted on the basis of the electrochemical theory of corrosion, in Appendix 3. The above general conclusions drawn from the present work are consistent with the prior information as interpreted in Appendix 3. The experimental data indicate that the sulfate and bisulfate ions have little if any detrimental effects on the corrosion of uranium despite the fact that soluble complexes are formed with U(IV) and U(VI). These ions may have beneficial effects if aggressive anions (chloride) are present.

Other notable observations made in the present work with uranium include the following:

d. The exchange current for reduction of H^+ in 1N H_2SO_4 was very low $\sim 10^{-10}$ amps/cm^2.

e. Reduction of O_2 on partially passivated uranium in 1N H_2SO_4 was inhibited. The mechanism of the inhibition is uncertain.

f. Reduction of O_2 on uranium in 0.1M K_2SO_4, pH 5.8 appeared more or less typical of that expected on oxide-coated surfaces.

g. Shallow pits were formed on the surfaces of specimens exposed to transpassive potentials ($E_{SCE} > .415 - .0591$ pH). This pitting can be explained in terms of local conversion of UO_2 to soluble UO_3.

h. Tafel-lines were formed by the polarization data in the transpassive regions. The slopes were 95 and 45 mv/decade at pH 5.3 and 0.55, respectively. These slopes can presumably be related to the kinetic mechanisms, but this has not been done. However, it can be assumed that some protective film of anhydrous UO_2 remains on the uranium surface at transpassive potentials.

Uranium Alloy

a. Anodic polarization in 0.1M K_2SO_4, pH 5.8.

The films formed during anodic polarization [up to 5v (SCE)] in K_2SO_4-solution were poor electronic conductors at the steady-state on the anodic side; water was not oxidized at the steady state and the film was not dissolved. The small steady-state currents were probably due to ion movement through the film. However, the transient currents which occurred upon a sudden increase in potential were well above those at steady-state, and it is possible that these currents were associated with transient electronic conduction. The stability of the film at potentials well above that at which UO_2 can be oxidized to UO_3 is probably due, at least in part, to the poor electronic conductivity. However, UO_3 may have been formed during the transient, high-current, conditions, and if so, the film-stability is also due in part to a low solubility, near neutral pH, of the oxide which contains Nb_2O_5 and ZrO_2 in addition to UO_3. The likelihood that solubility plays an important role in the film stability was supported by the results of a subsequent experiment in which one of the anodically-filmed specimens was anodically polarized in 0.1N H_2SO_4 - the film dissolved.

b. Cathodic polarization in 0.1M K_2SO_4 to potentials below those at which UO_2 and UH_3 are in thermodynamic equilibrium.

The results of the few experiments indicated that the behavior of the alloy, before and after anodization, is similar to that of uranium when the gas atmosphere is 4% H_2. However, when the specimen was anodically filmed and when the gas atmosphere was 20% O_2, the behavior

was different--the increase of cathodic current occurred well below the equilibrium potential, and the increase could be explained in terms of H_2O reduction to form H_2 rather than in terms of UH_3-formation.

c. Polarization behavior in 0.1N and 1N H_2SO_4.

It was concluded that the alloy exhibits transpassive behavior which is similar in the following respects to that of uranium in 1N H_2SO_4 and in 0.1M K_2SO_4: (1) the onset of transpassivity occurs near the potentials at which anhydrous UO_2 and UO_3 are in thermodynamic equilibrium, (2) Tafel relationships prevail in the transpassive regions, and (3) all dark films are removed from surfaces at transpassive potentials. The explanations for the transpassive behavior of the alloy are thought to be the same as those for uranium. The processes which control the anodic rate on the alloy in the transpassive region are probably the same as those for uranium in 0.1M K_2SO_4, pH 5.6 since the Tafel slopes are about the same (70-90 mv/decade). The transpassive behavior of the alloy differs from that of uranium in that no pits are formed on the alloy.

Transpassive polarization probably causes enrichment of the alloying elements, Nb and Zr, as oxides on the surface of the alloy. The enrichment is greater in 1N H_2SO_4 than in 0.1N H_2SO_4. The overvoltage for H^+-reduction on these enriched and unpassivated surfaces in H_2SO_4 is substantially less than that on uranium; -450 to -500 mv at -1 ma/cm^2 for the alloy in 1N H_2SO_4 compared with -735 mv at -1 ma/cm^2 for uranium.

Alloy specimens which are coated with passive films exhibit overvoltages for H^+-reduction which are comparable to those on uranium.

Reduction of oxygen takes place in a more or less normal manner on the alloy surfaces which are coated with passive films. The reduction

on the enriched and film-free surfaces is inhibited. This difference between the two types of surfaces probably involves differences between the concentrations of O_2 at the surface and/or between the amounts of O_2 adsorbed on the surface.

d. Pitting in solutions of 0.1M K_2SO_4 plus KCl

Most of the pitting behavior observed in this work was similar to that reported by others for other materials, and can be qualitatively explained by the mechanism and processes which others have postulated.

Pitting potentials were measured with air-filmed specimens in solutions containing 0.01M KCl (plus 0.1M K_2SO_4) and were between 0 and -100 mv (SCE). Cathodic plarization of a pitted specimen caused marked increases in the subsequently-measured pitting potential. The explanation for this effect is unknown.

The breakthrough potential depended, as expected, upon (Cl^-) and upon the type and amount of film on a specimen. In the case of the air-filmed specimen, it also depended upon the gas atmosphere - the breakthrough potential was lower with 4% H_2 than with 20% O_2. It is likely that this difference reflected a difference between types and amounts of film formed upon immersion of a specimen in the test solution.

e. Polarization behavior in 0.1N HCl and in 0.1M KCl at pH 8.66.

The anodic polarization behavior was typical of that expected with pitting in solutions containing chloride. However, the attack was in the nature of localized shallow attack rather than deep pitting. Pitting potentials were > -325 mv (SCE).

The overvoltage for reduction of H^+ on the corroded surface in 0.1N HCl was very low; -300 mv at -1 ma/cm^2.

An important conclusion which was drawn from these and the other experiments with chloride is that the film can be protected from Cl^- attack by maintaining a sufficiently low potential. With < 0.1 M Cl^-, the film on unstressed specimens would not be attacked at potentials < -325 mv (SCE). Stressed specimens may act differently, but these have not been investigated.

Tables

Electrochemistry of Uranium and Uranium-Alloys in Aqueous Solutions

G. H. Jenks

1. Introduction

Alloys of uranium with Nb and Zr are subject to stress corrosion cracking in aerated aqueous environments at room temperature. Cracking under these conditions probably involves electrochemical factors, and information on the electrochemistry of the alloys in aqueous environments was needed as part of an effort to understand the mechanism.

I have reviewed and analyzed literature information pertaining to the electrochemistry of uranium corrosion in aqueous environments below 100°C and to certain electrochemical aspects of pitting, crevice corrosion, and stress corrosion cracking. This literature review and the analyses are presented in Appendixes 1-5 of this report.

I have also made experimental electrochemical studies of corrosion of uranium and of the alloy U-7.5Nb-2.5Zr. This investigation had the principal objective of providing an outline of the electrochemistry of these materials at 25°C in the absence of aggressive anions. The alloy had been heat treated to form the γ phase, and specimens were machined from the heat treated material. The uranium was hot rolled and machined. The solutions were primarily 0.1M K_2SO_4, (pH 5-10) and 0.1 and 1N H_2SO_4. A few pitting experiments were made with solutions containing chloride in addition to 0.1M K_2SO_4 and in solutions of 0.1N HCl and 0.1N KCl at pH 8.7. Gas atmospheres

employed were : $4H_2$:96Ar, Ar, 20 O_2:80Ar. The potentials investigated ranged from -1.8v to 5v.* Most of the polarizations were carried out potentiostatically but some were conducted galvanostatically. In either case, current or potential values were recorded when judged to be within 5 to 10% of steady-state values. The experimental work is presented below.

2. Equipment for Electrochemical Measurements

2.1 Cell

The cell was made of Pyrex glass tubing with a flat bottom and a 55/50 standard taper joint at the top. The tube was water jacketed. Cell dimensions were: ID, 5 cm; depth below taper joint, 13 cm; solution volume during operation, about 150 cm^3.

A tapered Teflon cap was used to close the cell. Leads into the cell were passed through tapered holes in this cap.

Provisions were made for stirring, sweeping gas through the cell, adding of electrolyte and reagents, and for sampling the cell solution.

2.2 Test Electrode

The electrodes were in the form of cylinders; 0.25 in. OD, 0.063 in. ID, and 0.25 in. long. A sample was mounted such that only the outer surface was exposed to solution. The ends were sealed with Teflon gaskets. The portions of the specimen holder exposed to solution were comprised of glass and Teflon. The exposed specimen area was 1.25 cm^2.

---

*Vs SCE

2.3 Polarizing Electrode

A cylindrical tube, 4 cm in diameter and 2 cm long, made of platinum foil was the polarizing electrode. It was located such that the specimen was at the center of the cylinder.

2.4 Reference Electrode

A saturated calomel electrode (SCE) in a separate compartment served as the reference electrode. The bridge joining the Luggin probe to the calomel electrode was filled with cell solution. An ungreased stopcock adjacent to the reference cell prevented mixing of test and reference solutions.

2.5 Potentiostat

The potentiostat was an Anotrol (Model No. 4101) with a voltage range of ± 5.3v.

2.6 Cleaning of Cell Equipment

The cell and all other glass and Teflon surfaces which contacted cell solution were cleaned initially with a mixture of hot concentrated sulfuric and nitric acids—subsequent cleaning consisted of rinsing with the test solution.

2.7 Cleaning of Test Electrode

As received, machined samples were cleaned by brushing successively, in water, acetone, alcohol, and finally, triple-distilled water. Most samples of uranium were defilmed by immersion in concentrated HNO_3 for 1 min. They were then rinsed in distilled water and finally in triple-distilled water.

3. Experimental Conditions and Procedures

The experimental conditions and procedures for the different experiments with uranium and with the alloy are summarized in tables as follows:

Table 1	uranium
Table 2	U-7.5Nb-2.5Zr in 0.1M K_2SO_4 and in 0.1M K_2SO_4 with Cl^- at pH 5.8
Table 3	U-7.5Nb-2.5Zr in 0.1N and 1N H_2SO_4; also 0.1M K_2SO_4 at pH 9.6

4. Experimental Results, Discussion, and Conclusions - Uranium

4.1 Results and Correlations

The experimental results are presented graphically in Figs. 1 thru 11. Some results are included in Table 1. Additional information, correlations and comments on the results are presented below.

4.1.1 Initial Open Circuit Potentials of Defilmed Specimen in Deaerated Solution

All specimens except U-1 were defilmed prior to the initial measurements by immersion in concentrated HNO_3 for 1 min.

The initial open circuit potentials were in the neighborhood of -300 mv, but the potentials quickly dropped to the minimum values plotted in Fig. 9. With experiments U-2, U-4 and U-5, the potentials remained steady at the minimum values. With experiment U-3 (pH 9.6), the potential rose to higher values immediately after the minimum value was reached.

TABLE 1. SUMMARY OF EXPERIMENTAL CONDITIONS AND PROCEDURES FOR POLARIZATION MEASUREMENTS WITH URANIUM

(Some results also in this table)

Experiment Number[a]	Date	Solution[b] K_2SO_4 (M)	Solution[b] H_2SO_4 (N)	pH	Gas atm[c]	Polarization Range (mv)[d]	Polarization Data Fig. No.	Results of Examination of Surface for Pits.[n]	Remarks
U-1	10-21-69	0.1 (F)	---	5.8	air	0 to 300	1		Fresh specimens with dark, as received, film. (e)
U-1	10-22-69	0.1	---	5.8	air	-450 to 275	1	Several shallow pits	Specimens had been in cell over night. IOC = -36 mv.
U-2[f]	4-16-70	0.1 (F)	---	5.45	100 Ar	-1,100 to -1,500	2	No pitting	(h)
U-3[f]	4-17-70	0.1 (F)	---	9.6	100 Ar	-600 to -1350	3	No pitting	(i)
U-4[f]	4-20-70	0.1 (F)	---	(6.0)	$4H_2$	-950	4		(j)
U-4	4-21-70	0.1	---	(5.55) to (5.26)	$4H_2$	-400 to -1500	4		Solution became more acid upon standing over night and during polarization. (k)
U-4	4-22-70	0.1	---	(5.26) to (5.57)	$4H_2$	-300 to 300	5	Numerous shallow pits	pH decreased during anodic polarization.
U-5-1[f,l]	4-23-70	-----	1(F)	(.545)	$4H_2$	-----	-		Initial open circuit measurements. The value for this was -718 mv and steady.
U-5-2	4-23-70	----------same----------				-750 to -925	6		Tafel line with slope of -117 mv/decade. Put on O.C. following -925 mv polarization.
U-5-3	4-23-70	----------same----------				-650 to -500	6		Anodic polarization from O.C. of -712 mv. Put on O.C. following -500 mv polarization.
U-5-4	4-23-70	----------same----------				-400 to -100	6		Anodic polarization from O.C. of -700 mv. Put on O.C. following -100 mv polarization.
U-5-5	4-23-70	----------same----------				-800 to -950	6		Cathodic polarization from O.C. of -720 mv.
U-5-6	4-23-70	----------same----------				-100 and 0	6		
U-5-7	4-23-70	----------same			20 O_2	0	6		Changed atm to 20 O_2 during the 0 mv polarization. There was no sensible change in current.
U-5-8	4-23-70	----------same			20 O_2	-450 to -950	6		Cathodic polarization from O.C. of -400 mv. Put on O.C. following the -950 mv polarization.
U-5-9	4-23-70	----------same			20 O_2 to $4H_2$	----			Open circuit potential with 20 O_2 was -590 mv. This shifted to -720 mv when the O_2 was replaced with $4H_2$.
U-5-10	4-23-70	----------same			$4H_2$	0 to 225	6		System was put on O.C. following 225 mv polarization. O.C. went to -35 mv and constant.
U-5-11	4-24-70	-------	1	(.505)	$4H_2$	-100 to -950	6		Cathodic polarization from -35 mv O.C. following the -950 mv polarization, the O.C. was -665 mv.
U-6[m]	4-24-70	-------	1	.55	20 O_2	-650 to -950	7		Cathodic polarization from O.C. of -522 mv. Minimum initial O.C. was -650 mv.
U-6	4-24-70	-------	1	.55	20 O_2	83 to -1050	7		Cathodic polarization from O.C. of 81 mv.
U-6	4-29-70	-------	1	.55	20 O_2	250 to 475	8	Numerous shallow pits	Anodic polarization from O.C. of 140 mv.

(Table 1 cont'd.)

a. Experiments are identified by the combination of specimen number and date.

b. (F) means that the solution in cell was fresh. Otherwise, the solution was that used in previous experiment.

c. Where unspecified, the remainder of atmospheric pressure was supported by argon. Composition given in percent.

d. All potentials vs SCE.

e. No pretreatment of specimen other than washing and brushing. Initial exploratory measurements to +300 mv were made without close measurements of anodic currents.

Initial open circuit potential (I.O.C.) was -117 mv. Measurements numbered 1 thru 7 made on this date.

f. Fresh specimen defilmed by immersion in concentrated HNO_3 for 1 min.

g. Measurements 8 thru 26 on this date.

h. Initial open circuit potential dropped quickly to -1,065 mv and remained steady. Cathodic polarizations made in the numbered order.

i. Initial open circuit potentials dropped quickly to -1,260 mv and then rose. When the potential reached -570 mv, cathodic polarizations were started at -600 mv.

j. Initial open circuit potential dropped quickly to -1,010 mv and remained steady. Specimen was then polarized at -950 mv and then put on open circuit over night.

The initial current at -950 mv was +5.3μamp. The current diminished and changed sign with continued polarization. The value was -8.3μamp at the end of this polarization.

k. Continuation of run started on 4-20. The I.O.C. on this date was -308 mv.

l. Specimen U-5 used in experiments U-5-1 thru U-5-11.

m. Specimen U-6 was prepared from specimen U-5 by immersion in concentrated HNO_3 for 1 min.

n. The uranium surfaces had some pits as received. A specimen was examined after the final exposure, and a judgment made as to whether the number of pits had increased during the exposure.

TABLE 2. SPECIMENS, SOLUTIONS, INITIAL OPEN-CIRCUIT POTENTIALS AND RANGES OF POTENTIALS OR CURRENTS IN POLARIZATION EXPERIMENTS IN K_2SO_4 SOLUTIONS, pH 5.8, WITH AND WITHOUT KCl.

Experiment Number[c]	Date[a]	Solution[b]		Initial Open-Circuit Potential (mv)[f]	Potentiostatic Potential Range (mv)[f]	Galvanostatic Current Range (μamp)	Remarks
		KCl (M)	Atm[e]				
UA-2-89	11-6 thru 11-11	–	4% H_2	−200	−210 to 5000	–	
UA-3-89	11-12	–	4% H_2	−100	200 to 5000	–	
	11-13	–	Ar	7	200 to 4000	–	
	11-14	–	4% H_2	−155	−500 to 1500	–	
	11-14	0.0026	4% H_2	–	200 to 1000	–	
	11-17	0.0026	4% H_2	−280	20 to 5000	–	
	11-17	0.5	4% H_2	–	4000	–	Cl^- added with potential at 4000 mv, Table 4.
UA-4-89	11-18	–	air	−200	4500 to −200	–	
	11-19	–	air	−85	900 to −1100	–	
	11-19	0.01	air	–	100 to 300	–	
	11-20	0.01	air	−113	300 to 4500	–	Breakaway high current at 4500 mv, Table 4, Fig. 32.
UA-5-89	11-21	0.01	20% O_2	−150	0 to 550	–	Breakaway high current at 550 mv, Table 4, Fig. 32.
UA-6-89	11-21	0.01	4% H_2	−250	50 to 800	–	Breakaway high current at < 0 mv, Table 4, Fig. 32.
UA-7-89	12-2	0.01	4% H_2	–	–	Table 5	
UA-8-89	12-9	–	4% H_2	−850	−600 to −1300	–	
	12-10	–	4% H_2	−270	−1200 to 2000	–	
	12-11	–	4% H_2	−60	−1150 to 5000	–	
	12-12	–	4% H_2	–	–	−5 to −1940	
	12-17	–	4% H_2	−140	250 to 350	–	
	12-17	–	20% O_2	–	250	–	
	12-17	–	20% O_2	–	–	−6.3 to −3000	
	12-19	–	20% O_2	−50	600 to 5000	–	

(Table 2 cont'd.)

[a]1969.

[b]All solutions 0.1M K_2SO_4; pH 5.8; 25°C.

[c]One specimen used throughout each experiment. All specimens except UA-8-89 were machined and had an air film when placed in cell. The UA-8-89 specimen was abraded with Al_2O_3, grade 320, prior to placing in cell. All specimens were from quenched and aged material.

[e]Where unspecified, the remainder of atmospheric pressure was supported by argon. Composition given in percent.

[f]Potential versus SCE.

TABLE 3. SUMMARY OF EXPERIMENTAL CONDITIONS AND PROCEDURES FOR POLARIZATION MEASUREMENTS WITH U ALLOYS IN SOLUTION OF SULFURIC ACID[a]

Experiment Number[a]	Date[b]	K_2SO_4 (M)[f]	H_2SO_4 (N)[f]	pH[c]	Gas[d] atm	Polarization Range[e] (mv)	Polarization Data Figure Number	Footnote Remarks	Results of examination of Surface of specimen for pits.[v]
UA-8-89	1-15	----	.1(F)	1.2 (1.22)	4 H_2	-600 to 600	17	g,h	
UA-8-89	1-16	----	.1(F)	1.3	100 Ar	-800 to 800	18	i	
UA-8-89	1-19	----	1(F)	.25	4 H_2	0 to 600	19	j	No pits on UA-8-89
UA-11-89	1-19	----	1	.25	4 H_2	0 to 600	20	k	
UA-11-89	1-21	----	1	.25	20 O_2	150 to 450	20		
UA-11-89	1-22	----	1	.25	20 O_2	150 to 500		l	
UA-11-89	1-23	----	1	.25	20 O_2	-1000 to 550		m	
UA-11-89	1-26	----	1	.30 (.63)	4 H_2	-800 to 450	21	n	
UA-11-89	1-27	----	1(F)	.25 (.83)	4 H_2 20 O_2	-700 to 450	22	o	One shallow pit on UA-11-89
UA-12-89	1-27	----	1	.25	20 O_2	-800 to 550	22	o	
UA-12-89	1-28	----	1	.25	20 O_2	-600 to 750	23	p	
UA-12-89	2-2	----	1(F)	(.83)	4 H_2 100 O_2 100 Ar	-800 to 450	24	q	
UA-13-89	2-4	----	1(F)	.35 (.70)	4 H_2 100 O_2	-900 to 600	25a 25b	r	Few shallow pits on UA-13-89
UA-14-89	2-9	.1(F)	----	9.7 (10.1)	4 H_2	-1400 to 0	27	s	
UA-14-89	2-10	.1	----	9.6 (9.5)	4 H_2 20 O_2	-1600 to -350	28	t	
UA-14-89	2-12	----	1(F)	(.57)	4 H_2 100 O_2	-1100 to -200	26	u	Numerous shallow pits on UA-14-89

(Table 3 cont'd.)

a'. Two experiments at pH 9.6 are included; UA-14-89 on 2-9-70 and on 2-10-70.

a. Experiments are identified by the combination of number and date.

b. 1970

c. The number enclosed in parentheses was calculated from platinum potential. Other values were obtained using a glass electrode with samples of the solution.

d. Where unspecified, the remainder of atmospheric pressure was supported by argon. Composition given in percent.

e. All potentials vs SCE.

f. (F) means that the cell-solution was freshly charged. Otherwise the cell solution was that used in the previous experiment.

g. This specimen was used in previous experiments (Table 1) and had a heavy anodic film at the start. Following the measurements shown in Table 1, the specimen was exposed to air for several weeks and was then used in an experiment to measure N_2O reduction on 1-13-70.

h. Initial open circuit potential (I.O.C.) with 20% O_2 atm was 86 mv. Upon changing to 4% H_2, the potential shifted to 96 mv.

Visual and microscopic examination showed that the heavy oxide film had been dissolved during the anodic polarization on this date; there was no evidence of pitting.

i. Specimen had been in air over night. Initial open circuit potential was near zero mv.

j. Specimen had been in air over night.

Specimen was examined following this measurement. Its surface appearance was the same as that described under footnote h.

k. Fresh specimen with air-formed film on machined surface.

l. Specimen had been in air over night.

(Table 3 cont'd.)

Ran experiment to follow O.C. potentials. I.O.C. was 150 mv. After 450 mv polarization, O.C. went -100 mv in 39 min. O.C. increased to 55 mv over night.

m. Exploratory measurements of cathodic polarization behavior following anodic polarization to dissolve film.

After 550 and 450 mv polarizations, the potential was reduced rapidly to -1000 mv. Current was -770 μamp during 5 hr exposure. Upon putting specimen on O.C., the potential went positive very rapidly.

n. The O.C. in this experiment after cathodic polarization was very close to the Pt-potential, -240 mv, i.e., it was very close to the reversible potential for H^+-reduction.

o. The cathodic polarization data were near those obtained on 1-26-70. There was no observable reduction of O_2.

p. Cathodic behavior checked that of 1-27-70, anodic behavior also checked previous observations.

q. Cathodic behavior comparable to that obtained on 1-27-70. No observable reduction of O_2.

r. Fresh specimen with air-formed film on machined surfaces.

Initial cathodic polarization were made without prior anodization.

s. Fresh specimen abraded with Al_2O_3 grade 320.

There was close correlation between O.C. potentials and Pt-potentials in this experiment. Upon placing the specimen in cell, the O.C. was -625 mv while Pt-potential was -450 mv.

(Table 3 cont'd.)

Added KOH to decrease Pt-potential to -796 mv. Along with this change, the specimen potential decreased to -790 mv.

t. The specimen was left in the cell with 4% H_2 over night. The O.C. rose to -320 mv.

u. O_2 reduction was observable during some portions of the measurements.

v. These specimens were free of pits prior to exposures within the cell.

A correlation exists between minimum open circuit potentials and pH as can be seen in Fig. 9. The same functional relationship,

$$E_{O.C.} = -.059\ pH + constant, \qquad (1)$$

has been reported[1,2] for the initial corrosion potentials of Ti. However, no satisfactory explanation for this relationship has been offered, and I have none to propose for uranium. A possible connection with UH_3 is suggested by the location of the open circuit potentials between those at which UH_3 is in equilibrium with UO and with $U(OH)_3$.

The open circuit potential observed by Ward and Waber in a comparable experiment at 35°C (Appendix 3) is included in Fig. 9, and is in agreement with my results.

4.1.2 Effects of Cathodic Polarization to Potentials Below Those at Which UO_2 and UH_3 are in Equilibrium

Cathodic polarization to potentials below those at which UO_2 and UH_3 are in equilibrium in the reaction,

$$UH_3 + 2H_2O \rightleftharpoons UO_2 + 7H^+ + 7e^-, \qquad (2)$$

always produced a marked increase in the cathodic current (see Figs. 2, 4, and 7). The potential at which the break in the cathodic polarization curve was observed in each of the different experiments is plotted in Fig. 10 (see Appendix 1). The minimum potential which was employed in Exp. U-3 at pH 9.6 was above the potential for equilibrium between UH_3 and UO_2, and no break was observed in the cathodic polarization curve.

These results provide very strong evidence that UH_3 forms by reduction of UO_2 or by reaction between U and H_2O below the potential at which UH_3 is stable with respect to reaction with H_2O. The UH_3 could form on the surface of the UO_2 film with the electrons passing thru the oxide from the metal if the oxide is an electronic conductor, or it could form at the metal-oxide interface if the oxide is permeable to H_2O. The particular processes which actually prevail were not established by these experimental results.

4.1.3 Effects of Anodic Polarization Above the Initial Steady Open Circuit Potential but Below Potential of Equilibrium Between UO_2 and UO_3

4.1.3.1 Fig. 4, pH 6

Anodic polarization at -950 mv from the open circuit potential of -1.01v caused formation of passive film. This could be deduced from the facts that, (1) the current changed during polarization from 4μamps/cm^2 anodic to 6.7μamps/cm^2 cathodic, and (2) the steady open circuit potential shifted to -320 mv following the polarization to -950. Also, the open circuit corrosion rates changed from an estimated value of > 13μamps/cm^2 to ~ 1.2μamps/cm^2 as a result of the polarization (1μamp/cm^2 = .36 mpy). The corrosion rate prior to polarization was estimated from the effects of polarization on the current and from the estimated anodic current following polarization. The latter estimate was made from the cathodic polarization and open circuit potential data shown in Fig. 4.*

---

*See Appendix 5.

4.1.3.2 Fig. 6, pH 0.5

Passive film was formed during anodic polarization in this strongly acid solution. This could be deduced from the facts that, (1) the estimated anodic current at open circuit dropped from about 6μamps/cm^2 to about 1.5μamps/cm^2 after polarization to -100 mv, and (2) the slopes of the cathodic polarization curves increased as a result of the polarization.* The open circuit potential did not shift appreciably after anodic polarization to -100 or 0 mv presumably because of counter acting effects of the additional passive film on the rates of the anodic and cathodic processes. The open circuit potential was raised substantially by the subsequent polarizations to +200 and +225 mv.

4.1.4 Cathodic Processes Above Potentials at Which UH_3 and UO_2 are in Equilibrium

a. Fig. 3, pH 9.6, deaerated solution

The cathodic process in this case was, very likely, either direct reduction of H_2O with evolution of H_2 or formation of UH_3 by reaction between U and H_2O. There was insufficient H^+ or O_2 in the solution to account for the observed currents.*

b. Fig. 4, pH 5.6, deaerated solution

In this case, the (H^+) may have been barely sufficient to account for the highest cathodic currents. However, the line thru the data points is approximately parallel to that thru the data at pH 9.6, Fig. 3, and it seems likely that the reduction process was the same as that at pH 9.6.

---

*See Appendix 5.

c. Fig. 6, pH 0.5, deaerated solution

The cathodic process in this case was almost certainly H^+-reduction. The Tafel slope for the initial cathodic polarization was close to that expected with film-free surfaces, 118 mv/decade.* The higher slopes associated with subsequent cathodic polarizations can be ascribed to the presence of thicker passive films. The indicated exchange current was very small ($\sim 10^{-10}$ amps/cm^2).

d. Fig. 6, pH 0.5, aerated solution

No sensible amount of reduction of O_2 was observed on the partially passivated surface when the atmosphere of 4% H_2 was replaced with 20% O_2. An O_2-reduction current of 4 to 5μamps could have been detected, and a limiting diffusion current much greater than this would be expected on surfaces where O_2-reduction is not inhibited in some way, e.g., by high resistance to passage of electrons thru surface films or by slow or very low adsorption of O_2 on the surface. A limiting diffusion current of 200 to 400μamp/cm^2 was expected for uninhibited O_2 reduction in this experiment.*

e. Fig. 7, pH 0.5, aerated solution

Reduction of O_2 with a limiting current of about 10μamps/cm^2 was indicated by the results of this experiment. Here again, a limiting diffusion current of 200-400μamp/cm^2 was expected for uninhibited reduction of O_2.

---

*Appendix 5.

f. Fig. 1, pH 5.8, aerated solution

Oyxgen reduction in this experiment over the potential range tested was typical of that expected for an uninhibited surface. The high slope was consistent with the presence of passive film.* The limiting diffusion current was not determined in this experiment.

It might be noted that this specimen had been subjected to anodic polarization prior to the cathodic polarization and this may have affected the O_2-reduction properties by causing removal of the film and pitting of the surface.

4.1.5 Effects of Anodic Polarization to Potentials Above Those at Which Anhydrous UO_3 and UO_2 are in Equilibrium

Anodic polarization to potentials near those at which anhydrous UO_2 is in equilibrium with UO_3 always resulted in a shift from a passive to an active state as shown in Figs. 1, 5 and 8. The potentials at which the transition occurred are plotted vs pH in Fig. 11.

A Tafel relationship prevailed in the transpassive region. Visual examinations showed that all dark film was removed at potentials above the transpassive potential and that it reformed below this potential. Also, shallow pits were formed on the surfaces of specimen which had been exposed at transpassive potentials (Table 1).

These results provide clear evidence that protective UO_2 is converted to soluble UO_3 at and above the potential of equilibrium between UO_2 and UO_3.

---

*Appendix 5

The shallow pits are probably explained by the occurrence of processes similar to those which explain pit-initiation and growth in the presence of aggressive anions (Appendix 4). In the present case, it can be postulated that UO_3 formulation and dissolution begins at localized sites where the electronic conductivity of the UO_2 film is the highest. The conductivity at the site would increase as the film thickness decreases, and so the dissolution would continue at an increasing rate until the UO_2 film is penetrated.* When the metal is exposed, the high local corrosion rate would cause changes in the local potentials and solutions componsitions; the potentials would decrease, and H_2SO_4 would accumulate within the pit solution (Appendix 5). At equilibrium, the pit-potential would presumably be below the surface-potential but above the potential at which the net pit-current would be cathodic. Consideration of the experimental polarization data reported above, Figs. 4, 5, and 6 led to the conclusions that the equilibrium potential would be above about -700 mv (SCE) at $< 1N\ H_2SO_4$ within the pit, and that the equilibrium rate of corrosion within the pit would be $< 10\mu amp/cm^2$. The potentials and reactions which might prevail prior to equilibrium are unknown. It can be speculated that the potentials could go to very low values immediately after exposure of bare metal. However, cathodic reactions, including UH_3-formation, would occur at the low potentials so that the net anodic current would decrease and the potential would rise toward the equilibrium value. It seems possible that overshoots would occur, leading to oscillations of potential within the pit during the approach to equilibrium.

*Of course, the rate of dissolution must remain below a level at which the local potential is significantly decreased.

The slopes of the Tafel-lines were 95 and 45 mv/decade at pH 5.3 and 0.55, respectively. The value for the acid solution can be compared with the value of 40 at 37°C in H_2SO_4 reported by Kindlimann and Greene.[3,4] No previous experimental information is available on transpassive behavior in neutral solutions at 25°C.

The transpassive Tafel slopes can presumably be related to the kinetic mechanisms, but this has not been done. It can be noted that while most of the oxide film is dissolved at transpassive potentials, it must be assumed that some protective film remains on the surface and that this protective film is UO_2. The first assumption appears necessary because the anodic rates are below those which would be expected in the complete absence of film. The second assumption is necessary because the transpassive dissolution appears to be an activation-controlled redox reaction with an equilibrium potential corresponding to that for equilibrium between anhydrous UO_2 and UO_3.

4.2 Summary of Conclusions for Uranium

The experimental results lead to the following general conclusions regarding the electrochemistry of uranium in solutions of 0.1M K_2SO_4, (pH 5 to 6) and 1N H_2SO_4 with one or more of the gas atmospheres; Ar, $4H_2$: 96Ar, 20 O_2 : 80Ar (or $80N_2$).

a. A passive film of UO_2 forms on uranium above potentials near those for the equilibrium,

$$UH_3 + H_2O \rightleftharpoons UO + 5H^+ + 5e^-;\ E^\circ = -.655 - .0591\ pH \qquad (3)^*$$

*Potential vs SCE

b. The passive film is removed, and increasing anodic rates occur above potentials near those for the equilibrium between UO_2 and soluble UO_3,

$$UO_2(anh) + H_2O \rightleftharpoons UO_3(anh) + 2H^+ + 2e^-;\ E^\circ = .415 - .0591\ pH \quad (4)^*$$

c. The cathodic rate on the passive metal increases sharply below potentials near those for the equilibrium,

$$UH_3 + 2H_2O \rightleftharpoons UO_2 + 7H^+ + 7e^-;\ E^\circ = -.958 - .0591\ pH \quad (5)^*$$

This indicates that UH_3 is formed from UO_2 and/or from U by reaction with H_2O or with H^+ below these potentials.

The above conclusions probably are valid for solutions of other pH values but this remains to be verified. Given below for convenient reference is a list of pH and gas atmospheres used in experiments which led to the above conclusions.

General Conclusion	pH (gas atm)
a.	0.5(4% H_2), 5.5(Ar), 6(4% H_2), 9.6(Ar)
b.	0.6(20% O_2), 5.3(4% H_2), 5.8(air)
c.	0.5(20% O_2), 5.4(Ar), 5.6(4% H_2)

Prior information on the corrosion of uranium in aqueous solutions at temperatures of 25 to 100°C is summarized, and is correlated and interpreted on the basis of the electrochemical theory of corrosion, in Appendix 3. The above general conclusions drawn from the present work are consistent with the prior information as interpreted in Appendix 3. The experimental data indicate that the sulfate and

---

*Potential vs SCE

bisulfate ions have little if any detrimental effects on the corrosion of uranium despite the fact that soluble complexes are formed with U(IV) and U(VI). These ions may have beneficial effects if aggressive anions (chloride) are present. This is discussed elsewhere in this report.

Other notable observations made in the present work include the following

d. The exchange current for reduction of H^+ in 1N H_2SO_4 is very low, $\sim 10^{-10}$ amps/cm^2.

e. Reduction of O_2 on partially passivated uranium in 1N H_2SO_4 is inhibited. The mechanism of the inhibition is uncertain.

f. Reduction of O_2 on uranium in 0.1M K_2SO_4, pH 5.8 appeared more or less normal.

g. Shallow pits were formed on the surfaces of specimens exposed to transpassive potentials ($E_{SCE} > .415 - .0591$ pH). This pitting can be explained in terms of the occurrence of processes similar to those which explain pit initiation and growth in the presence of aggressive anions (Appendix 4). Pit initiation in this case results from local conversion of UO_2 to soluble UO_3.

h. Polarization in the transpassive regions followed Tafel behavior. The slopes were 95 and 45 mv/decade at pH 5.3 and 0.55, respectively. Presumably these slopes can be related to the kinetic mechanisms, but this has not been done. It can be assumed that some protective film remains on the surface at transpassive potentials and that this film is anhydrous UO_2.

5. Experimental Results and Discussion; U-7.5Nb-2.5Zr in 0.1M K_2SO_4, pH 5.8*

5.1 Results and Correlations

The experimental results are presented graphically in Figs. 12 thru 16. Additional information, correlations, and comments on the results are presented below.

5.1.1 Anodic Polarization Behavior Prior to Cathodic Polarization of Filmed Specimens

The polarization behavior determined potentiostatically in these experiments is illustrated by curves representing data from experiments UA-2-89, UA-3-89, UA-4-89, and UA-8-89, Figs. 12 and 13.

Notable features of the results are:

(a) Steady-state currents remained very small out to the maximum voltage imposed (~ 5v). There was no evidence for the oxidation of water which would be expected at the high voltages if the oxide films were electronic conductors (Appendix 5).

(b) There was no significant difference between the behavior with air and with 96% Ar, 4% H_2.

(c) Prior cathodic polarization of an unfilmed specimen (UA-8-89) did not appreciably alter subsequent anodic behavior.

(d) There was a noticeable reduction of current at a given potential following a small amount of anodization. After this initial effect, the subsequent anodizations which occurred as part of the measurements did not appreciably affect the steady-state currents.

(e) In general, the transients which occurred upon increasing the voltage gave rise to currents in excess of those at the steady state. Upon decreasing the voltage, the transient currents were negligible.

(f) The specimens took on a gold-brass appearance during anodic polarization. Specimen UA-8-89 had a deep purple color; possibly a result of the extensive anodization and cathodization with this specimen.

5.1.2 Anodic Polarization Behavior After Prior Cathodic Polarization of Anodically Filmed Specimens

Cathodic polarization of anodically filmed specimens resulted in a reduction in current at a given anodic potential during subsequent anodic polarizations. This effect is illustrated in Fig. 14. No correlation was noted between the cathodic current or voltage and the extent of this effect.

5.1.3 Cathodic Polarization Behavior

The results of cathodic polarization to -1.5 v in experiment UA-8-89 using an atm of 4% H_2, 96% Ar are illustrated in Fig. 15a, 15b, and 16. Those for polarizations to -1.8 v in the same experiment using an atm of 20% O_2, 80% Ar are illustrated in Figs. 15a and 15b. Other cathodic polarization experiments to -1.04 v are also illustrated in Fig. 15a.

Notable features of these results are:

(a) Sharply increasing cathodic rates occurred below about -1.18 v when the gas atm was 4% H_2. This effect occurred both before and after anodization.

(b) An increase in cathodic current also occurred at low potential when the gas atm was 20% O_2. However, the increase started at a lower potential, ~ -1.45 v, and was less marked than that in the 4% H_2 atm.

(c) The maximum cathodic currents prevailing prior to the transitions to high cathodic currents were less than those expected for limiting diffusion currents; the expected limiting currents were about 5 to 10μamp for the 4% H_2, pH 5.8 solutions, and about 500 to 1000μamp for the air or 80% Ar, 20% O_2 atmospheres.

(d) The cathodic currents at a given voltage in solutions with O_2 atmospheres differed significantly from one experiment to another, indicating that the cathodic behavior was dependent upon the conditions under which prior anodization (and possibly prior cathodization) were performed.

The potentials at which transitions to high cathodic current occurred in UA-8-89 are plotted in Fig. 10 where they can be compared with the transition-potentials for uranium. The potentials of alloy-transition in 4% H_2 and in 20% O_2 were, respectively, about 125 mv above and 150 mv below that for uranium at the same pH.

5.1.4 Open-Circuit Potentials

The open-circuit potential prior to the start of an experiment is listed in Table 2.

Fragmentary evidence was obtained that these potentials shifted considerably after polarization. At the end of experiment UA-8-89, 12-19-69, the specimen was placed on open circuit following polarization at 600 mv. The open-circuit potential was 400 mv and was drifting slowly downward. (The initial open-circuit potential was -50 mv on this date.) The potential was then held at 5 v until

a steady state was reached and then put on open circuit. The initial potential was about 2 v. It dropped quickly to the neighborhood of 400 mv and then dropped to about 300 mv over a period of several hours. The next morning, the potential was +70 mv.

A shift in the cathodic direction during cathodic polarization was also noted. During experiment UA-8-89, 12-10-69, the specimen was placed on open circuit following cathodic polarization at -1400 mv. The potential was -720 mv when first observed; it increased to -322 during an observation period of 72 minutes. (The initial open-circuit potential in this experiment was -280 mv.)

5.1.5 Open Circuit Corrosion Rates

Corrosion rates at open circuit could not be estimated accurately from these experimental data. However, it was estimated that these rates were < 10μamp/cm^2 (< 6.3 mpy) in all experiments.

5.2 Discussion

The films formed during anodic polarization in K_2SO_4-solution are apparently poor electronic conductors at the steady-state on the anodic side; water was not oxidized at the high potentials. The observed steady-state currents were probably due to ion movement thru the film. However, the transient currents which occurred upon a sudden increase in potential were well above those at steady-state, and it is possible that these currents were associated with transient electronic conduction. The stability of the film at potentials well above that at which UO_2 can be oxidized to UO_3 (Section 4) is probably due, at least in part, to the poor electronic conductivity

(This oxidation is a redox reaction, Appendix 5, and it is reasonable to assume that electrons must pass thru the film in order to oxidize UO_2 at the oxide solutions interface.) However, UO_3 may have been formed during the transient, high-current, conditions, and if so, the film-stability is also due in part to a low solubility, near neutral pH, of the oxide which contains Nb_2O_5 and ZrO_2 in addition to UO_3.

The results of the cathodic polarizations in experiment UA-8-89 indicate that the behavior of the alloy at low potentials in the absence of O_2 is similar to that of uranium. As discussed previously, it is believed that this behavior results from formation of UH_3 by reaction between UO_2 (or U) and H_2O or H^+ below potentials at which UH_3 and UO_2 are in thermodynamic equilibrium (Section 4). In the presence of O_2 the indicated cathodic behavior is quite different. The observed increase in cathodic current starting at -1.45 v can be ascribed to the onset of direct reduction of water to evolve H_2 (Section 7), and it is not necessary to assume that UH_3 was formed.

No explanation is offered at this time for the observation that cathodic polarization of an anodically-filmed specimen led to a reduction in the anodic current during subsequent anodic polarization.

6. Experimental Results and Discussion; U-7.5Nb-2.5Zr in 0.1N and 1N H_2SO_4*

---

*Experimental condition and procedures in Table 3.

6.1 Results and Correlations

The experimental results are presented graphically in Figs. 17 thru 26. Some results are included in Table 3. Additional information, correlations, and comments are presented below.

6.1.1 Effects of Anodic Polarization to Potentials Above Those at Which UO_2 and UO_3 are in Thermodynamic Equilibrium

Figs. 11, 17, 18, 19, 20, 23, and 25b.

Anodic polarization to potentials above those at which anhydrous UO_2 and UO_3 are in thermodynamic equilibrium produced results similar, in many respects, to those observed with uranium in 1N H_2SO_4 and in 0.1M K_2SO_4. Specifically, (1) the anodic current increased markedly with increasing potentials above the equilibrium potentials, (2) Tafel behavior prevailed in the transpassive potential region, and (3) all dark film was removed from surfaces above the transpassive potential. It should be noted that the above remarks apply to all specimens including UA-8-89, 1-15-70, which was coated with an anodic film in K_2SO_4 prior to exposure in the 0.1N H_2SO_4. This anodic film dissolved during anodization in the H_2SO_4 (Fig. 17).*

The Tafel slopes for the alloy (Figs. 17-20, 23, and 25b) ranged from 70 to 90 mv/decade. These are well above the 45 mv/decade found with uranium in 1N H_2SO_4 but they are comparable to that for uranium in 0.1M K_2SO_4, pH 5.3.

There were no significant effects of gas atmosphere on the transpassive behavior and on the potential of transition.

---

*Tests with another specimen showed that a pre-formed anodic film did not dissolve in aerated 0.1N H_2SO_4 at open circuit potentials.

It appears that, in general, the behavior of the alloy at high potentials in 0.1 and 1N H_2SO_4 is comparable to that of uranium in 1N H_2SO_4 and in 0.1M K_2SO_4 at pH 5 to 6 and, accordingly, that the explanations for the behavior are the same as those discussed above for uranium (Section 4.2). The rate controlling processes for the alloy in the transpassive region in H_2SO_4 are probably the same as those for uranium in 0.1M K_2SO_4, pH 5.5 since the Tafel slopes are about the same.

The fact that a pre-formed anodic film was dissolved during anodic polarization in 0.1N H_2SO_4 indicates that the film was an electronic conductor in H_2SO_4. As discussed previously, these films are poor electronic conductors at the steady-state in 0.1M K_2SO_4 (pH 5.8) although they probably are electronic conductors under the transient conditions which prevail after the potential is increased. It can then be postulated that UO_3 is formed during the transients and that the resulting film which contains UO_3 is soluble in 0.1N H_2SO_4 but insoluble in K_2SO_4 at pH 5.8 (Section 5.2).

6.1.2 Cathodic Polarizations

6.1.2-1 Cathodic Reductions of H^+ and O_2 in 1N H_2SO_4. Occurrence of Pits.

The experimental results for the cathodic reduction of H^+ and O_2 and for the occurrence of pitting fall into two groups with the grouping apparently dependent upon specimen polarization history and other pretreatment. The results for the two different groups are described separately below.

Group 1

Each specimen had an air-formed film when immersed in 1N H_2SO_4 within the cell. Each specimen was anodized to +450 mv or above prior to cathodic measurements. All visible oxide film was dissolved during these anodizations (Section 6.1.1). The change to a cathodic potential after anodization was made rapidly, and in some cases instantaneously.

The experimental results which pertain to H^+-reduction are summarized by lines 1, 2 and 3 in Fig. 29.* As can be seen, the results from different experiments are in near agreement. The data formed good Tafel lines over many orders of magnitude of current. The slopes of the lines were about 112 mv/decade. The exchange currents were in the neighborhood of a few tenths $\mu amp/cm^2$ (Fig. 21). The indicated corrosion rate at open circuit was $<< .1\ \mu amp/cm^2$ (Fig. 21).

No reduction of O_2 could be detected on these specimens (Figs. 22 and 24). In one set of measurements (Nos. 2, 7, 8, 11 and 12, Fig. 24) which provided a sensitive test for O_2-reduction, the expected diffusion-limited current from O_2 was > 500 μamp (see Fig. 30 and Appendix 5), and a current of 20-30 $\mu amps$ due to O_2-reduction could have been readily detected; no O_2-reduction current was detected.

With the exception of a single pit on specimen UA-11-89, these specimens were free of pits after experimentation (Table 3).

---

*A line representing H^+-reduction on uranium is included in this and other figures for convenient reference.

Group 2

The experimental results pertaining to H^+-reduction are illustrated by lines 4, 4a and 5 in Fig. 29. The data which were obtained when the gas atmospheres was 4% H_2 formed good Tafel lines over several orders of magnitude of current. However, the slopes were significantly greater than 112 mv/decade. No reliable estimates of the exchange currents could be made because the Tafel slopes were apparently affected by film (Appendix 5). However, it is apparent in Fig. 29 that the current at a given potential was far below that for specimens in group 1.

Reduction of O_2 was observed in experiment UA-14-89, Fig. 26, and the characteristics were more or less as expected for uninhibited reduction. Reduction of O_2 was also observed during one part of experiment UA-13-89 (Fig. 25a) although the apparent contribution of O_2-reduction to the current changed during the course of the measurements.

Pits were found after experimentation on each of the two specimens in this group (Table 3).

Pretreatments for these specimens are summarized below:

Line 4, Fig. 29. Specimen UA-13-89 which was used in these measurements had an air-formed film when it was immersed in H_2SO_4 within the cell. There were no polarizations above the initial open circuit potential.

Line 4a. Following the line 4-measurements, specimen UA-13-89 was anodized at transpassive potentials and then employed in these 4a measurements.

Line 5. Specimen UA-14-89 was first abraded and then used in polarization experiments at pH 9.5 (Figs. 27 and 28 and Section 7) prior to use in the experiments represented by line 5. At no time was the specimen polarized in H_2SO_4 at anodic potential where film-dissolution was expected.

6.1.2-2 Cathodic Reduction of H^+ in 0.1N H_2SO_4

The results of the one cathodic experiment in 0.1N H_2SO_4 are illustrated in Fig. 29 where they can be compared with those in 1N H_2SO_4. The slope of the Tafel line was 112 mv/decade. The indicated exchange current was much less than those in 1N H_2SO_4. The relationship between H^+-reduction in 0.1N and 1N H_2SO_4 is discussed in more detail in Section 6.1.2-3.

6.1.2-3 Summary and Discussion

Values and/or comments pertaining to certain parameters which summarize the observed cathodic polarization behavior of U-7.5Nb-2.5Zr in 1N H_2SO_4 are listed in Table 4. Listings for uranium specimen U-5, Fig. 6, in 1N H_2SO_4 and for U-7.5Nb-2.5Zr in 0.1N H_2SO_4 are included for comparison. In addition, it can be noted that the data for H^+-reduction on U-7.5Nb-2.5Zr in 0.1 and 1N H_2SO_4 (group 1 specimens) are adequately expressed by the equation,

$$i_c(\text{amps/cm}^2) = 1.2 \times 10^{-9}(H^+)^{3/2}\exp-\left(\frac{.53F}{RT}\ \Delta\phi\right), \qquad (6)^*$$

where $\Delta\phi$ is the electrode potential (V vs SCE).

Experimental and theoretical information regarding the kinetics of reduction of O_2 and H^+ and regarding factors which affect the

Table 4. Summary of Observed Cathodic Polarization Parameters for U, 7.5 Nb, 2.5 Zr and Uranium in 1N H_2SO_4

Specimen Material and/or Group	Parameter				
	H^+-reduction			Detectible Reduction of O_2	Occurrence of Pitting[g]
	Tafel Slope (mv/decade)[c]	Cathodic Transfer Coefficient[d]	Overvoltage at -1 ma/cm^2 (mv)		
U,7.5Nb, 2.5Zr					
Group-1	112	.53	-450 to -500	No	No
Group-2	154-210	.38 to .28	-750[i] to -930[i]	Yes	Yes
Uranium					
Group-1[a]	112	.53	-735[e]	-	-
Group-2[b]	150	.38	-915[f]	No	-
[alloy in 0.1N H_2SO_4][h]	112	.53	-605[i]	-	-

[a] No prior anodization to form passive film, Fig. 6.

[b] After anodization to form passive film, Fig. 6.

[c,d] See Appendix 5.

[e,f] Estimated by extrapolations from the maximum measured current densities of about -500 and -100 μamp/cm^2, respectively.

[g] As determined by visual examination following experimentation.

[h] Included for comparison.

[i] Estimated by extrapolations from the maximum, measured current densities of -100 to -200 μamp/cm^2.

kinetics are reviewed in Appendix 5. The following tentative conclusions can be drawn from the experimental observations using information in this review.

a. The surface films on the group 1 specimens of U-7.5Nb-2.5Zr were thin and did not affect the transfer of electrons to hydrogen ions in solutions adjacent to the surfaces. The same is true for the group-1 uranium specimen in 1N H_2SO_4 and for the alloy specimen in 0.1N H_2SO_4. These conclusions were indicated by the experimental Tafel slopes, 112 mv/decade, and transfer coefficients, 0.53. They were also indicated by the histories of these specimens which were such that only very thin films were expected to be present during the cathodic measurements.

b. The surfaces of the group-2 alloy and uranium specimens were coated with passive films.

Again, this conclusion was indicated by the Tafel slopes, $>>$ 112 mv/decade, and by the transfer coefficients, $<<$ 0.5. They were also indicated by the histories of these specimens except that of specimen UA-13-89, Figs. 25a and 29, line 4a. This specimen was anodized at transpassive potentials prior to the line 4a measurements. However, the specimen had been cathodically polarized to -850 mv prior to the anodizations, and it is possible that this pretreatment effected changes in the composition of the surface material which survived the anodizations and affected the subsequent cathodic results.*

---

*However, the anodic currents in the transpassive region were not significantly different from those for group-1 alloy specimens (Fig. 25b).

c. The overvoltages for H^+-reduction on the alloying elements (Nb and Zr) are much lower than those on uranium, and these alloying elements are probably exposed and enriched on the surface of the alloy during anodic polarizations at transpassive potentials.

These conclusions were suggested by the low overvoltages on the group-1 alloy specimens and by the relatively high overvoltage on the group-1 uranium specimen.

d. The relative concentrations of Nb and Zr on the surfaces of alloy specimens after transpassive polarization in 0.1N and 1N H_2SO_4 are greatest when the polarization is done in 1N H_2SO_4.

This conclusion was suggested by the appearance of the factor, $(H^+)^{3/2}$, in Eqn. 6. Theoretically, the current at a given $\Delta\phi$ should depend on the concentration of H^+ to a power of 0.5 to 1.

e. The concentrations of O_2 and/or the amounts of adsorbed O_2 at the surfaces of the group-2 alloy specimens were greater than those for the group-1 alloy specimens.

This conclusion was based on the observation that reduction of O_2 could be detected with the group-2 specimens but not with the group-1 specimens, and also on the observation that the hydrogen overvoltage was highest on the group-2 specimens. The latter observation led to a discounting of the possibility that differences between energetics of electron transfer from the surfaces accounted for the differences between O_2-reduction characteristics.

It may be noted that the expected diffusion limited current for O_2-reduction with P_{O_2}= 1 atm was 1 to 2 ma/cm^2. The data show

that this limiting current was reached during some of the measurements with group-2 alloy specimens.

f. Pitting. There is no obvious explanation for the differences between pitting characteristics of the alloy specimens. However, it can be noted that the histories of the specimens which were pitted included early cathodic polarizations to potentials below or near those at which UH_3 can be formed by reduction of UO_2. It is possible that localized UH_3-formation occurred and that later oxidation of the UH_3 resulted in the pits.*

6.2 Summary of Conclusions and Notable Features of Results.

It was concluded that the alloy exhibits transpassive behavior which is similar in the following respects to that of uranium in 1N H_2SO_4 and in 0.1M K_2SO_4: (1) the onset of transpassivity occurs near the potentials at which anhydrous UO_2 and UO_3 are in thermodynamic equilibrium, (2) Tafel relationships prevail in the transpassive regions and (3) all dark films are removed from surfaces at transpassive potentials. The explanations for the transpassive behavior of the alloy are thought to be the same as those discussed for uranium in a previous section (Section 4.2). The processes which control the anodic rate on the alloy in the transpassive region are probably the same as those for uranium in 0.1M K_2SO_4, pH 5.6 since the Tafel slopes are about the same (70 to 90 mv/decade).

Transpassive polarization probably causes exposure and enrichment of the alloying elements, Nb and Zr, on the surface of the alloy. The

*Also, it is possible that the abrasion-pretreatment of UA-14-89 produced the shallow pits in the specimen.

enrichment is greater in 1N H_2SO_4 than in 0.1N H_2SO_4. The overvoltage for H^+-reduction on these enriched and film-free surfaces in H_2SO_4 is substantially less than that on uranium.

Alloy specimens which are coated with passive films exhibit overvoltages for H^+-reduction which are comparable to those on uranium.

Reduction of oxygen takes place in a more or less normal manner on the alloy surfaces which are coated with passive films. The reduction on the enriched and film-free surfaces is inhibited. This difference between the two types of surfaces probably involves differences between the concentrations of O_2 at the surface and/or between the amounts of O_2 absorbed at the surface.

Pits were found on the surfaces of certain specimens after experimentation. The exposure histories for these specimens differed from those which did not exhibit pits. In particular, these histories included early cathodic polarizations to potentials below or near those at which UH_3 can be formed by reduction of UO_2. It is possible that localized UH_3-formation occurred and that later oxidation of the UH_3 (below transpassive potentials) resulted in the pits. Also, one of the specimens was abraded, and it is possible that this pretreatment affected pit formation.

7. Experimental Results and Discussion; U-7.5Nb-2.5Zr in 0.1M K_2SO_4, pH 9.5*

7.1 Results

The experimental results are presented graphically in Figs. 27 and 28.

*Experimental conditions and procedures in Table 3.

7.2 Discussion

Polarizations were made at potentials $\leq$ 0v, and atmospheres of 4% H_2 or 20% O_2 were used. The polarization data showed a low corrosion rate and a more-or-less ideal behavior with respect to O_2-, H^+- and H_2O-reduction. An anodic polarization to -200 mv preceded the cathodic polarization (Fig. 27). Accordingly, it can be inferred that the surface of the specimen was coated with a passive film during the cathodic polarizations and that the high Tafel slopes for H_2O-reduction resulted from the presence of this film (Appendix 5 and Section 6).

The H_2O-reduction data provided a basis for interpretation of the high cathodic currents observed with a previous, anodically-filmed, specimen in K_2SO_4 (pH 5.8) with an atm of 20% O_2. As shown in Fig. 31, the present data are in near agreement with those of the prior experiment, and it can be inferred that the same cathodic processes prevailed i.e., H_2O-reduction with evolution of H_2 in both cases.*

8. Pitting Experiments in Solutions of 0.1M K_2SO_4 plus KCl (pH 5.8) U-7.5Nb-2.5Zr

8.1 Introduction

Potentiostatic and galvanostatic experiments of pitting were made in solutions of 0.1M K_2SO_4 containing also .0026, .01 or .5 M KCl. Specimen history and procedures are summarized in Tables 2 and 5.

---

*As discussed in Appendix 5, the reduction of water in neutral and alkaline solutions containing an excess of supporting electrolyte is expected to be independent of pH.

TABLE 5

BREAKDOWN POTENTIALS IN K_2SO_4–KCl SOLUTIONS[a]

Potentiostatic Measurements

Experiment[b] Number	KCl (M)	Breakdown Potential[c] (mv)	Atmosphere	Remarks
UA-3-89	0.0026	>5000	96 Ar 4 H_2	Specimen anodically filmed in prior measurements. Maximum prior voltage: 5000 mv. No pits.
UA-3-89	0.5	<4000	96 Ar 4 H_2	Cl^- added with potential at 4000 mv. Badly corroded.
UA-4-89	0.01	4000	air	Specimen anodically filmed in prior measurements. Maximum prior voltage: 4500 mv. One pit only.
UA-5-89	0.01	550	80 Ar 20 O_2	Some anodic film formed during measurements of steady-state currents at 9 potentials prior to reaching breakdown potential. Several pits. Fig. 32
UA-6-89	0.01	<0	96 Ar 4 H_2	Some anodic film formed during measurements of steady-state currents at 11 potentials prior to reaching breakdown potential. Several pits. Fig. 33

[a] All solutions 0.1 M K_2SO_4; pH, 5.8; temperature, 25°C.

[b] All specimens were machined and had an air film when placed in cell.

[c] Potential versus SCE.

Theoretical and experimental aspects of pitting in the presence of aggressive anions are reviewed and discussed in Appendix 4.

8.2 Results

The results of potentiostatic measurement of breakthrough potential on preanodized and on air-filmed specimens are listed in Table 5 and shown graphically in Figs. 32 and 33 for experiments UA-5-89 and UA-6-89.

These results demonstrated that the breakthrough potential depended, as expected, upon (Cl^-) and upon the type and amount of film on a specimen. In the case of the air-filmed specimens (UA-5-89 and UA-6-89), it also depended upon the gas atmosphere--the breakthrough potential was lower with 4% H_2 than with 20% O_2. However, it is likely that this difference reflected a difference between types and amounts of film formed upon immersion of a specimen in the test solution. Pitting potentials were measured in experiments UA-5-89 and UA-6-89 and were between 0 and -100 mv, Figs. 32 and 33.

The results of galvanostatic measurements of breakthrough and pitting potentials with 0.01M KCl and an atmosphere of 4% H_2 are listed in Table 6. The specimen was air-filmed. The initial measurements showed potentials near those found in the potentiostatic measurements. However, a cathodic polarization to a minimum of -1.15 v resulted in a large increase in pitting potential.

8.3 Discussion

Most of the pitting behavior observed in this work is similar to that which has been reported by others for other materials, and

TABLE 6

BREAKDOWN AND PITTING POTENTIALS IN K_2SO_4–KCl SOLUTION

Galvanostatic Experiment UA-7-89[a,b,i]

Number[c]	Current (μamps)	Breakdown[d,f] Potential (mv)	Pitting Potential[e,f] (mv)
1	10	300	0 to −100
2	100	750	0 to −50
3	4.5	750	0 to +50
4	9	750	0 to +50
5	15	850	0 to +50
6	45	1050	0 to +50
7	−10[g]	–	–
8	22	850	+50 to +100
9	−10[h]	–	–
10	10	1500	+500 to +800
11	90	1500	+500
12	150	–	+500 to +750
13	225	–	+500 to +750
14	450	1500	+500 to +750

[a]Solution 0.1 M K_2SO_4, 0.01 M KCl; pH, 5.8; temperature, 25°C; atmosphere, 96Ar, 4H_2.

[b]Specimen was machined; air film when placed in cell.

[c]Successive measurements as numbered.

[d]Maximum potential.

[e]Approximate steady potential at given current.

[f]All potentials versus SCE.

[g]Two minutes to -500mv.

[h]Nine minutes to -1150mv.

[i]There were numerous pits on the surface after these exposures.

can be qualitatively explained as discussed in Appendix 4. The marked effects of cathodic polarization on the pitting potential is unexplained. It seems reasonable to assume that these effects resulted from changes in the structure and/or composition of the film during cathodic polarization, but the nature of these changes is unknown.

9. Polarization Behavior in 0.1N HCl and in 0.1M KCl, pH 8.66, U-7.5Nb-2.5Zr

Major results of these experiments are shown graphically in Figs. 34-37. Both specimens were coated with an air-formed film when immersed in the test solutions.

The anodic polarization behavior was typical of that expected with pitting in solutions containing chloride. However, the attack was in the nature of localized shallow attack rather than deep pitting.

The appearances of the films on those surfaces which did not undergo localized attack were not changed by the anodic or cathodic polarization in HCl. In the 0.1M KCl, pH 8.66, the films adjacent to the corroded areas exhibited temper colors.

The cathodic polarization data in Fig. 36, points 13 to 17, indicate that most of the H^+-reduction took place on the corroded surfaces. Accordingly, they also indicate a very low overvoltage for H^+-reduction on these surfaces. Thus, assuming that all H^+-reduction took place on the estimated 5 to 10% of the surface which had undergone localized attack, the extrapolated overvoltage at -1 ma/cm^2 would be about -300 mv. This compares with values of -450 to -500 mv for film-free specimens in 1N H_2SO_4.

An important conclusion which can be drawn from these and previous experiments with chloride is that the film can be protected from Cl^--attack by maintaining a sufficiently low potential. With $< 0.1M\ Cl^-$, the film on unstressed specimens would not be attacked at potentials <-325 mv (SCE). Stressed specimens may act differently, but this point was not investigated.

References

1. T. R. Beck, "Electrochemical Aspects of Titanium Stress Corrosion Cracking," Proc. of Conference on Fundamental Aspects of Stress Corrosion Cracking," R. W. Staehle, Ed., Nat. Ass. Corr. Engr., Houston, Texas, 1969, p. 605.

2. C. M. Chen, F. H. Beck and M. G. Fontana, "Stress Corrosion Cracking of Ti-8Al-1Mo-1V Alloy," Corrosion, 26, 135 (1970).

3. L. E. Kindlimann and N. D. Greene, "Dissolution Kinetics of Nuclear Fuels, 1. Uranium," Corrosion, 23, 29 (1970).

4. L. E. Kindlimann and N. D. Greene, "Mechanism of the Acid Corrosion Behavior of Neutron Irradiated Uranium," Corrosion, 26, 189 (1970).

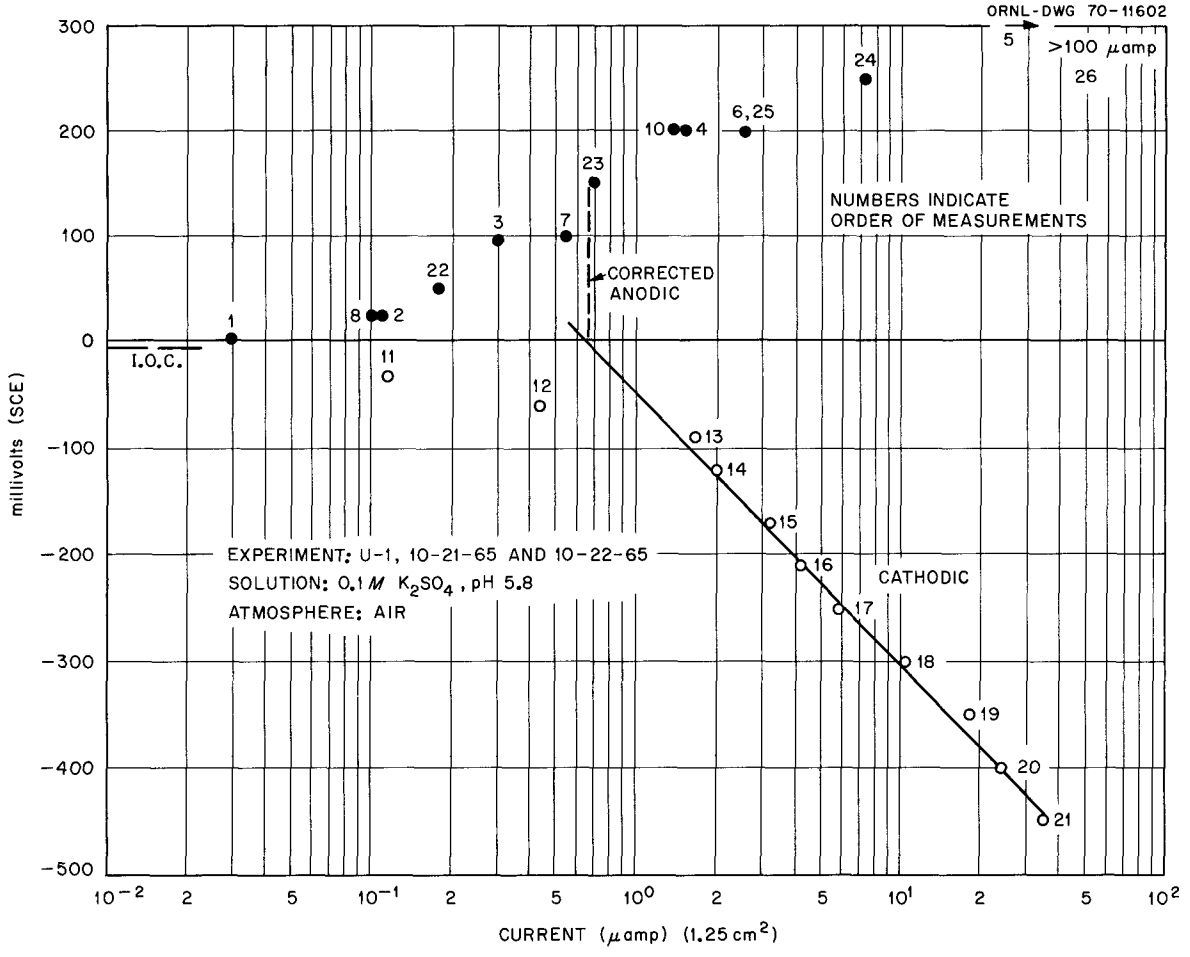

Fig. 1. Polarization of Uranium in K_2SO_4

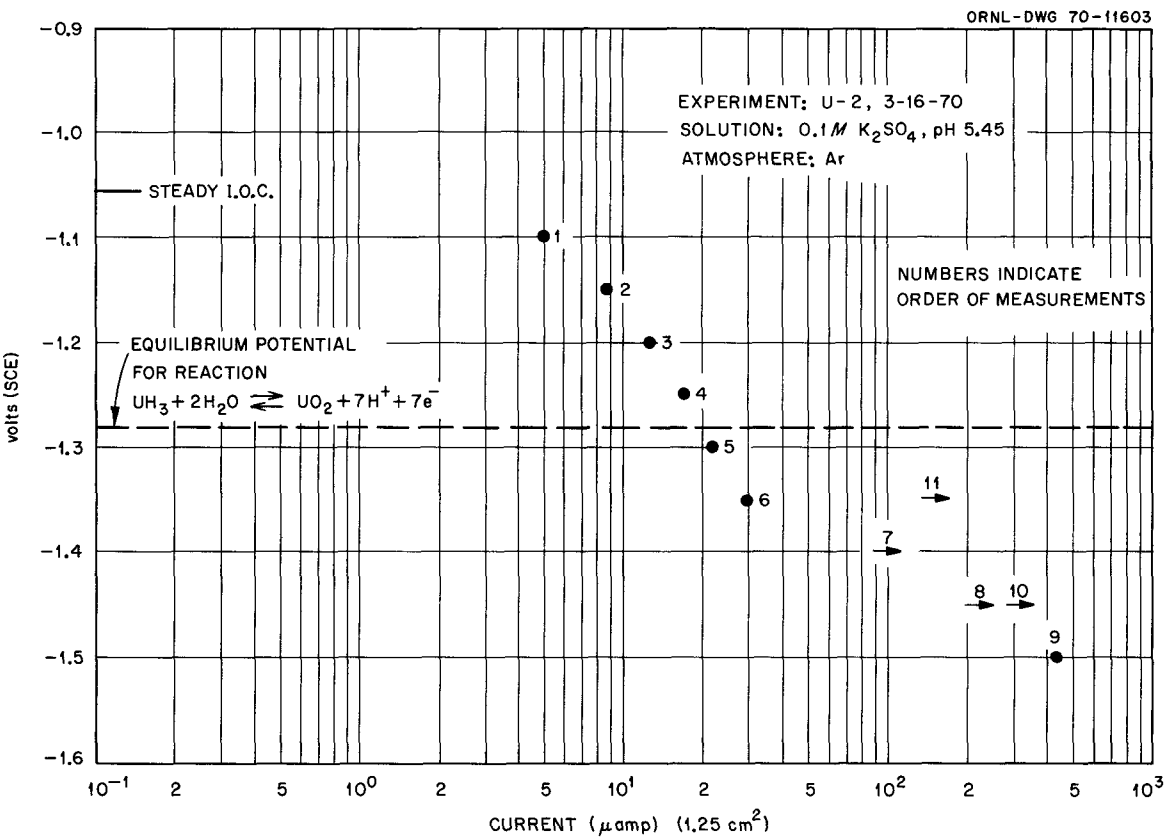

Fig. 2. Cathodic Polarization of Uranium in K_2SO_4

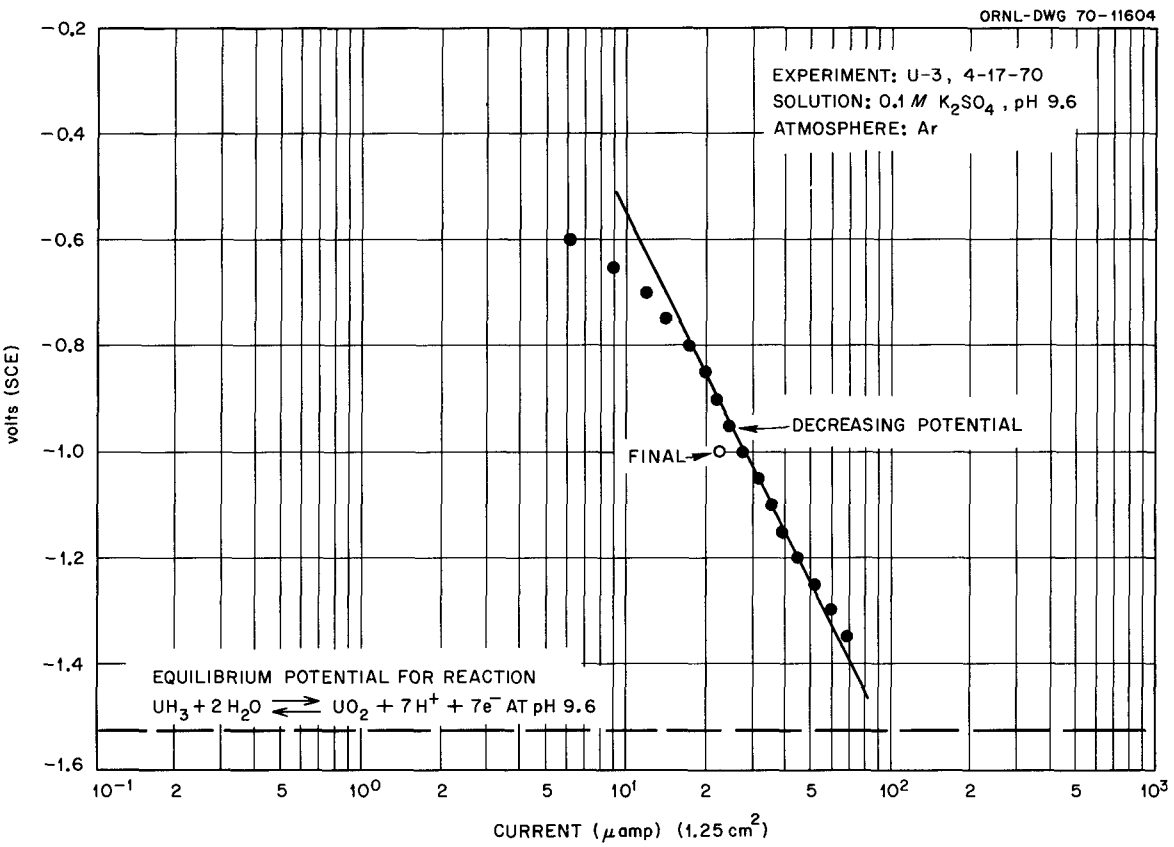

Fig. 3. Cathodic Polarization of Uranium in K_2SO_4

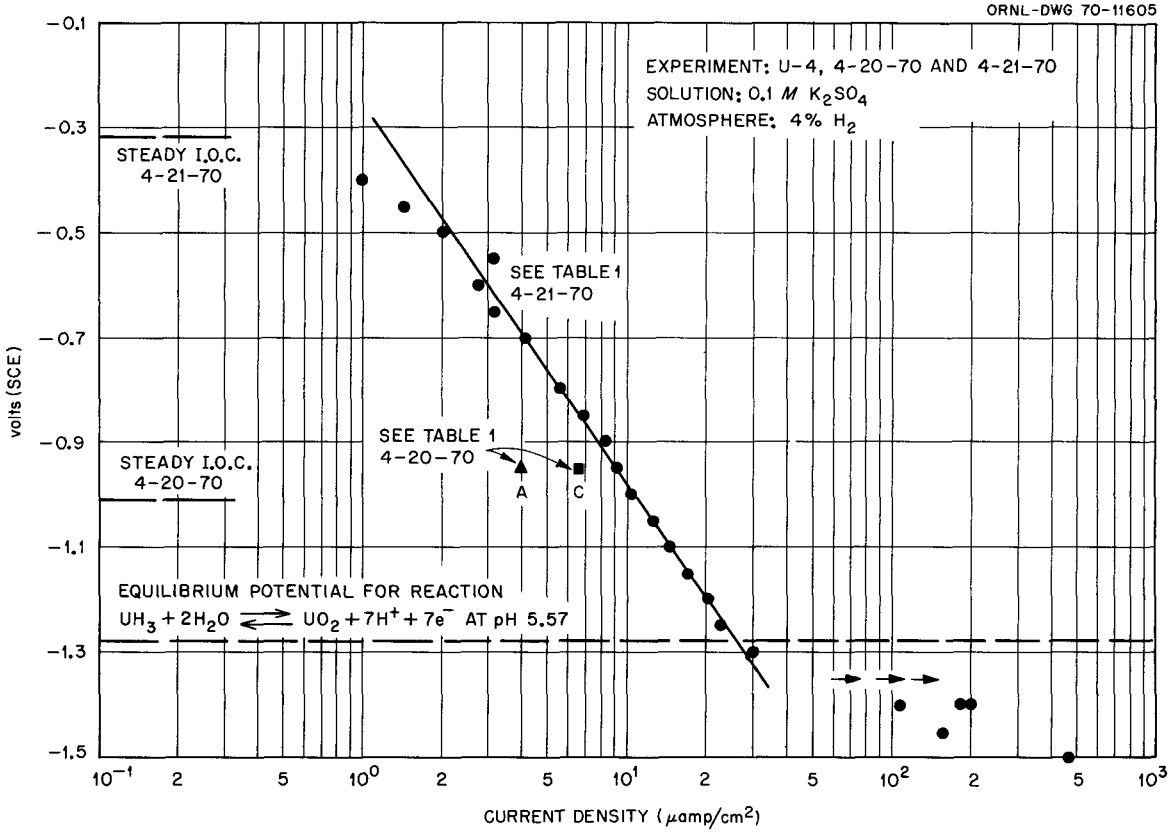

Fig. 4. Anodic and Cathodic Polarization of Uranium in K_2SO_4

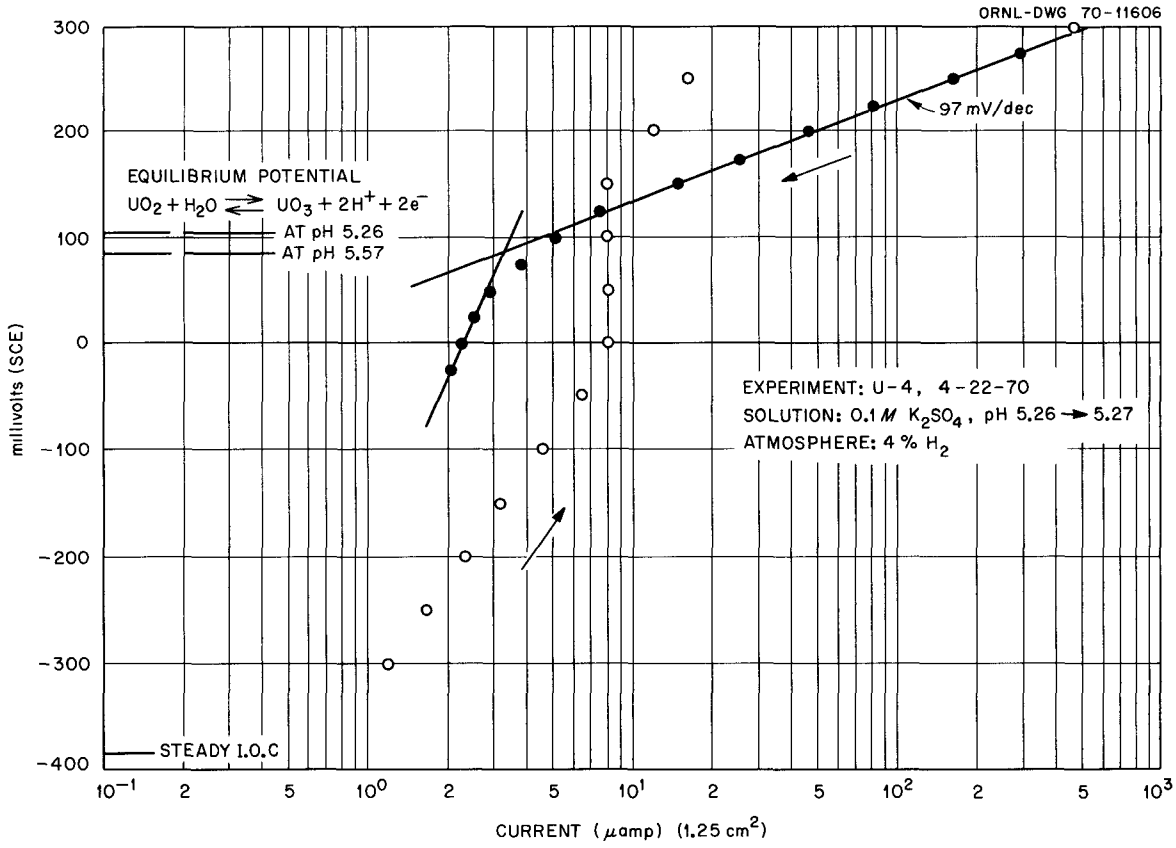

Fig. 5. Anodic Polarization of Uranium in K_2SO_4

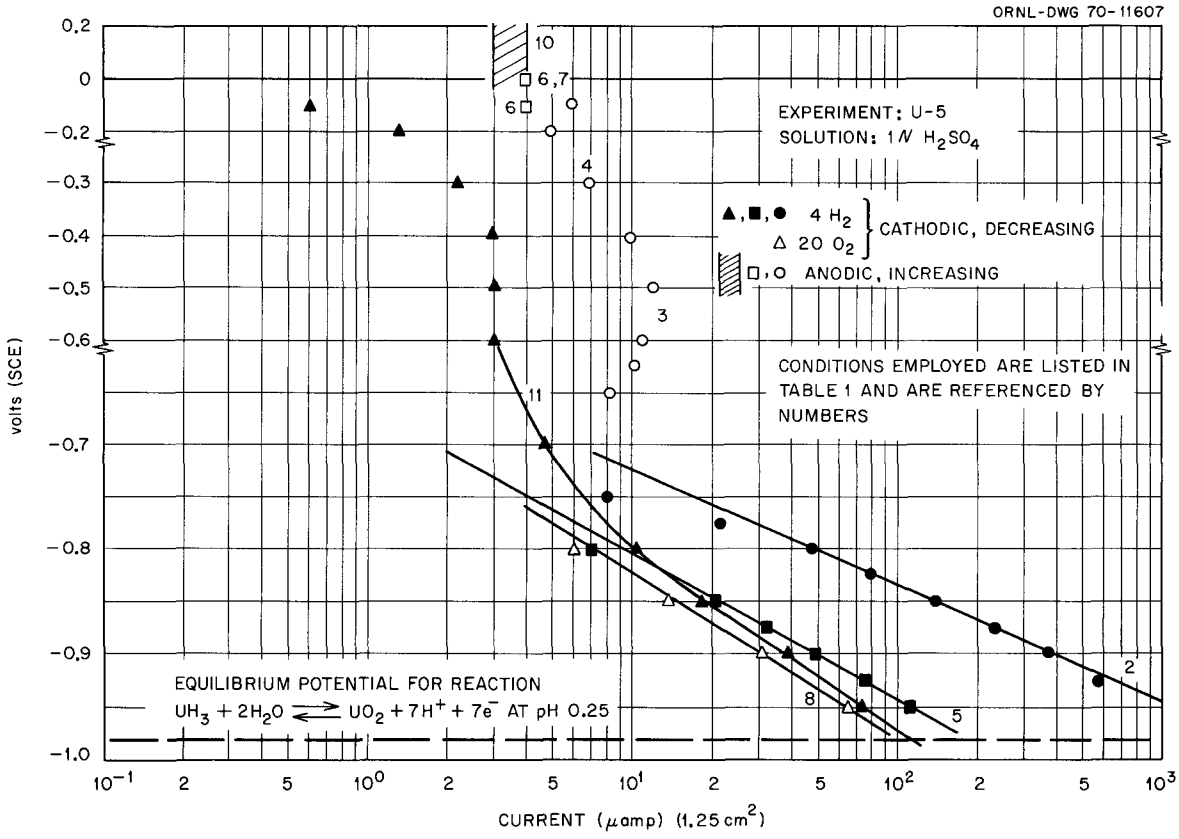

Fig. 6. Anodic and Cathodic Polarization of Uranium in H_2SO_4

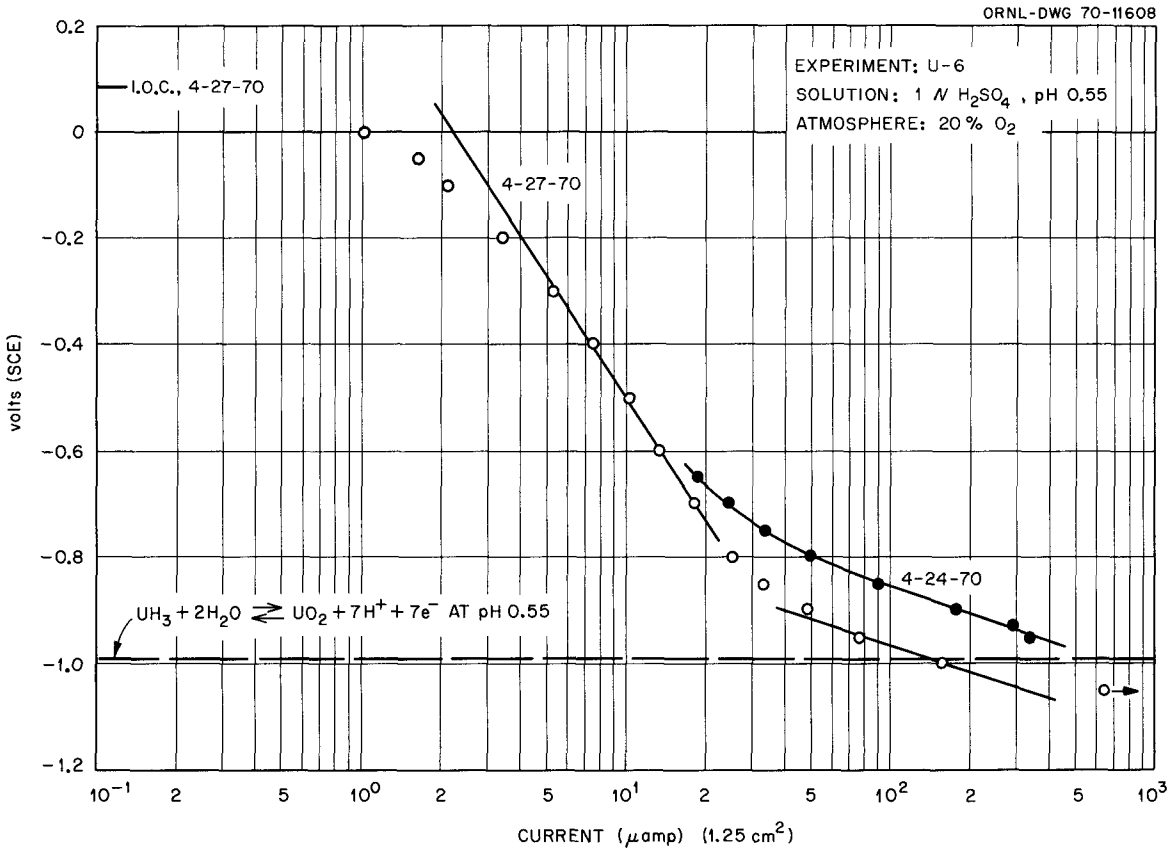

Fig. 7. Cathodic Polarization of Uranium in H_2SO_4

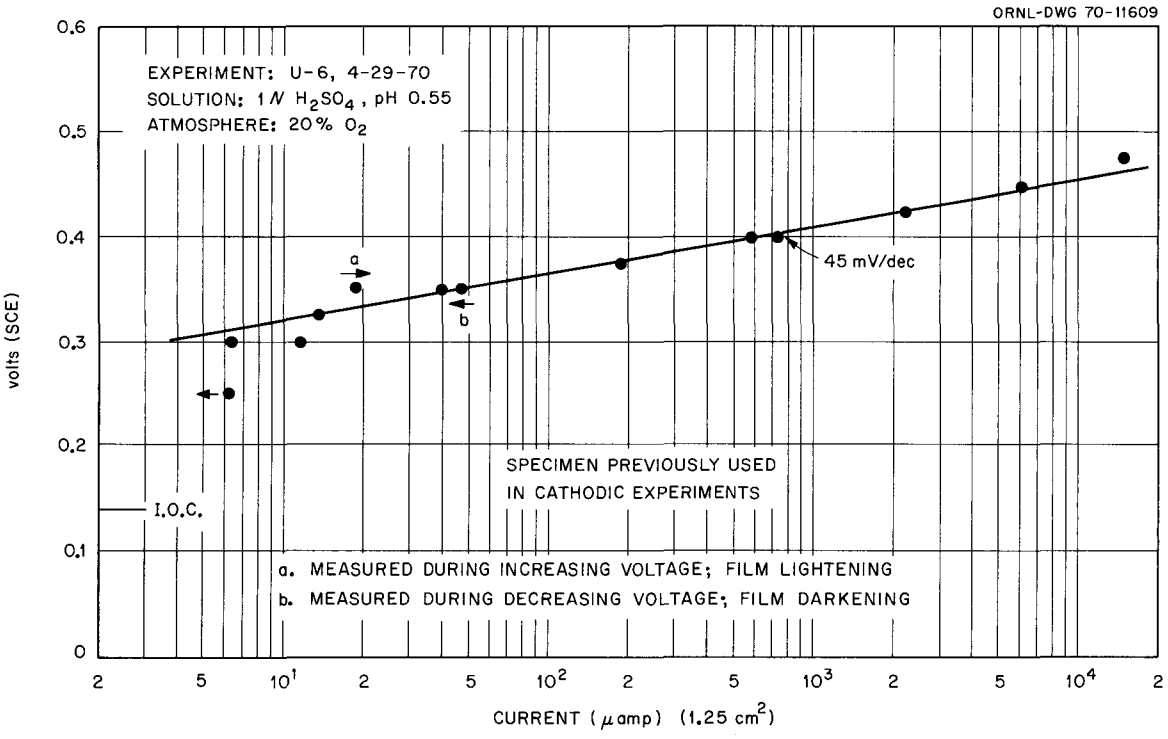

Fig. 8. Anodic Polarization of Uranium in H_2SO_4

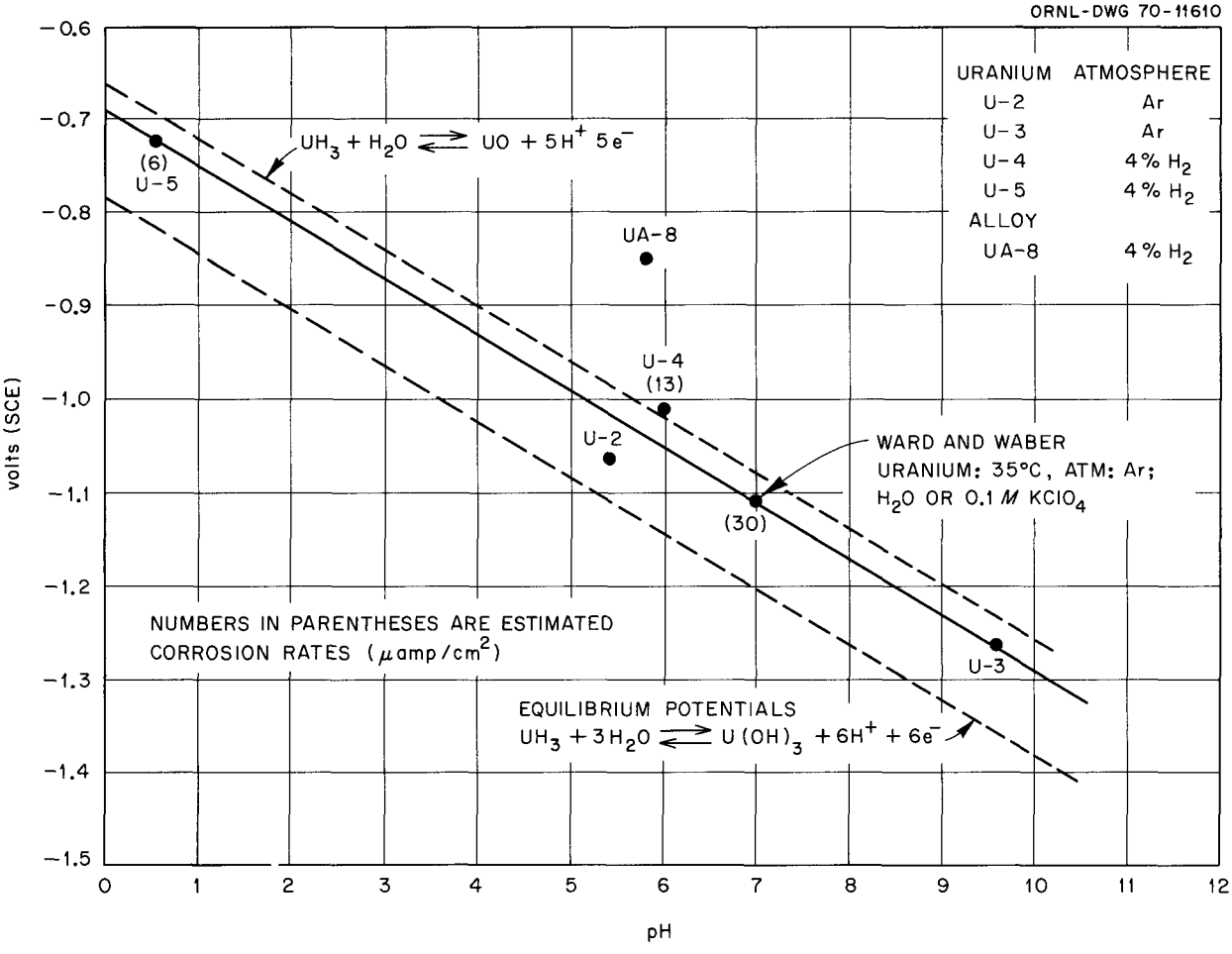

Fig. 9. Open Circuit Potentials vs pH for Uranium

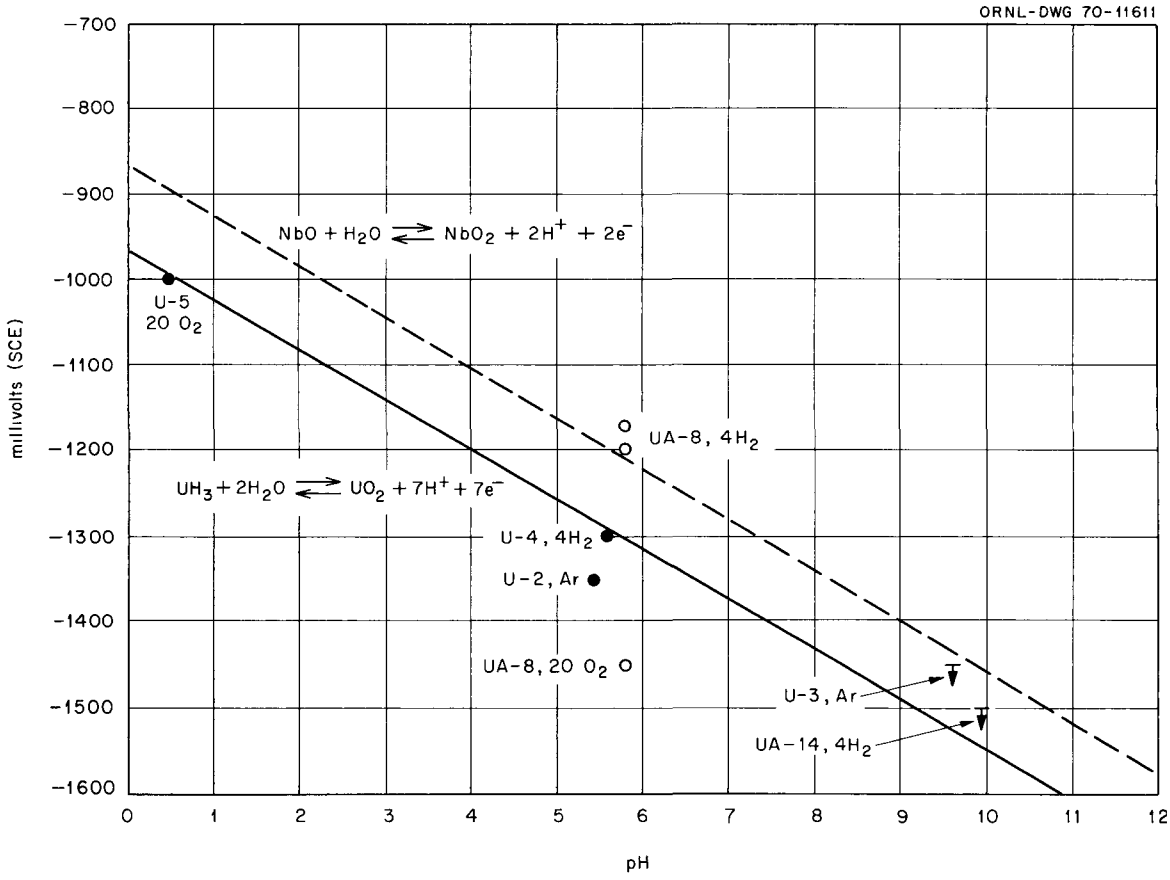

Fig. 10. Potential of Transition to High Cathodic Currents

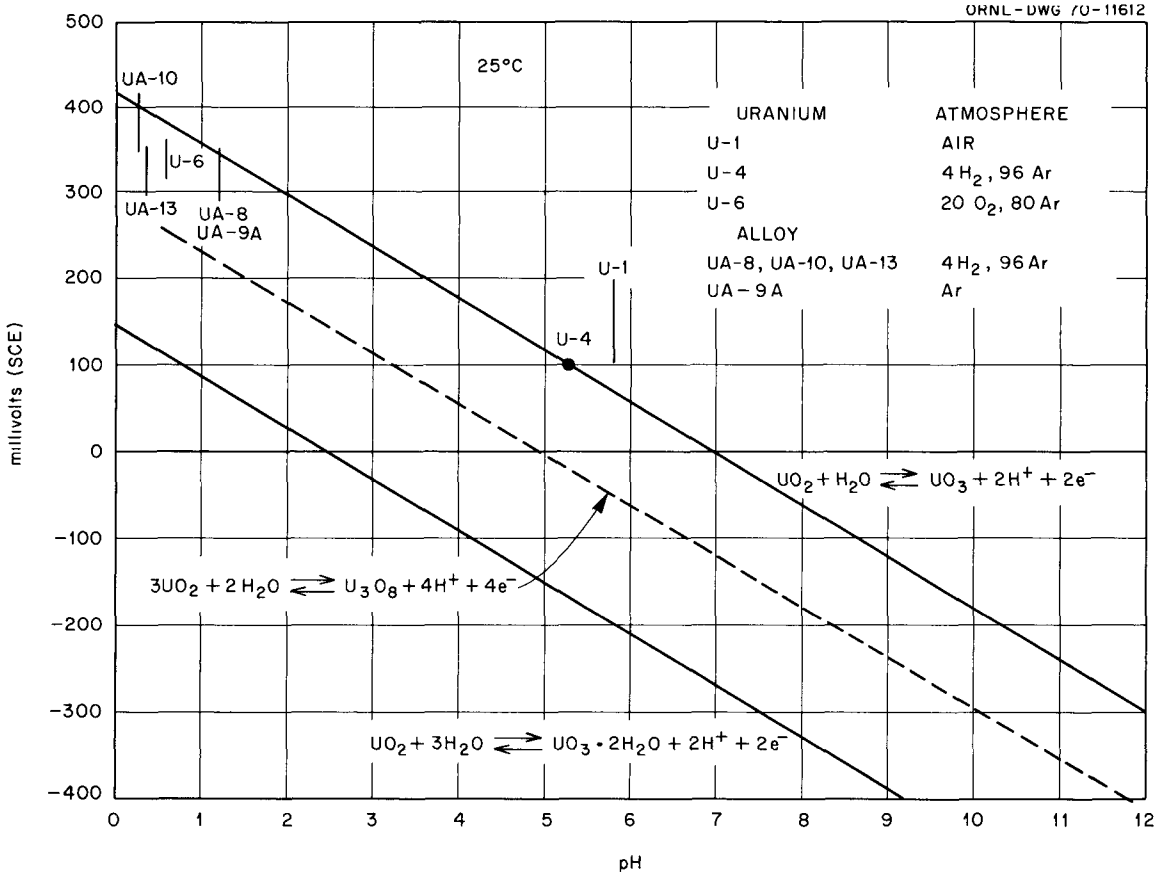

Fig. 11. Transpassive Potential vs pH

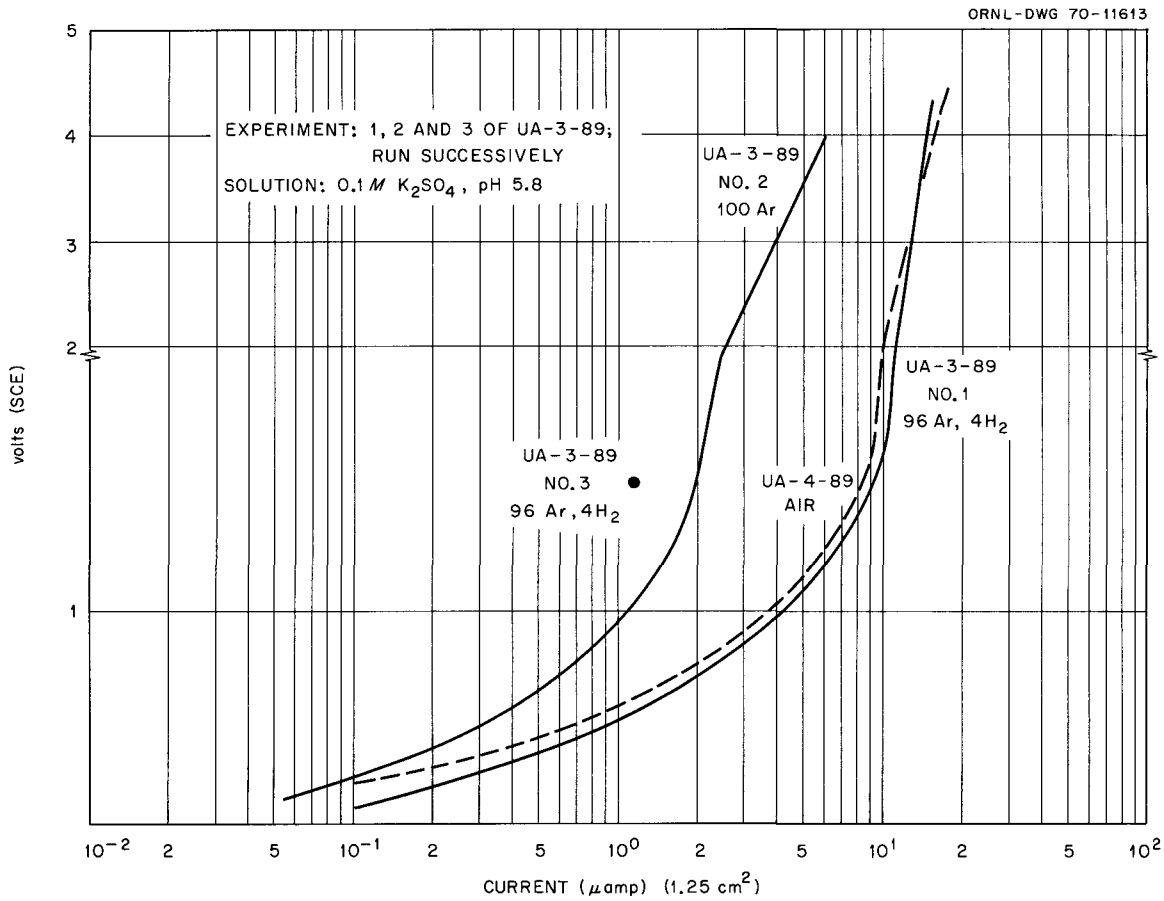

Fig. 12. Anodic Polarization of Alloy in K_2SO_4, No Prior Cathodic Polarizations

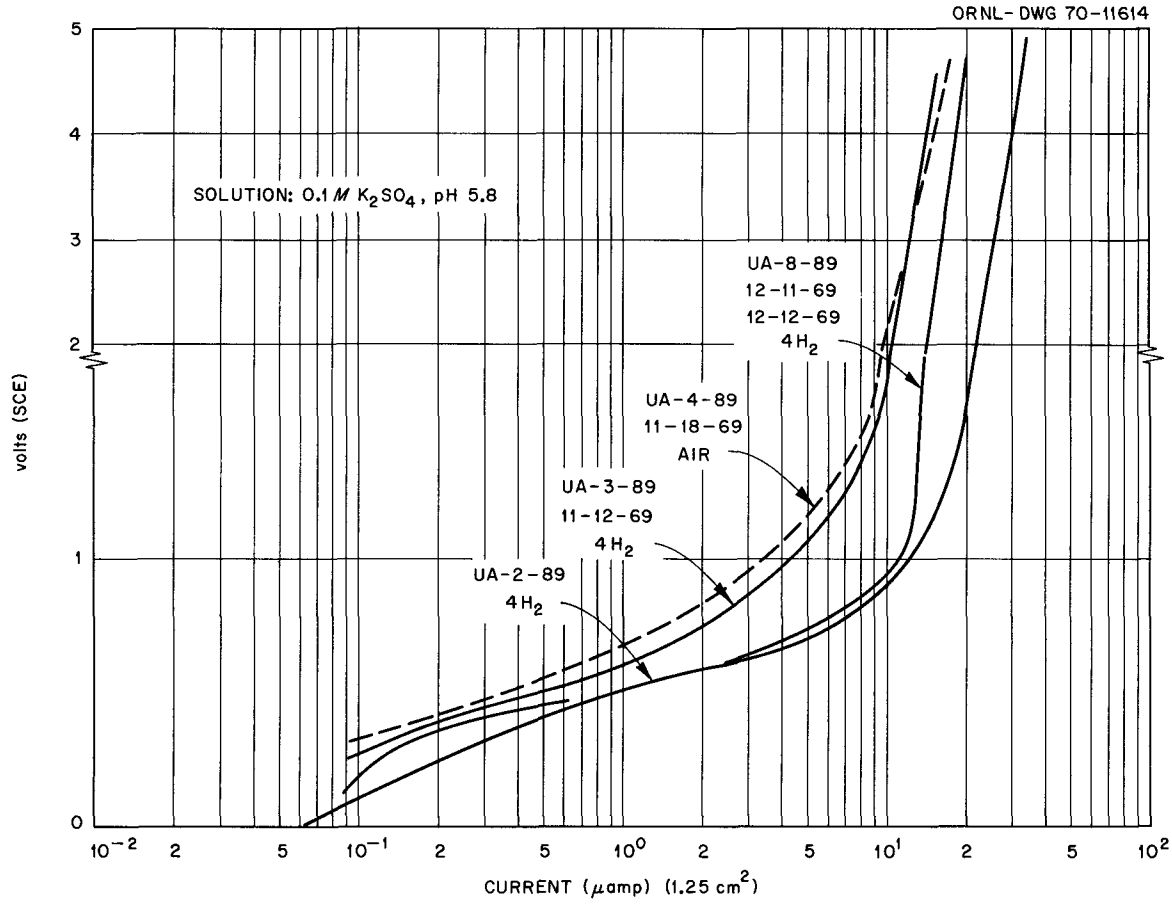

Fig. 13. Anodic Polarization of Alloy in K_2SO_4, No Prior Cathodic Polarizations

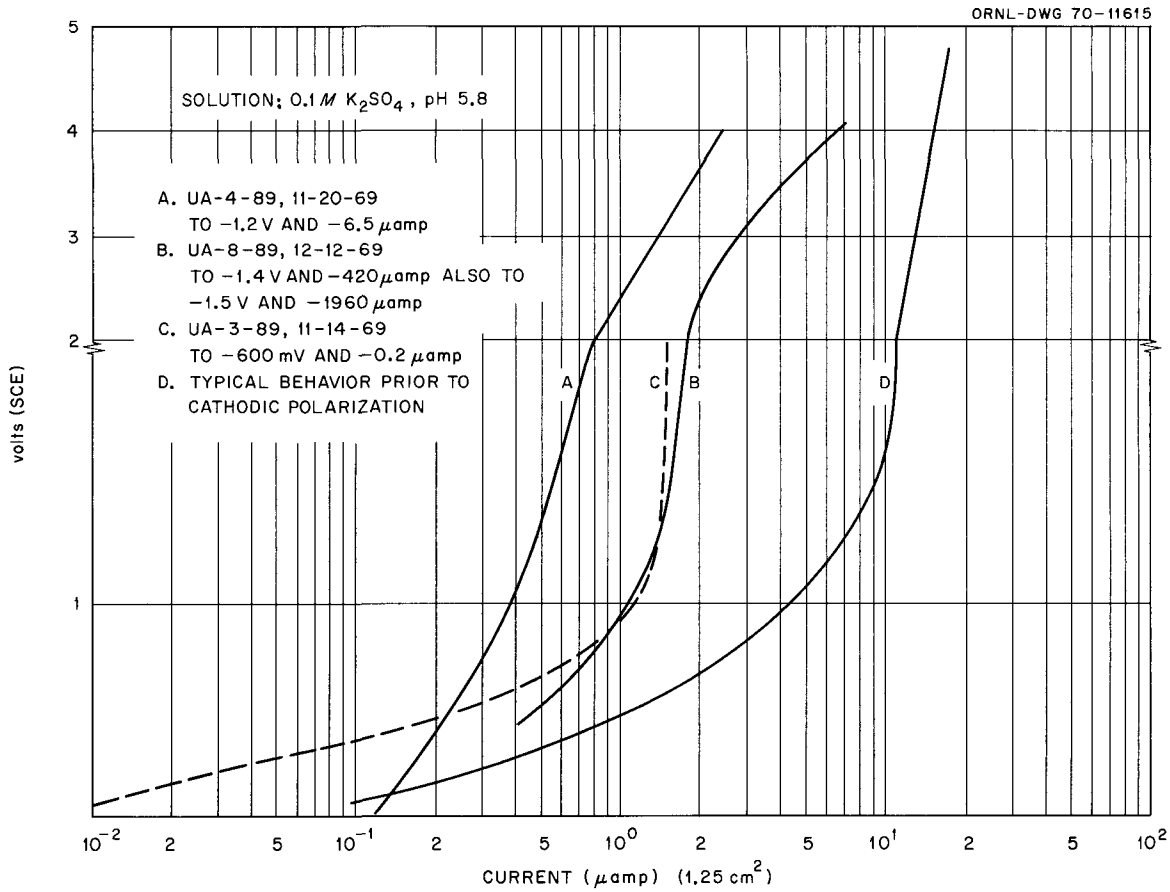

Fig. 14. Effects of Cathodic Polarization of Anodically-Filmed Specimen of Alloy on Subsequent Anodic Behavior; K_2SO_4 Solutions

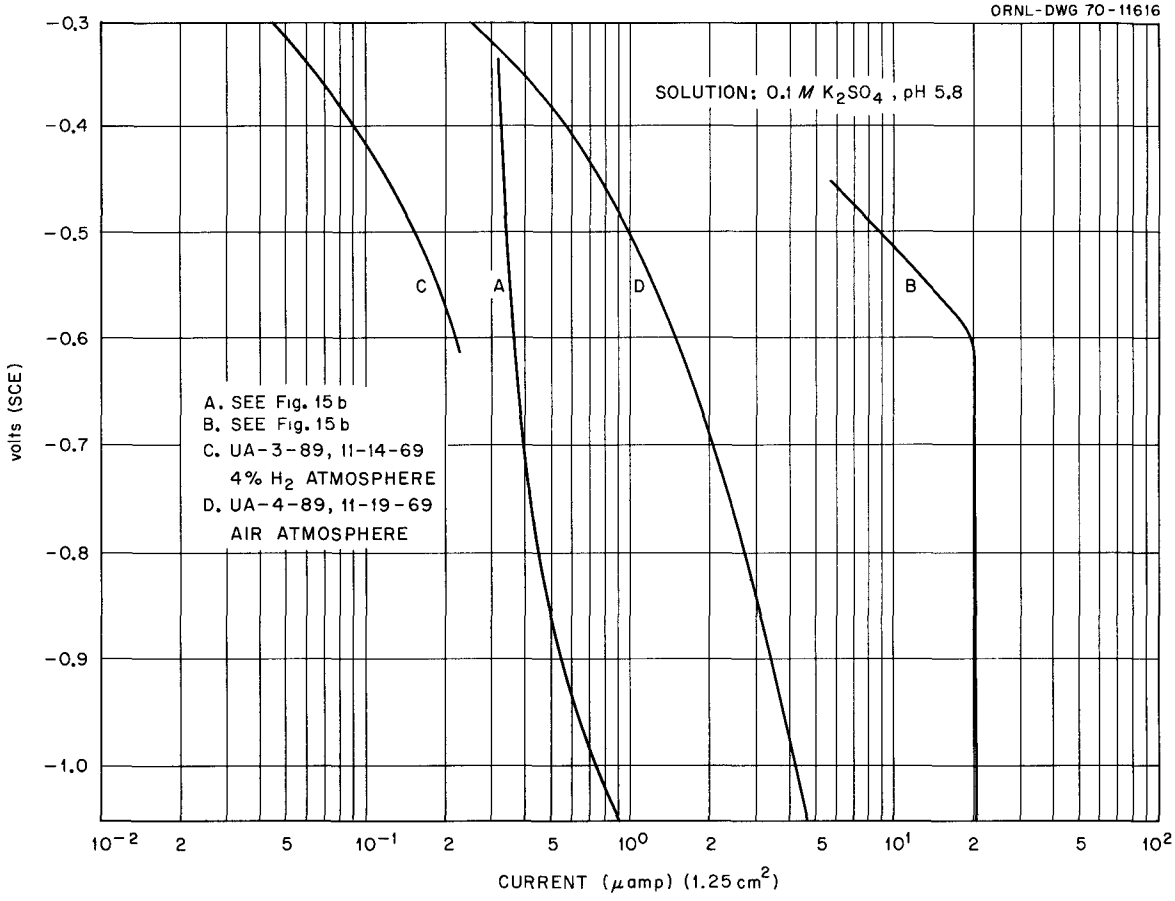

Fig. 15a. Cathodic Polarization of Alloy After Anodization; K_2SO_4 Solutions

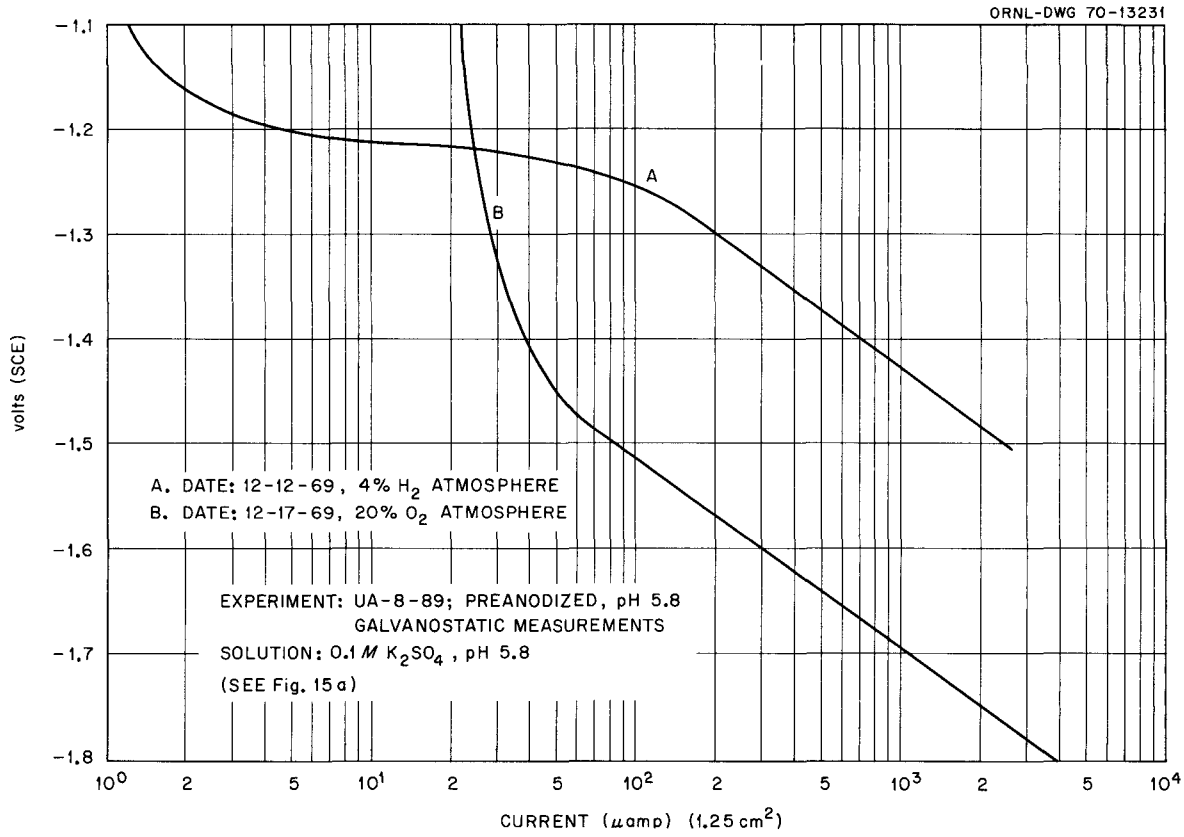

Fig. 15b. Cathodic Polarization of Alloy After Anodization; K_2SO_4 Solutions

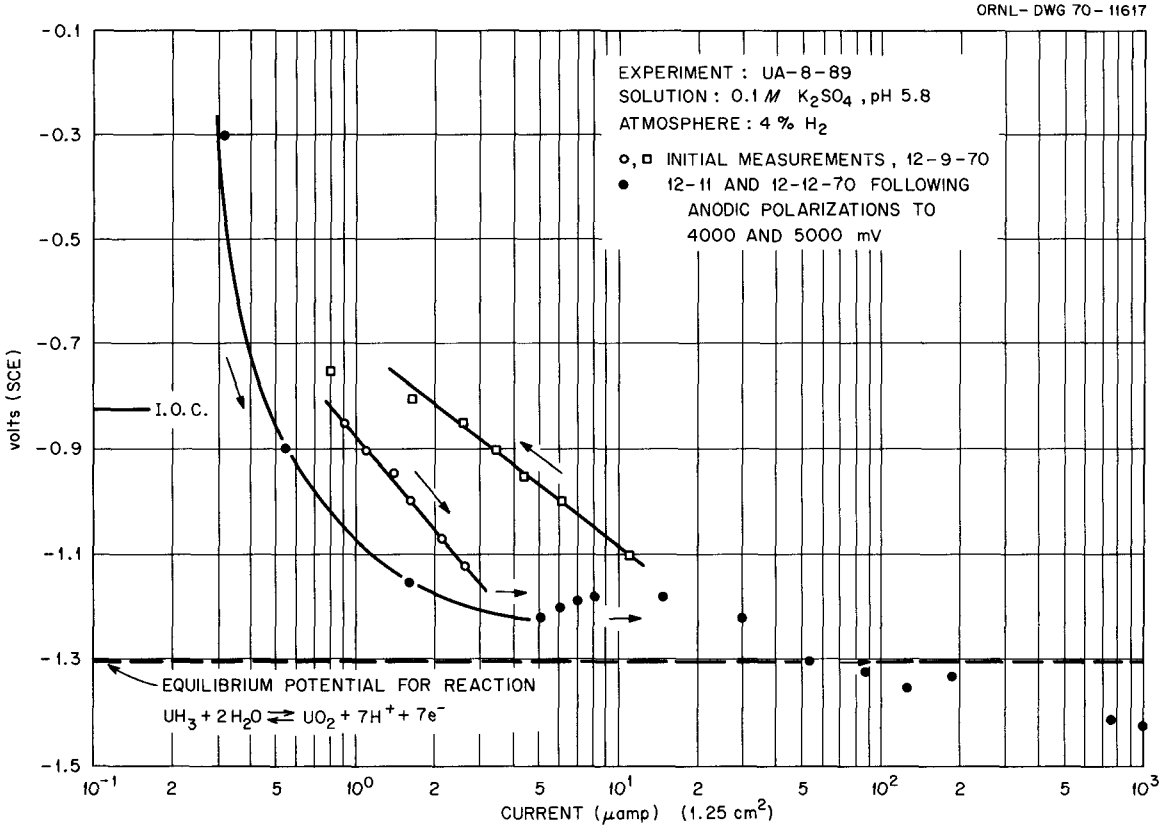

Fig. 16. Cathodic Polarization of Alloy, K_2SO_4 Solutions

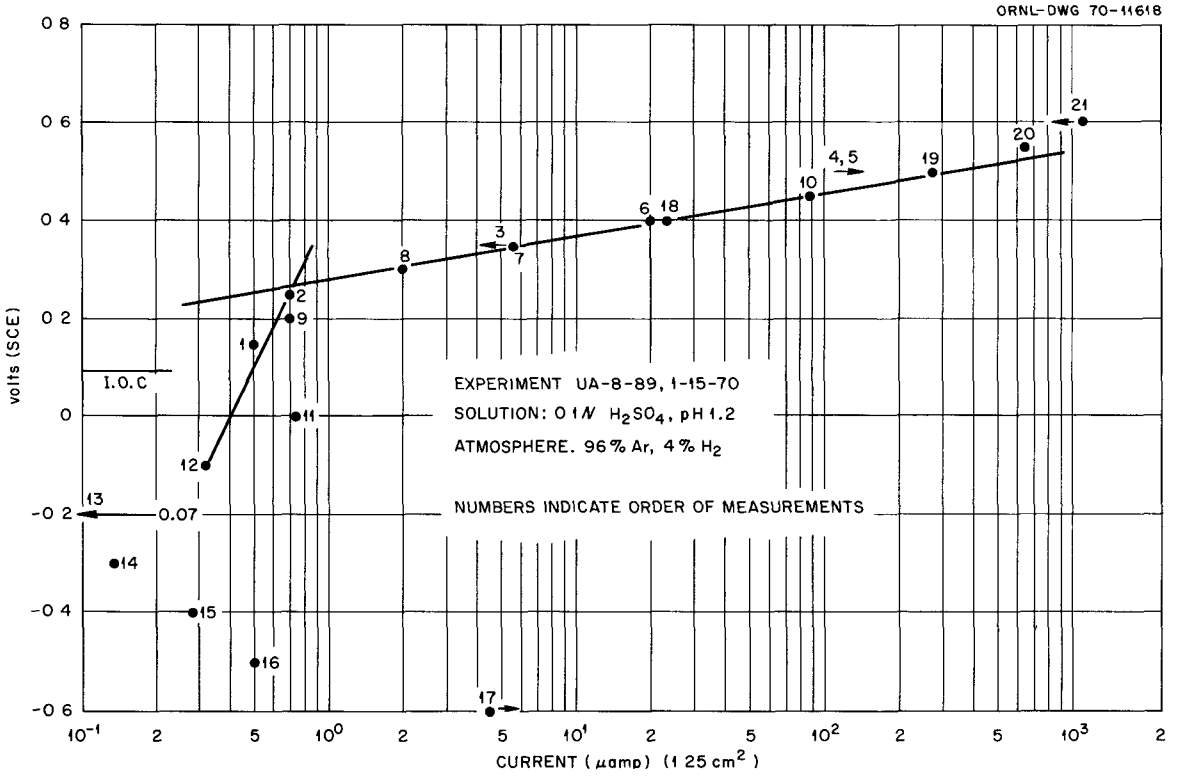

Fig. 17. Polarization of Alloy in 0.1N H_2SO_4

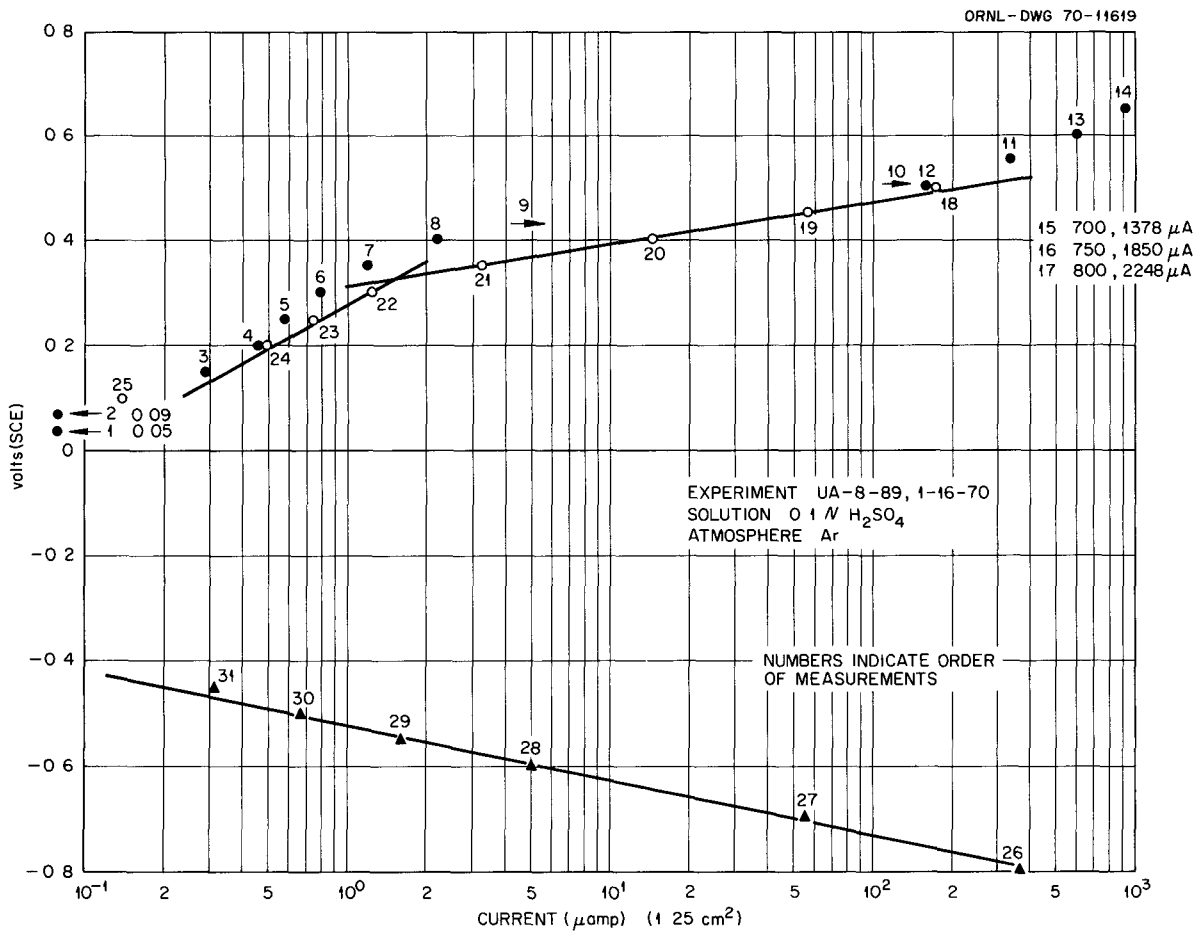

Fig. 18. Polarization of Alloy in 0.1N H_2SO_4

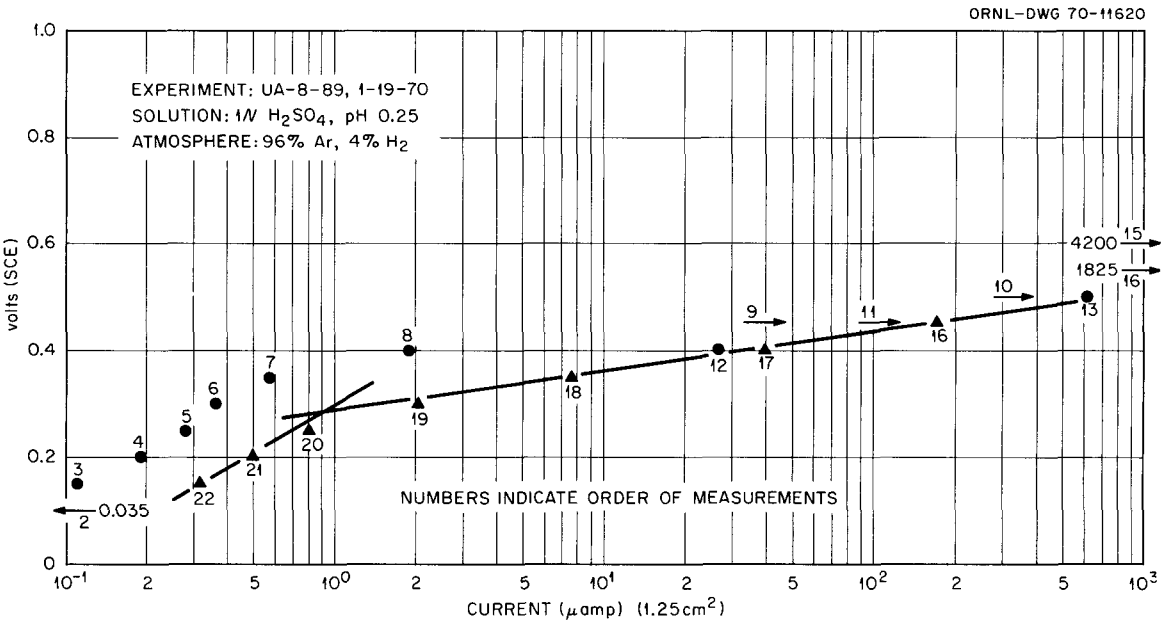

Fig. 19. Polarization of Alloy in 1N H_2SO_4

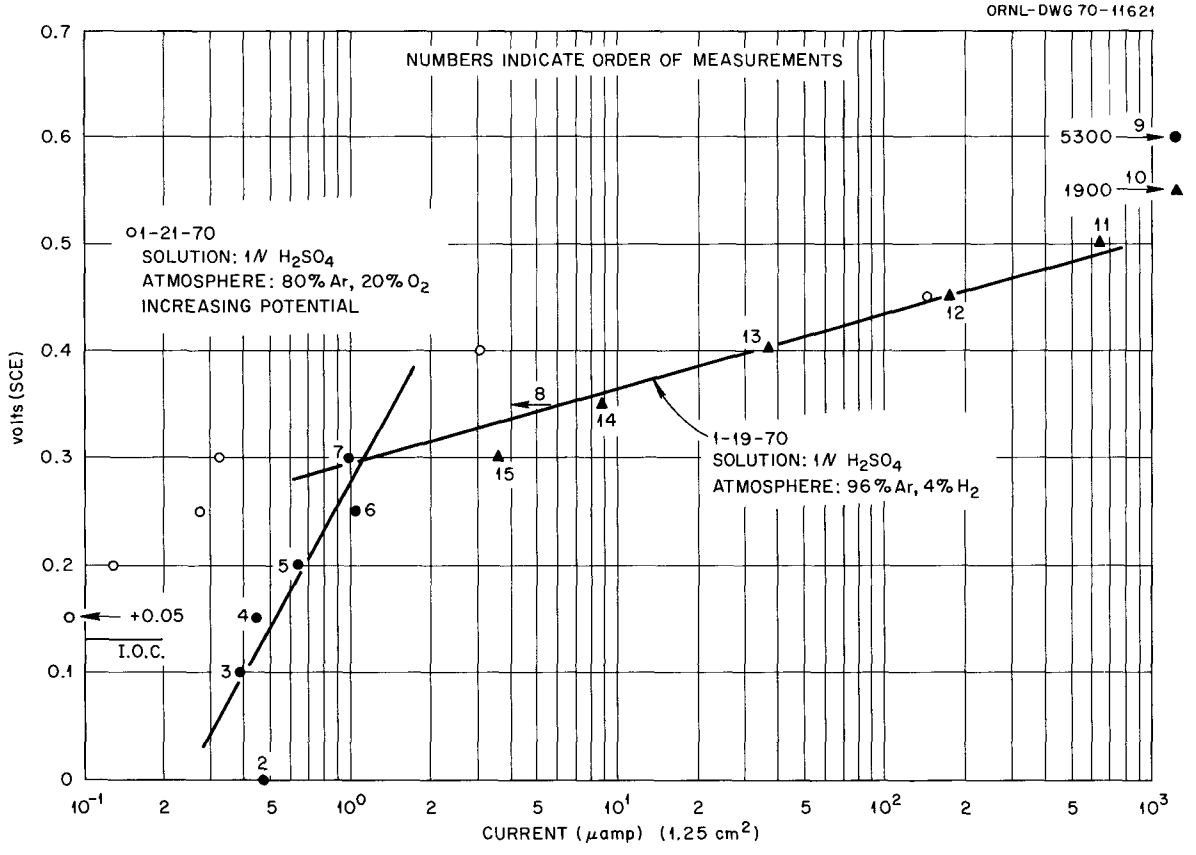

Fig. 20. Polarization of Alloy in 1N H_2SO_4, Experiment UA-11-89

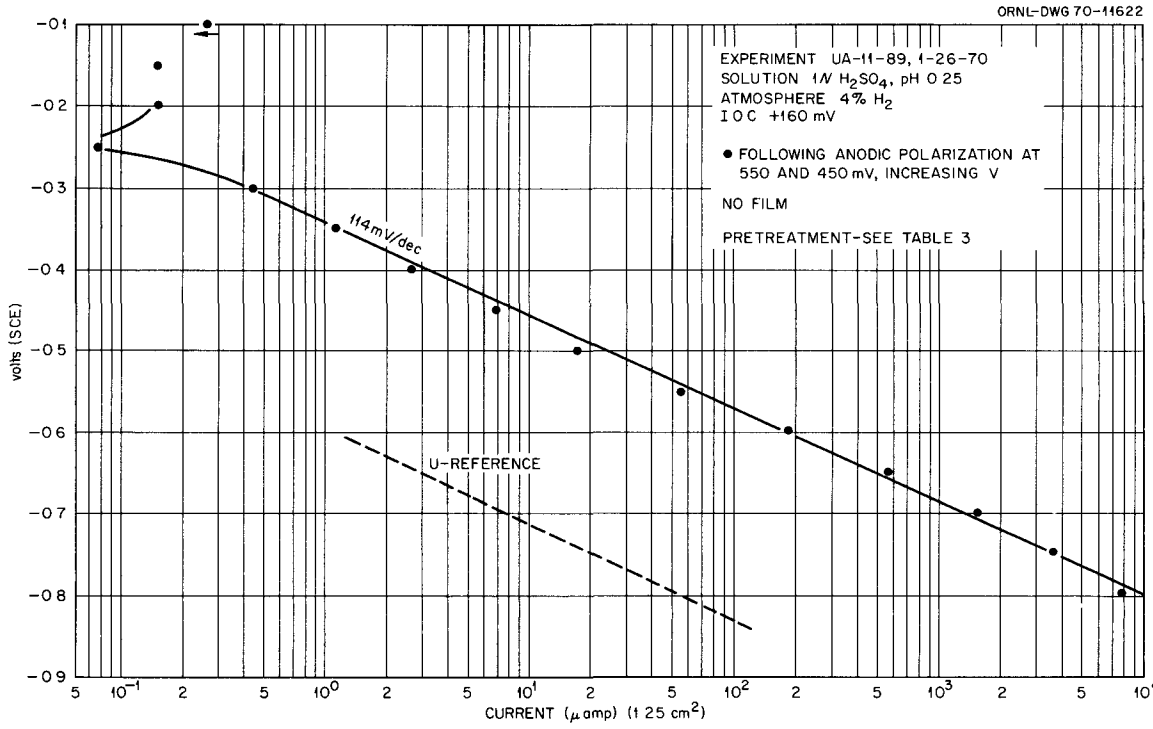

Fig. 21. Cathodic Polarization of Alloy in 1N H_2SO_4, Reduction of H^+

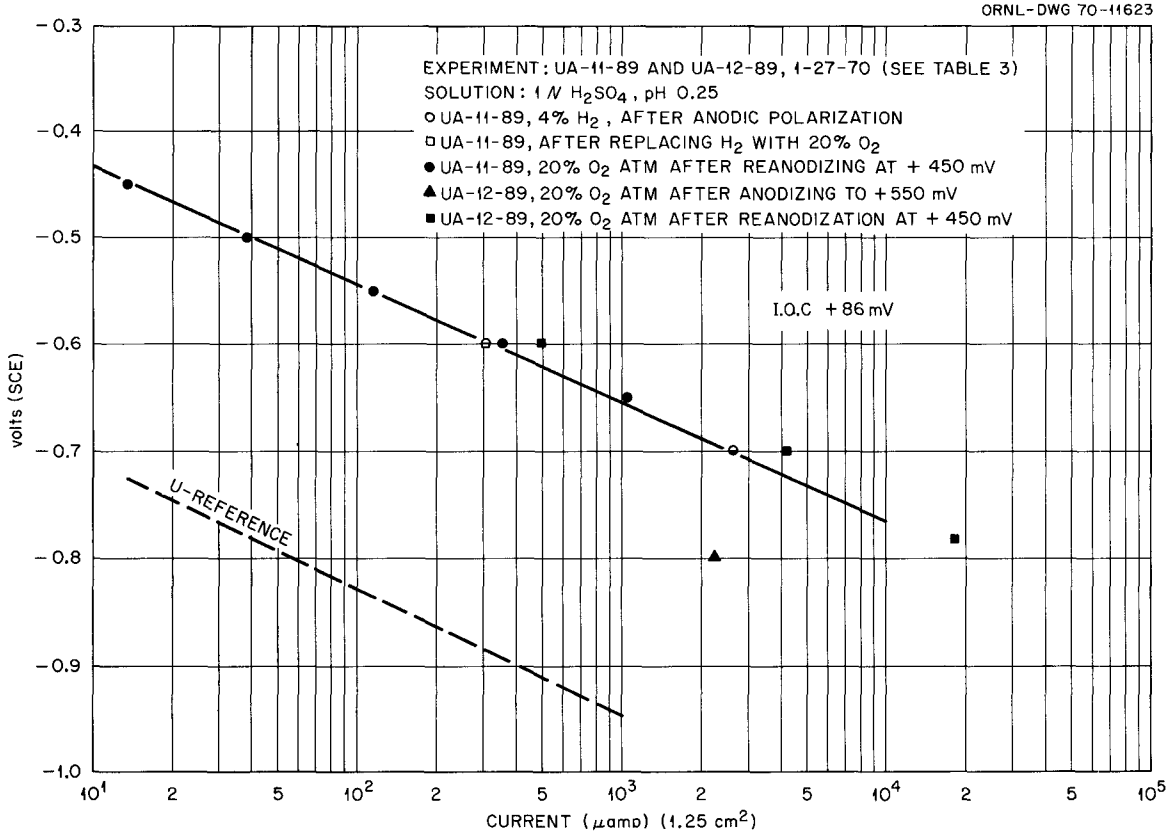

Fig. 22. Cathodic Polarization of Alloy in 1N H_2SO_4

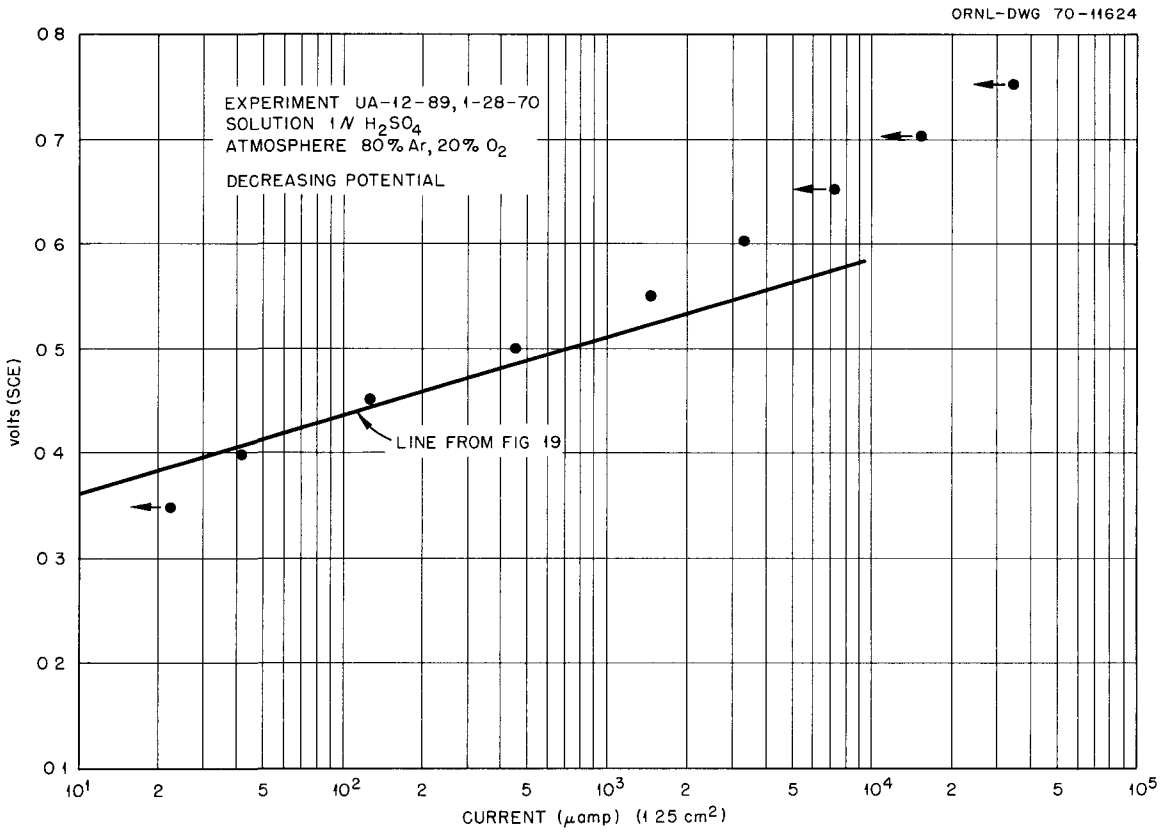

Fig. 23. Anodic Polarization of Alloy in 1N H_2SO_4

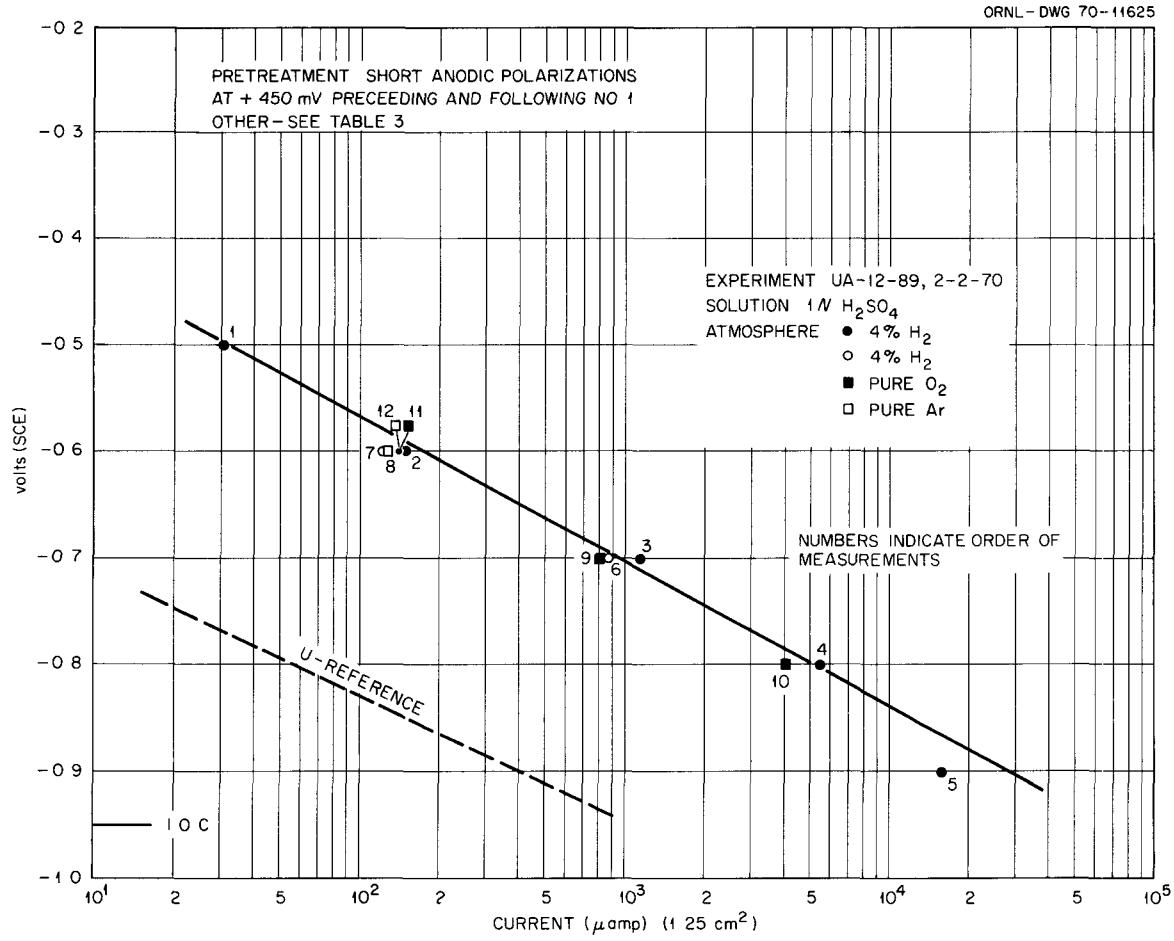

Fig. 24. Cathodic Polarization of Alloy in 1N H_2SO_4

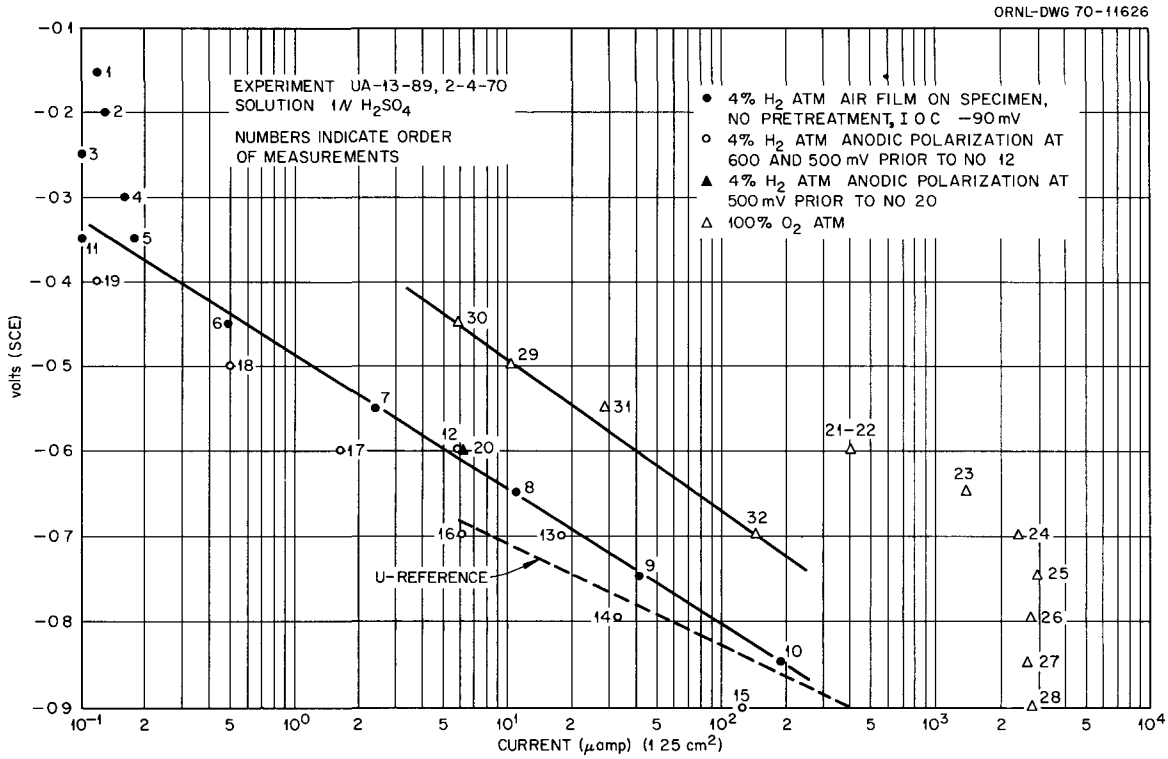

Fig. 25a. Cathodic Polarization of Alloy in 1N H_2SO_4

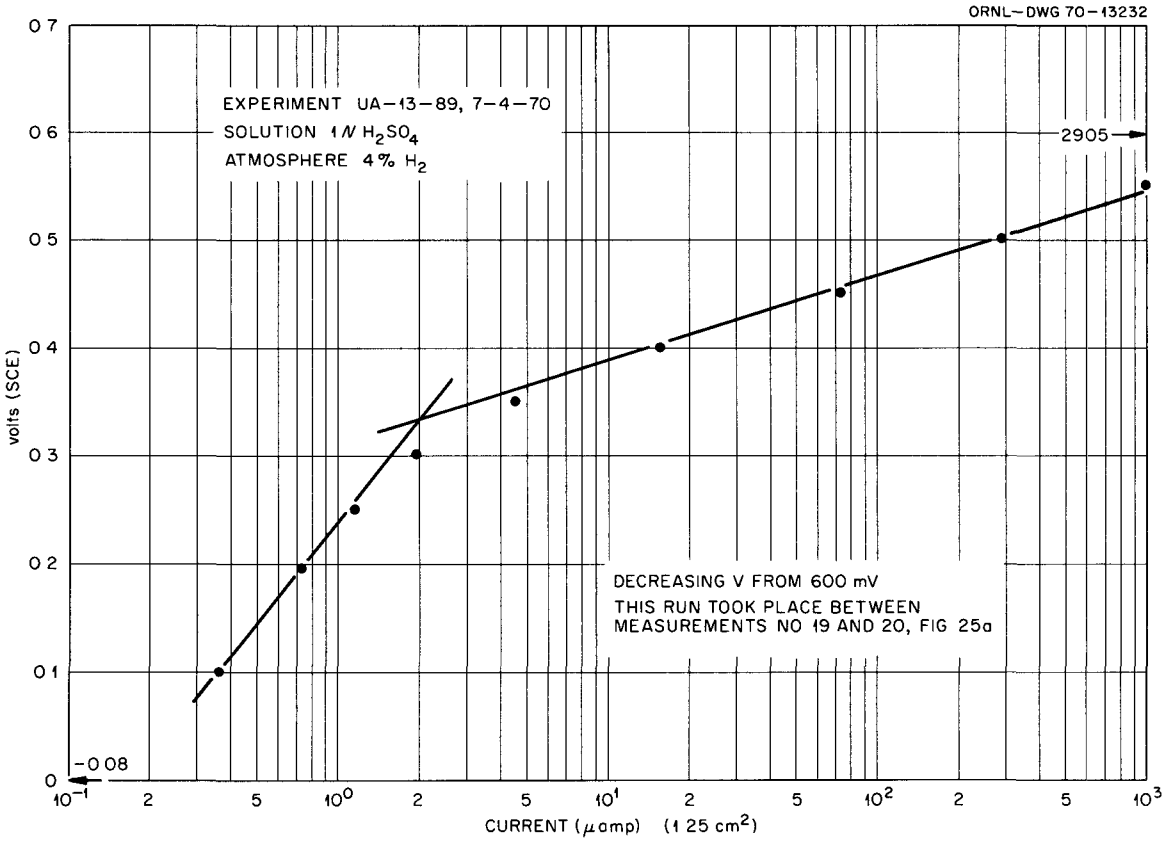

Fig. 25b. Anodic Polarization of Alloy in 1N H_2SO_4

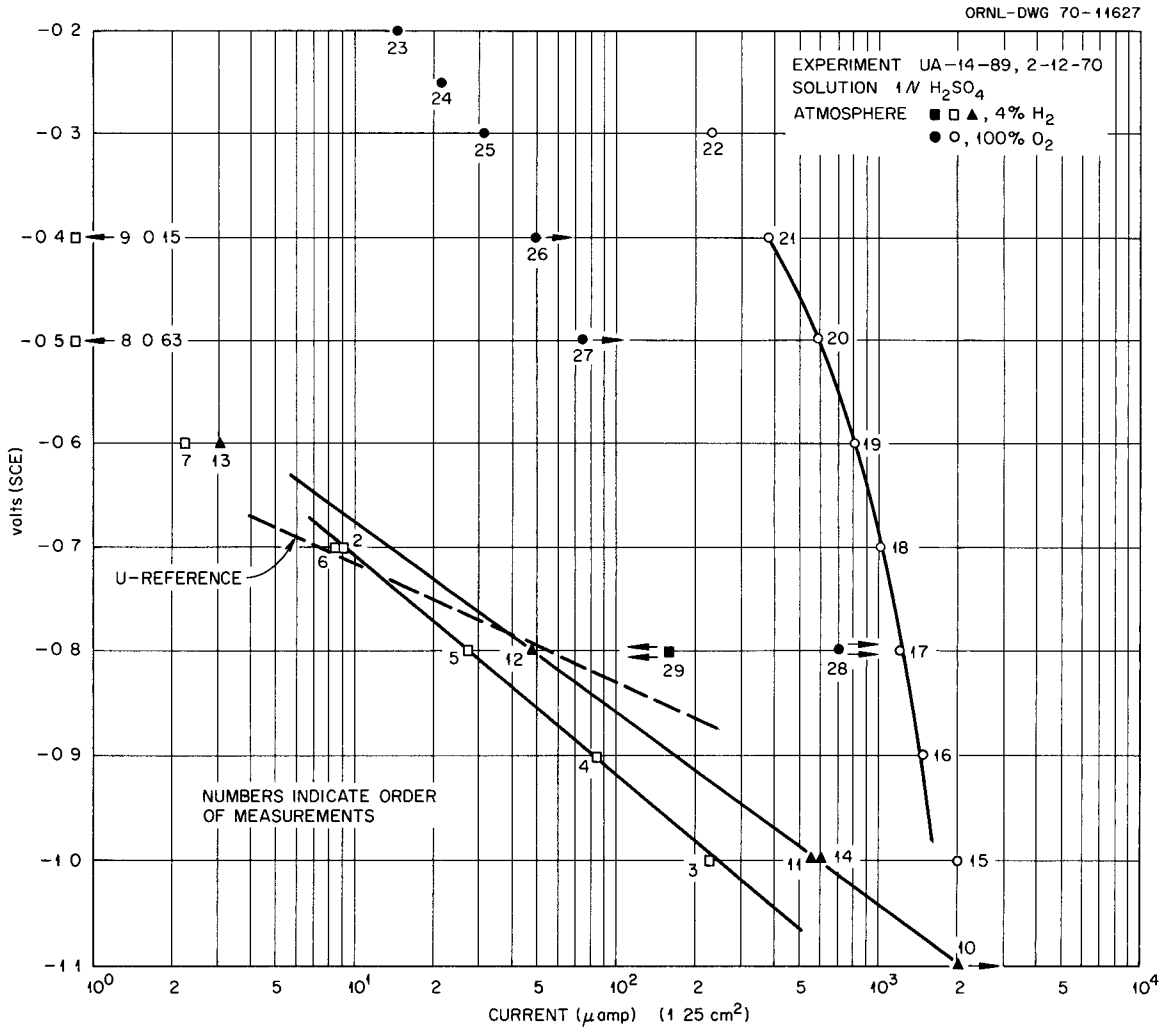

Fig. 26. Cathodic Polarization of Alloy in 1N H_2SO_4

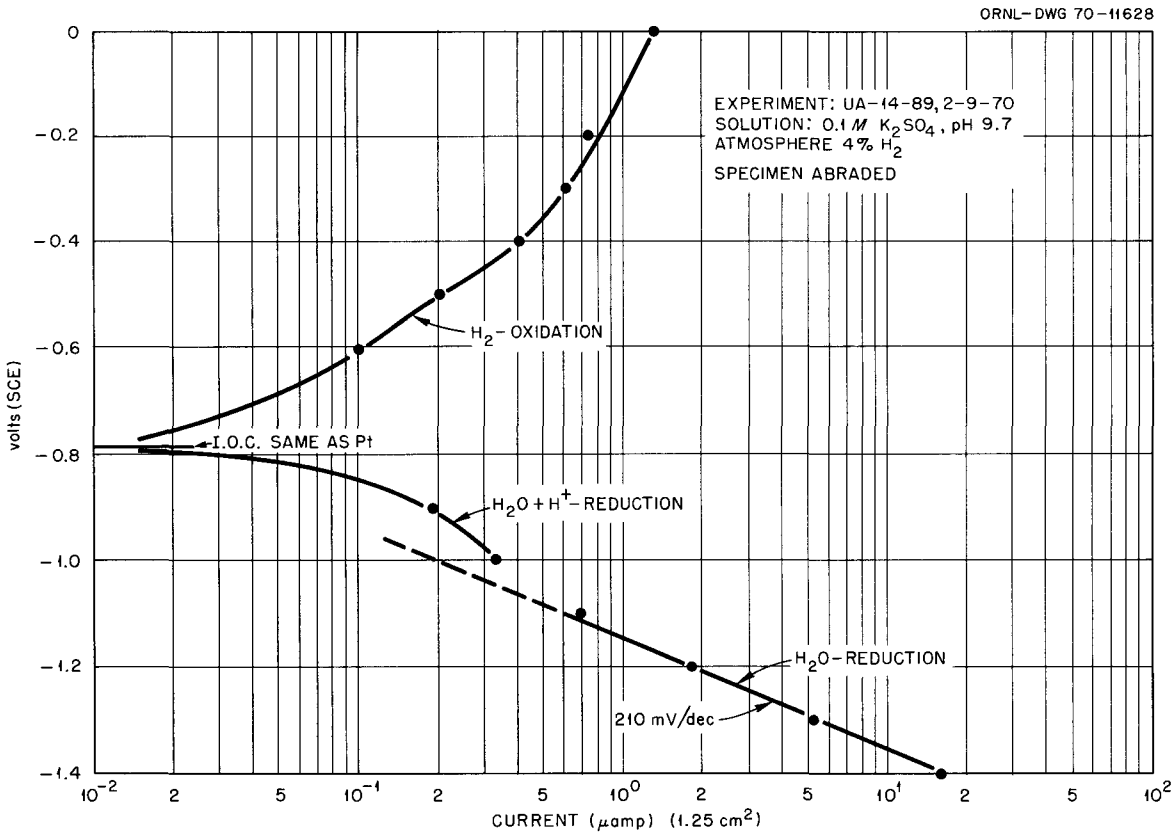

Fig. 27. Polarization of Alloy in K_2SO_4 at pH 9.7

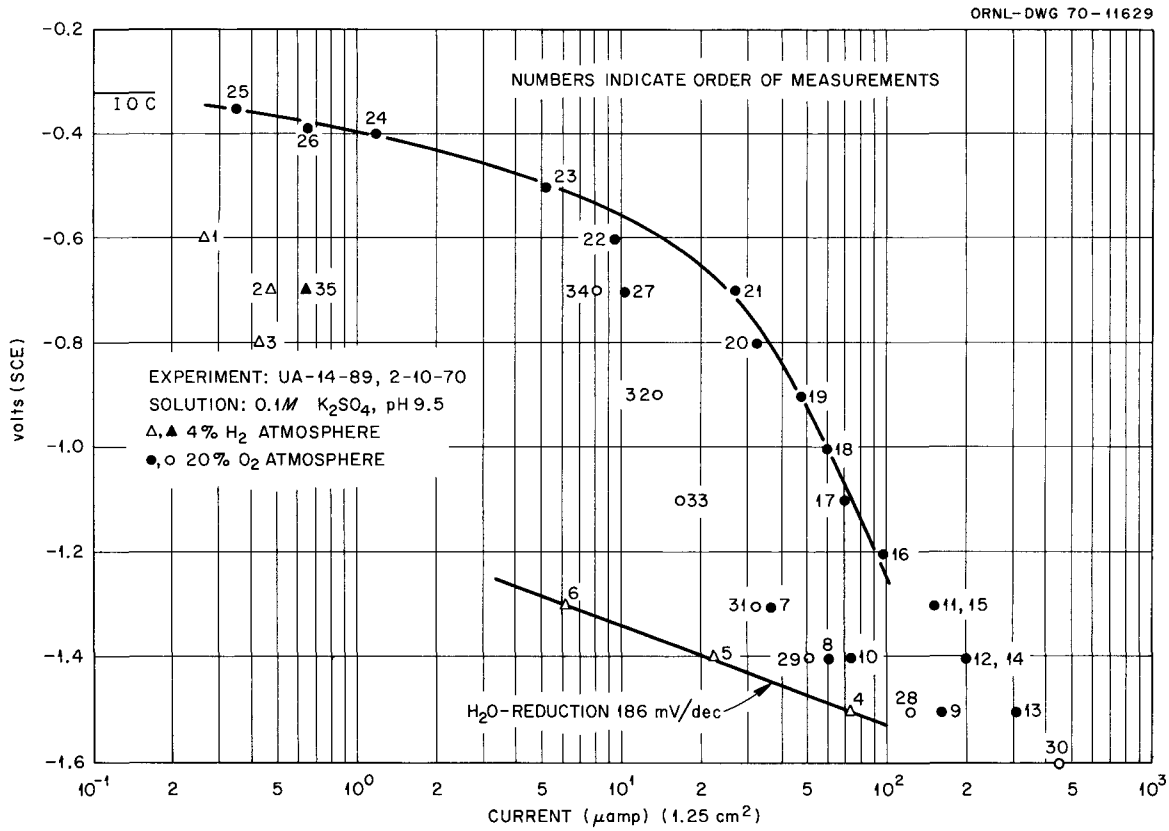

Fig. 28. Reduction of H_2O and O_2 on Alloy in K_2SO_4 at pH 9.5

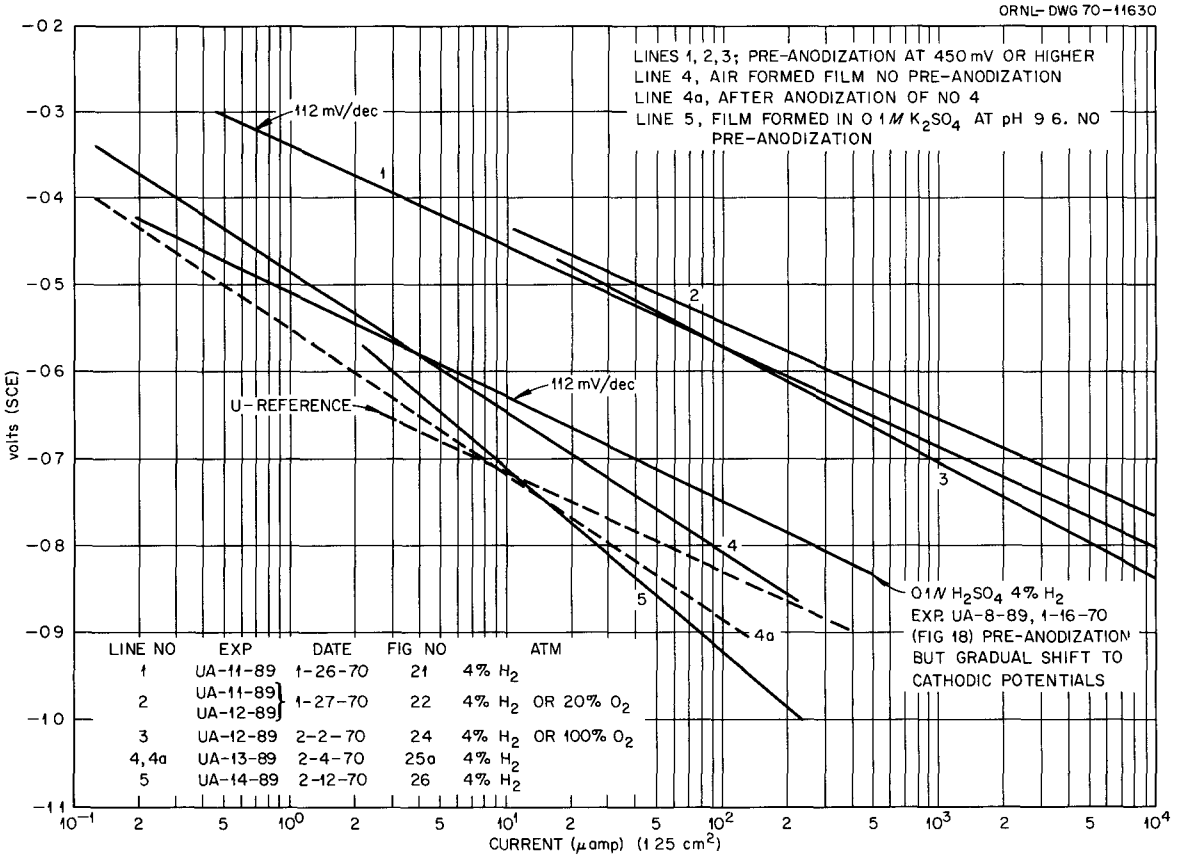

Fig. 29. Comparison Between H^+ Reduction on Alloy in 1N H_2SO_4 in Several Experiments

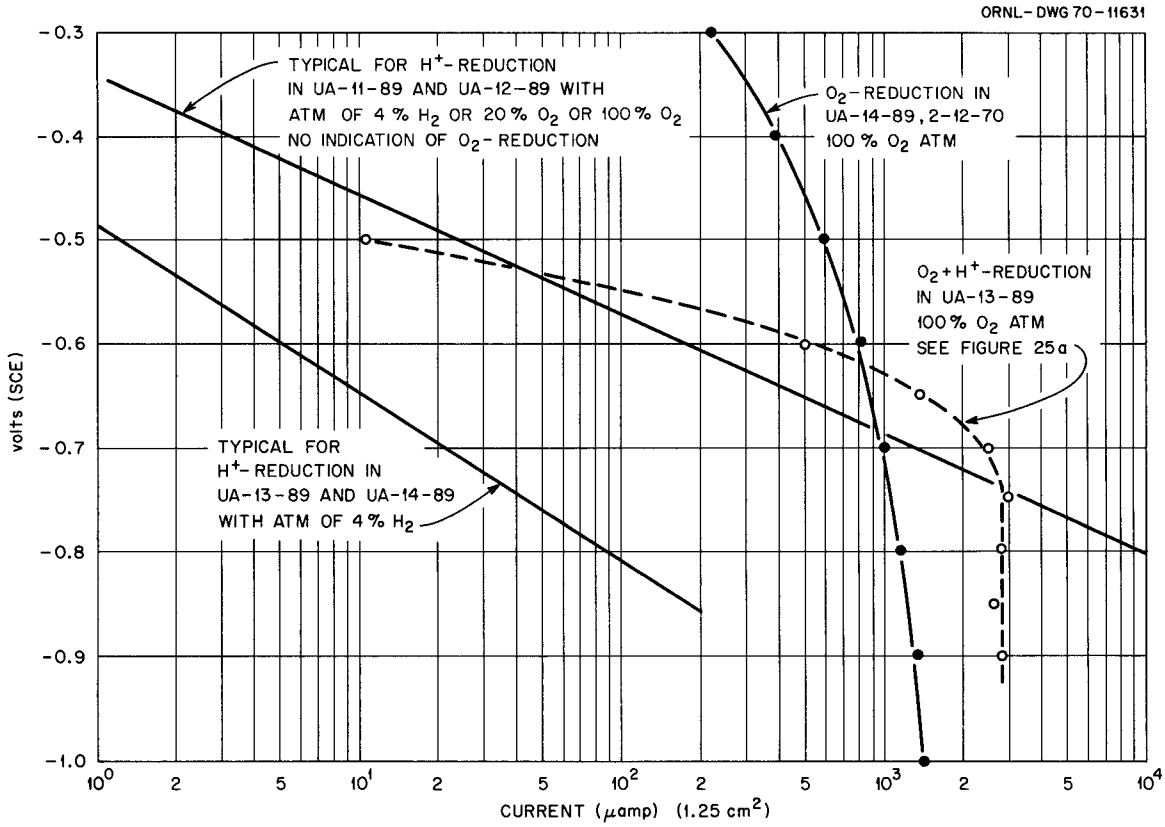

Fig. 30. Illustration of Occurrence and Absence of O_2-Reduction

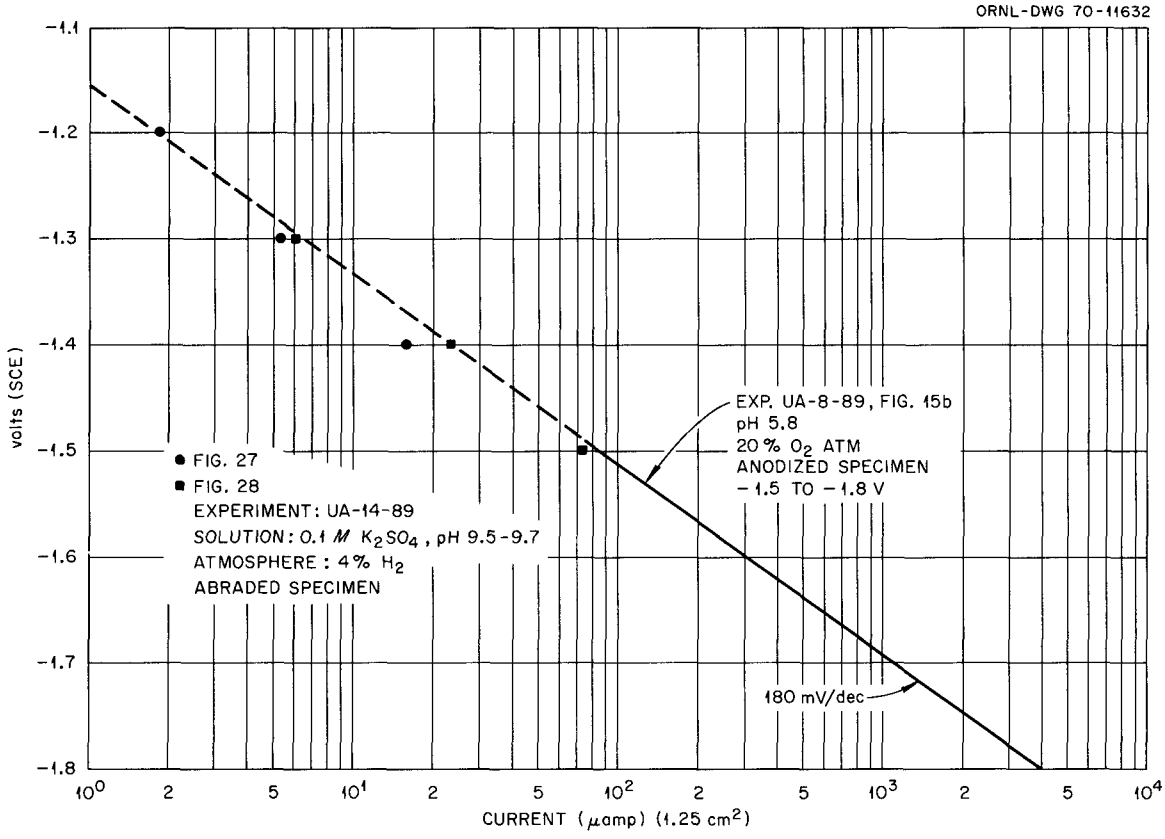

Fig. 31. Comparison Between Data for H_2O-Reduction on Alloy at pH 5.8 and 9.5 to 9.7

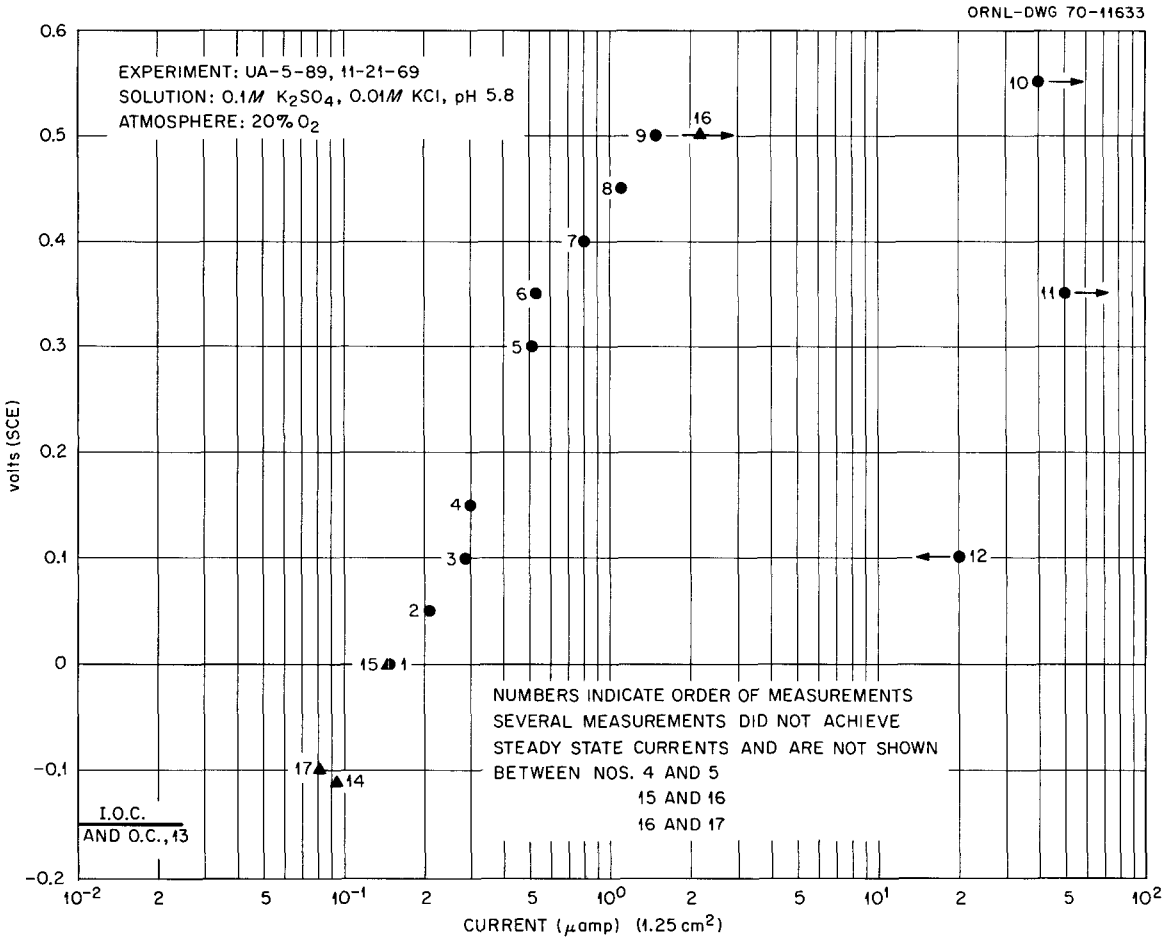

Fig. 32. Breakthrough Potential for Pitting of Alloy in K_2SO_4-KCl

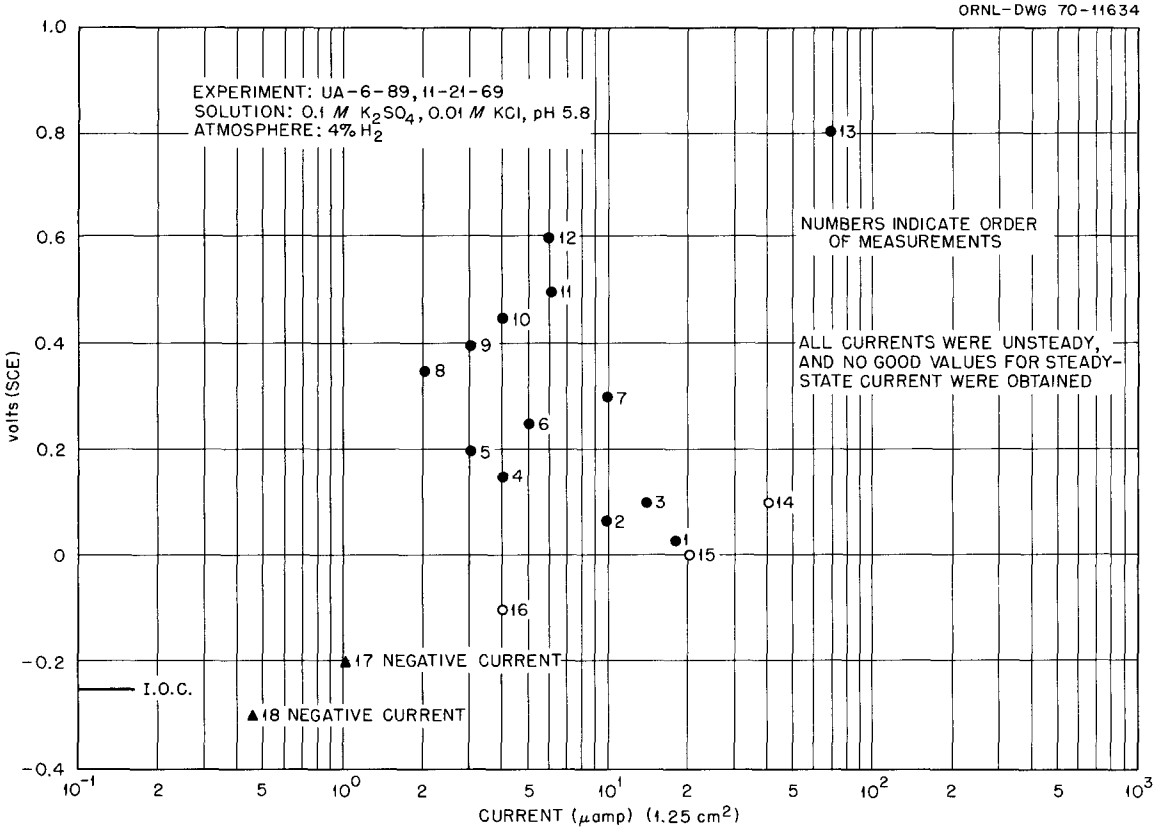

Fig. 33. Polarization of Alloy in K_2SO_4-KCl

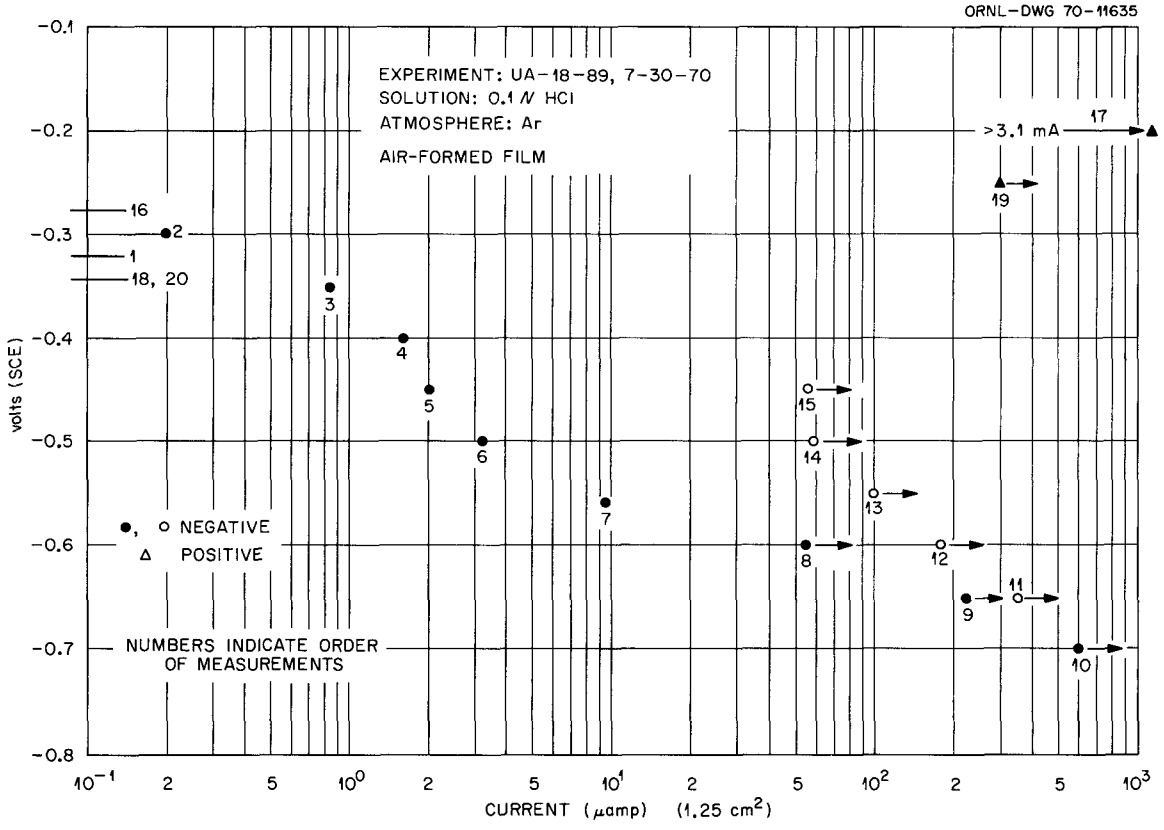

Fig. 34. Polarization of Alloy in 0.1N HCl

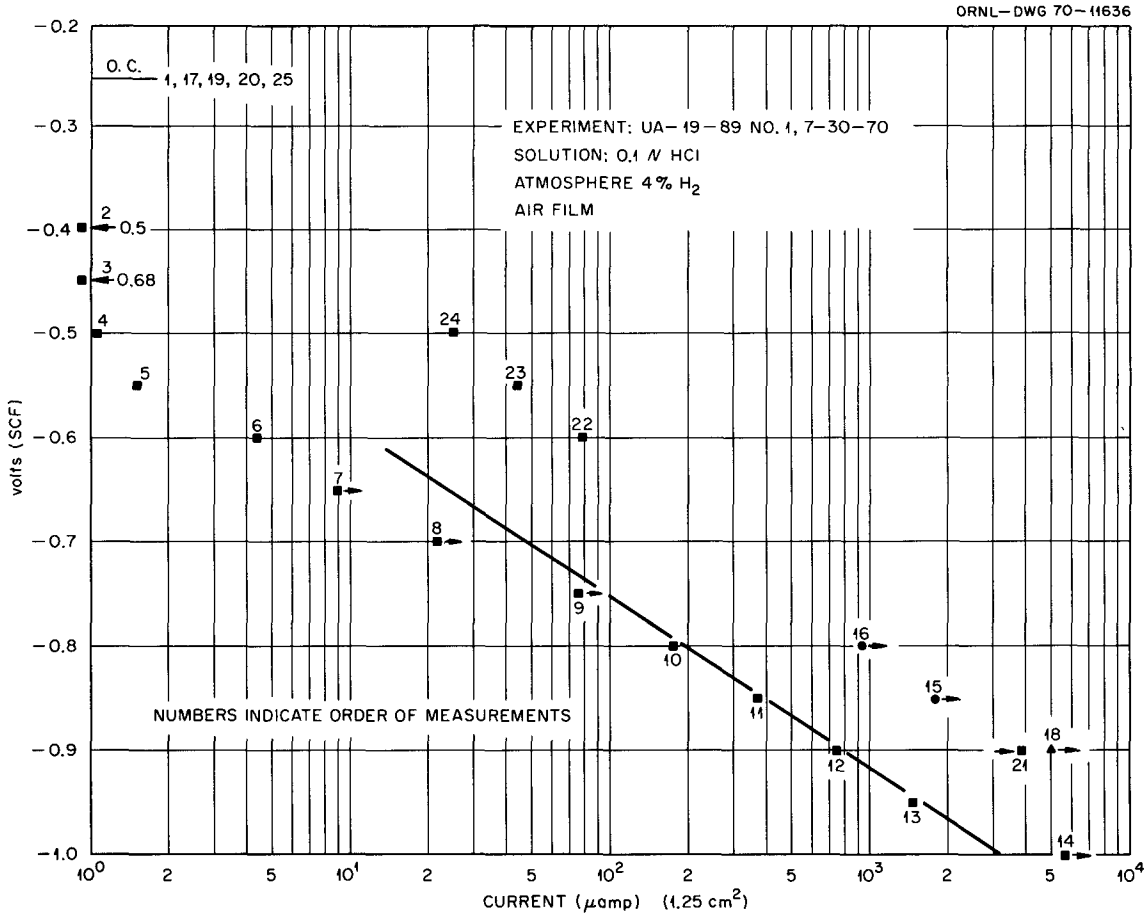

Fig. 35. Polarization of Alloy in 0.1N HCl

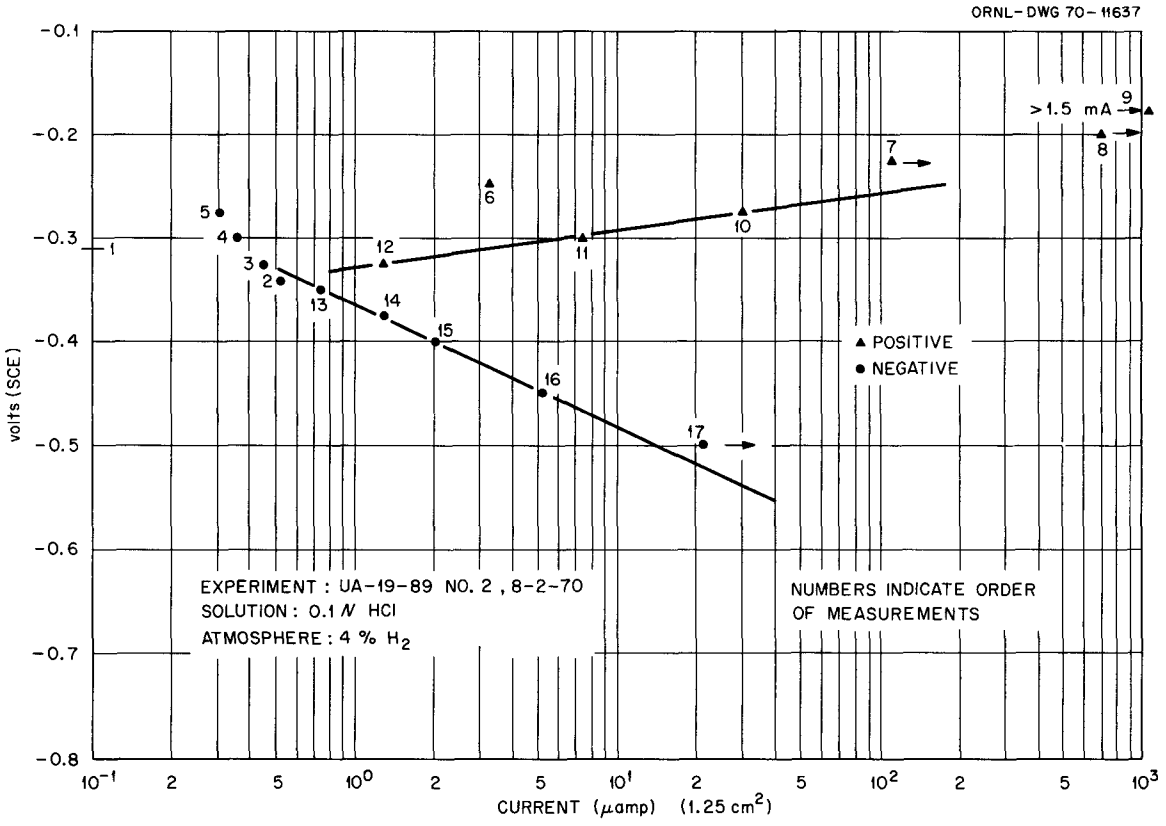

Fig. 36. Polarization of Alloy in 0.1N HCl

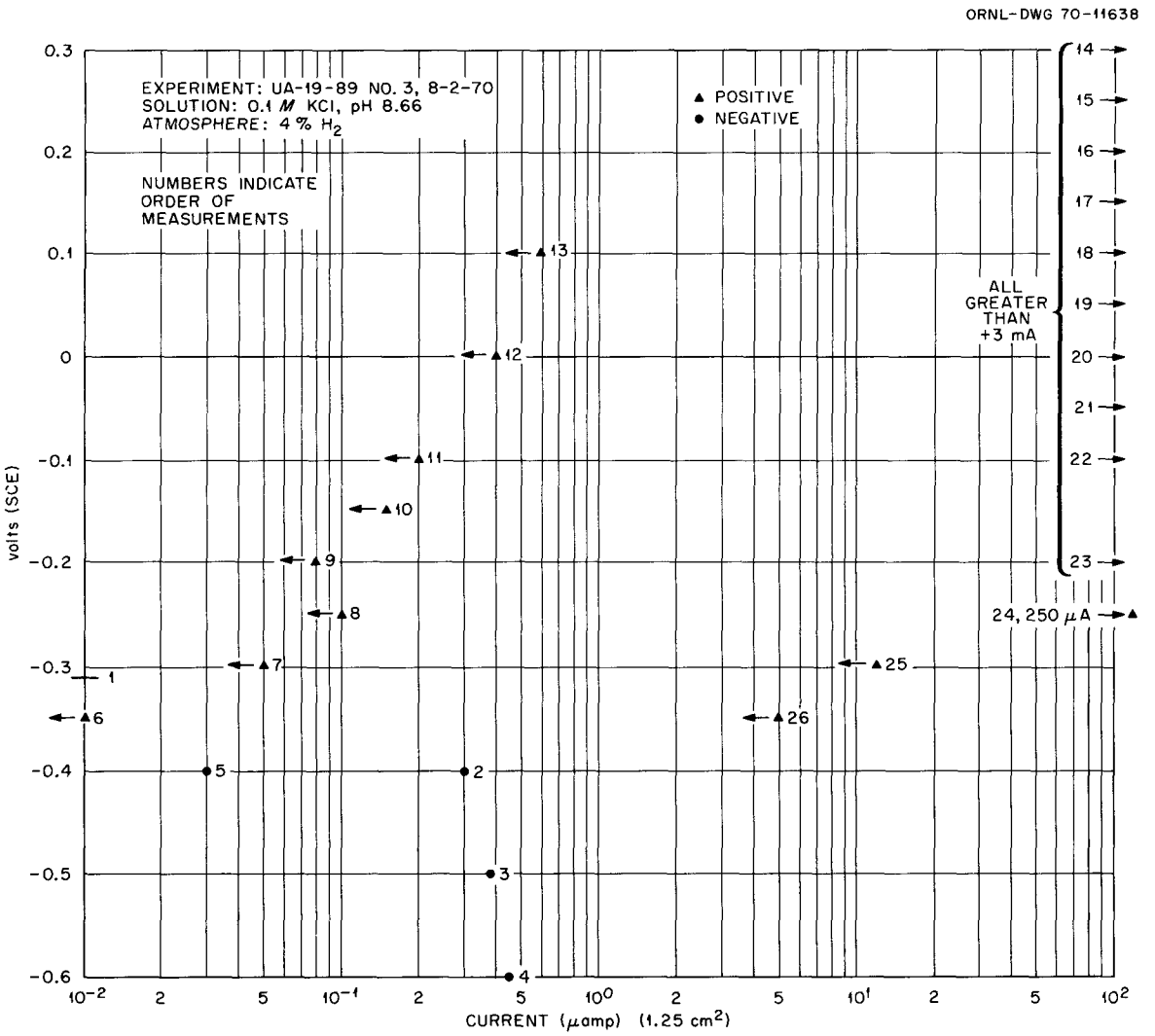

Fig. 37. Polarization of Alloy in 0.1N HCl

Appendix 1. Review of Thermodynamic Information for Uranium-Water Systems; Pourbaix Diagrams

1. Introduction

Thermodynamic information on the uranium-water system which is presented by Pourbaix[1.1] is reviewed and discussed in this section. Some of the information presented by Pourbaix is in the form of the familar potential-pH diagrams, and I include a review of the diagrams which is intended to be a brief summary of the types of information included therein, and of the mechanics of calculating the illustrated thermodynamic properties. No discussion is given of the thermodynamic bases for the mechanics of the calculations. Discussions of these are included in the Atlas.[1.1]

2. Summary of information presented in Pourbaix diagrams and of construction methods

The Pourbaix potential-pH diagrams for a metal and its aqueous corrosion products in aqueous solution present the following information, in the general case, for the equilibrium systems.

A. Lines expressing the conditions of pH and potential under which the concentrations of two dissolved substances are equal.

B. Lines which represent the conditions of pH and potential at which two different solid substances are in equilibrium.

C. Lines representing conditions of pH and potential for which the solubility of the different solid substances in all the different dissolved forms have the same value. These lines

usually pertain to concentrations of 10^{-6}, 10^{-4}, 10^{-2}, and 10^{0} moles of metal per liter. Where only one line is presented, it refers to a concentration of 10^{-6}M.

D. Lines a and b which represent, respectively, the equilibrium conditions of the reduction of water (or its H^+ ions) to gaseous hydrogen and the oxidation of water to gaseous oxygen when the partial pressure of hydrogen or oxygen is one atm at 25°C.

The products considered are usually oxides, hydrides, metal ions and compound ions with oxygen or with oxygen and hydrogen. The diagrams are not valid when the solution contains substances capable of forming soluble complexes or insoluble salts with the metal unless these are specifically considered.

The information used in plotting the lines is obtained by thermodynamic calculations using literature information on standard chemical potentials of reacting species.* Two types of reactions are recognized and considered in establishing the diagrams: chemical and electrochemical.

A chemical reaction is defined as one in which only neutral molecules and positively or negatively charged ions take part, with the exclusion of electrons. For example,

$$Fe(s) + 2H^+(aq) \rightleftharpoons Fe^{++}(aq) + H_2(g) \qquad (1)$$

---

*Lists of standard chemical potentials are included in the Pourbaix Atlas (ref. 1.1).

In the general case, we write,

$$\upsilon_1 A + \upsilon_2 B + ... \rightleftharpoons \upsilon_3 C + \upsilon_4 D + ... \quad (2)$$

where υ_1, υ_2.....are stoichiometric numbers, and A, B, C, D are chemical species. The equilibrium conditions for a chemical reaction are obtained by applying the equations,

$$\Sigma\upsilon \log (M) = \log K, \quad (3)$$

and

$$\log K = -\Sigma \frac{\upsilon\mu^\circ}{1363} \quad (4)$$

where K is the equilibrium constant for the reaction, (M) is the activity of a species taking part in the reaction, and υ represents stoichiometric numbers. The sign of υ is negative when the species is on the left-hand side of the reaction as written (e.g., reaction 2). It is positive when the species is on the right hand side. μ° is the standard chemical potential of the species.

To illustrate the use of Eqs. (3) and (4), consider the reaction,

$$Fe(OH)_2(s) \rightleftharpoons Fe^{+2}(aq) + 2\ OH^-(aq) \quad (5)$$

For this reaction,

$$\log K = \log (Fe^{+2}) + 2 \log (OH^-)^{**} \quad (6)$$

$$\log K = \log (Fe^{+2})\ (OH^-)^2 \quad (7)$$

and

$$\frac{-\Sigma\upsilon\mu^\circ}{1363} = \frac{\mu^\circ_{Fe^{+2}} + 2\,\mu^\circ_{OH^-} - \mu^\circ_{Fe(OH)_2}}{1363} \quad (8)$$

---

*Lists of standard chemical potentials are included in the Pourbaix Atlas (ref 1.1).

**The activity of a solid is one. That of water is also one.

An electrochemical reaction is defined as being a reaction involving, besides molecules and ions, negative electrons arising from a metal or other substance by metallic conduction. For example,

$$2H^{+}(aq) + 2e \rightleftharpoons H_2(g), \tag{9}$$

or in the general case,

$$\upsilon_1 A + \upsilon_2 B + \text{---} + ne^{-} \rightleftharpoons \upsilon_3 C + \upsilon_4 D + \text{----} \tag{10}$$

The equilibrium conditions for an electrochemical reaction at 25°C are evaluated from the equation

$$E^{\circ} = E_0^{\circ} + \frac{0.0591}{n} \Sigma \upsilon \log (M), \tag{11}$$

where

E° is the equilibrium electrode potential (volt vs SHE),

E_0° is the standard electrode potential at 25°C and is given by,

$$E_0^{\circ} = \frac{\Sigma \upsilon \mu^{\circ}}{23{,}060n} \tag{12}$$

n is the value for the number of electrons taking part in the reaction. It has a negative sign if the electrons are on the left in the reaction as written (e.g., reaction 10). The other symbols have the meanings stated above.

To further illustrate the application of these equations, we consider below the derivation of three different relationships for uranium-water. Values of standard chemical potentials (free energies of formation) needed in the derivations are included in Table 1.1. These values were taken from Pourbaix's Atlas.[1.1]

a. Derive expression for conditions of pH and potential giving equal solubility of U^{+3} and UOH^{+3} in the equilibrium,

$$U^{+3} + H_2O \rightleftharpoons UOH^{+3} + H^{+} + e^{-} \tag{13}$$

Table 1.1. List of Standard Chemical Potentials (After Pourbaix)[1]

Species	μ°(cal)	Name, Color, Crystalline System
H_2O (gaseous)	-54,635	-
H_2 (gaseous)	0	-
O_2 (gaseous)	0	-
H_2O (liquid)	-56,690	-
H^+ (dissolved)	0	-
OH^- (dissolved)	-37,595	-
CO_2 (gaseous)	-94,260	-
H_2CO_3(dissolved)	-149,000	-
UOH^{+3} (dissolved)	-193,500	-
U^{+4} (dissolved	-138,400	-
U^{+3} (dissolved)	-124,400	-
UO_2^{+2} (dissolved)	-236,400	-
UO_2 (anh)	-246,600	Uranium oxide, black oxide, brown-black, cubic or rhomb.
UO_3 (anh)	-273,000	Uranic oxide, yellow-red, rhomb.
$UO_3 \cdot H_2O$	-343,000	Monohydrated uranic oxide, yellow-orange, amorphous or orthomb.
$UO_3 \cdot 2H_2O$	-398,840	Dihydrated uranic oxide, yellow-green α f.c. tetrag, β orthomb.
UO	-123,000	Uranium monoxide, grey, f.c. cubic
U_2O_3 (hyd)	-263,200	Hypouranous hydroxide, brown
UH_3	-17,700	Uranium hydride, grey-brown, cubic

Using Eq. 11 with reaction 13, we can write

$$E^\circ = E_0^\circ + 0.0591[\log (UOH^{+3}) - \log(U^{+3}) - \log (H^+)] \qquad (14)$$

or

$$E^\circ = E_0^\circ - 0.0591\ pH + 0.0591 \log (UOH^{+3})/(U^{+3}) \qquad (15)$$

From Eq. 12,

$$E_0^\circ = \frac{\mu^\circ_{UOH^{+3}} - \mu^\circ_{U^{+3}} - \mu^\circ_{H_2O}}{23{,}060} \ . \qquad (16)$$

Introducing μ° values from Table 1.1 in Eq. 16 and substituting in Eq. 15, we have

$$E^\circ = - 0.538 - 0.0591\ pH + 0.0591 \log (UOH^{+3})/(U^{+3}). \qquad (17)$$

Setting (UOH^{+3}) equal to (U^{+3}) we have,

$$E^\circ = - 0.538 - 0.0591\ pH, \qquad (18)$$

which expresses the conditions of potential and pH at equal solubility of UOH^{+3} and U^{+3}.

b. Derive expression for the conditions of pH and potential under which anhydrous UO_2 and anhydrous UO_3 are in equilibrium in the reaction,

$$UO_2 + H_2O \rightleftarrows UO_3 + 2H^+ + 2e^- \qquad (19)$$

For this reaction we have, using Eq. 11,

$$E^\circ = E_0^\circ - 0.0591\ pH. \qquad (20)$$

From Eqn. 12,

$$E_0^\circ = \frac{\mu^\circ_{UO_3} - \mu^\circ_{UO_2} - \mu^\circ_{H_2O}}{(2)\ (23{,}060)} \ . \qquad (21)$$

Introducing values for μ° in Eq. 21, and substituting in Eq. 20, we have,

$$E^\circ = 0.656 - 0.0591\ pH \qquad (22)$$

Eqn. 22 expresses the conditions under which UO_2 and UO_3 are in equilibrium in reaction 19.

c. Determine the expression for solubility of anhydrous UO_3 as a function of pH in the reaction,

$$UO_2^{+2} + H_2O \rightleftharpoons UO_3 + 2H^+ \tag{23}$$

From Eqs. 3 and 4

$$\Sigma\, \upsilon \log (M) = -\Sigma \frac{\upsilon\mu^\circ}{1363} \tag{24}$$

$$\Sigma\, \upsilon \log (M)_\circ = 2 \log_\circ (H^+) - \log_\circ (UO_2^{+2}) = -2pH - \log_\circ (UO_2^{+2}). \tag{25}$$

$$\Sigma \frac{\upsilon\mu^\circ}{1363} = \frac{\mu^\circ_{UO_3} - \mu^\circ_{UO_2^{+2}} - \mu^\circ_{H_2O}}{1363} \tag{26}$$

Introducing values for μ° from Table 1.1, we have,

$$\Sigma \frac{\upsilon\mu^\circ}{1363} = 14.73. \tag{27}$$

Combining Eqs. 25 and 27 in Eq. 24, we have,

$$\log (UO_2^{+2}) = 14.73 - 2pH \tag{28}$$

This is the expression for the solubility of anhydrous UO_3 in aqueous solution as a function of pH. It is interesting to note that the solubility is about 1 molar at pH 7 and that it increases with decreasing pH.

Pourbaix[1.1] and others[1.2,1.3] emphasize that the diagrams provide thermodynamic information for the systems considered. They do not provide any information regarding the kinetics of a particular reaction. Also, importantly, the solid phases which form in the actual system may differ from the theoretical ones so that the equilibrium conditions may differ from those predicted. Accordingly, the behavior of a system cannot be predicted reliably on the basis of the diagrams alone. Kinetic and structural information is indispensable for thorough understanding of the system.

3. Review of Pourbaix diagrams for uranium

The published Pourbaix diagrams for uranium in aqueous solution are illustrated in Fig. 1.1. The solid substances considered by Pourbaix for the Fig. 1.1a diagrams were U, UO, U_2O_3(hydrous), UO_2, U_3O_8, UO_3(anhydrous). Those considered for the Fig. 1.1b diagram were: U, UO, U_2O_3(hydrous), UO_2, U_3O_8, $UO_3 \cdot 2H_2O$, UH_3.

In each figure, a dotted line other than line a or b, represents conditions of equal solubility of the two dissolved species on opposite sides of the line. The lines labeled 0, -2, -4, and -6 show the conditions under which the solubility of the different dissolved substances in all the dissolved forms have the same value of 1, 10^{-2}, 10^{-4}, or 10^{-6} molar. The lines between two solid phases show the conditions under which these phases are in equilibrium. The equilibrium conditions which are represented are listed in Pourbaix's Atlas,[1.1] and are identified by the numbers appearing in the diagrams.

The stable equilibria at 25°C of the system uranium-water are those in Fig. 1.1b. Uranium hydride is more stable than uranium so that this compound appears instead of uranium in the stable system. The dihydrated uranic oxide, $UO_3 \cdot 2H_2O$, is the most stable of the three forms of UO_3 considered (Table 1.1), and so the $UO_3 \cdot 2H_2O$ appears in the diagram of the stable system.

4. Additional thermodynamic information on uranium-water systems

Additional thermodynamic information on the uranium-water systems, including information on non-equilibrium systems, is presented in Fig. 1.2 and Table 1.2. The non-equilibrium conditions should generally

be included in corrosion considerations because they may occur as transient conditions which may affect the course of corrosion.

Fig. 1.2 illustrates the conditions of potential and pH for equilibrium between several different pairs of solids. These conditions were set forth by Pourbaix[1.1] under the reaction numbers included in Fig. 1.2.

Table 1.2 has information on the thermodynamic solubilities of several oxides of uranium. Most of this information was presented by Pourbaix[1.1] under the reaction numbers listed in Table 1.2. I calculated the solubility of U_2O_3 using values for standard chemical potentials given by Pourbaix.[1.1] No information on U^{+2} solubility was given.

It should be emphasized that the solubility relationships pertain to only the reactions listed. In practice, the dissolved species may undergo other reactions which would lead to precipitation. For example, the UO_2^{+2} formed in solution by reaction 23ae would be expected to hydrolyze at pH 7 and precipitate as $UO_3 \cdot 2H_2O$. Also, U^{+3} is unstable with respect to U^{+4} under some conditions of pH and potential where the U^{+4} is insoluble (see Figs. 1.1a and 1.1b).

5. General conclusion from thermodynamic data for uranium

General conclusion which can be drawn for the thermodynamic data include the following.

a. Uranium hydride can form by reaction between H_2O and U at potentials below line 9, Fig. 1.2. The UH_3 is not stable with respect to formation of UO_2 by reaction H_2O and UH_3 until the potentials are below line 12a, Fig. 1.2.

Table 1.2 Solubility of Uranium Oxides[a]

Numbers[b]	Z	Solid	Dissolved Ion	Reaction	General Solubility Relationship	Solubility (moles/ℓ) at pH			
						0	7	10	5
α	+2	UO	---	---	----	---	---	----	---
β	+3	U_2O_3(hyd)[f]	U^{+3}[c]	$U^{+3} + 3H_2O \rightleftharpoons U(OH)_3 + 3H^+$	$\log (U^{+3}) = 22.94 - 3\ pH$	10^{23}	$10^{1.9}$	10^{-7}	$10^{7.9}$
21a	+4	UO_2	U^{+4}[d]	$U^{+4} + 2H_2O \rightleftharpoons UO_2(anh) + 4H^+$	$\log (U^{+4}) = 3.80 - 4\ pH$	$10^{3.8}$	10^{-24}	10^{-36}	10^{-16}
21b	+4	UO_2(hyd)[e]	U^{+4}[d]	$U^{+4} + 4H_2O \rightleftharpoons U(OH)_4 + 4H^+$	$\log (U^{+4}) = 9.95 - 4\ pH$	$10^{9.95}$	10^{-18}	10^{-30}	10^{-10}
22a	+4	UO_2	UOH^{+3}[d]	$UOH^{+3} + H_2O \rightleftharpoons UO_2(anh) + 3H^+$	$\log (UOH^{+3}) = 2.63 - 3\ pH$	$10^{2.6}$	10^{-18}	10^{-28}	10^{-12}
22b	+4	UO_2(hyd)[e]	UOH^{+3}[d]	$UOH^{+} + 3H_2O \rightleftharpoons U(OH)_4 + 3H^+$	$\log (UOH^{+3}) = 8.78 - 3\ pH$	$10^{8.8}$	10^{-12}	10^{-21}	10^{-6}
23ae	+6	UO_3(anh)	UO_2^{+2}[g]	$UO_2^{+2} + H_2O \rightleftharpoons UO_3(anh) + 2H^+$	$\log (UO_2^{+2}) = 14.74 - 2\ pH$	$10^{14.7}$	$10^{.74}$	$10^{-5.3}$	$10^{4.7}$
23ac	+6	$UO_3 \cdot 1H_2O$	UO_2^{+2}[g]	$UO_2^{+2} + 2H_2O \rightleftharpoons UO_3 \cdot 1H_2O + 2H^+$	$\log (UO_2^{+2}) = 4.97 - 2\ pH$	$10^{5.0}$	10^{-9}	10^{-15}	10^{-5}
23ad	+6	UO_3	UO_2^{+2}[g]	$UO_2^{+2} + 3H_2O \rightleftharpoons UO_3 \cdot 2H_2O + 2H^+$	$\log (UO_2^{+2}) = 5.60 - 2\ pH$	$10^{5.6}$	$10^{-8.4}$	10^{-14}	$10^{-4.4}$

a. Calculated from standard chemical potentials in the listed reaction

b. Reaction numbers and equations are those presented by Pourbaix[1.1]. I calculated the relationship for number (β) from standard chemical potentials given by Pourbaix[1.1].

c. Hypouranous ion; pink or purple

d. Uranous ions; green

e. Uranous hydroxide; green

f. Hypouranous hydroixde; brown

g. Uranyl ion; yellow

b. Uranium hydride is stable with respect to formation of UO at potentials below line 10, Fig. 1.2; with respect to formation of hydrous U_2O_3 below line 11, Fig. 1.2.

c. UO_2 is the stable oxide and is insoluble ($< 10^{-6}M$) in the potential-pH domain bounded by lines 12, 22, and 19, Fig. 1.1b.

d. UO_2 and other oxides, or U^{+3} can form at potentials well below lines 12 and 24, Fig. 1.1b, as illustrated in Fig. 1.1a. However, these species are unstable with respect to formation of hydride at potentials below these lines.

e. At potentials above line 19ad (Fig. 1.2) UO_2 can be oxidized to $UO_3 \cdot 2H_2O$; above line 19ae (Fig. 1.2) the UO_2 can be oxidized to anhydrous UO_3.* The anhydrous UO_3 is soluble ($> 10^{-6}M$) below pH 10.4 while the $UO_3 \cdot 2H_2O$ is soluble below pH 5.8; Figs. 1.1a and 1.1b.

Finally it should be repeated that the corrosion behavior of a metal in aqueous solution cannot be confidently predicted on the sole basis of thermodynamic considerations. Kinetic and structural information on these factors is discussed elsewhere in this report. Experimental information bearing on these factors was obtained as part of the present work and is presented elsewhere in this report.

---

*Formation of $UO_2 \cdot H_2O$ can occur at potentials near those of line 19ad.

References

1.1 Marcel Pourbaix, "Atlas of Electrochemical Equilibria in Aqueous Solutions," English Edition, Pergamon Press, New York, 1966.

1.2 R. Piontelli, loc. cit. p. 11-15.

1.3 Pierre Van Rysselberghe, loc. cit. p. 21-27.

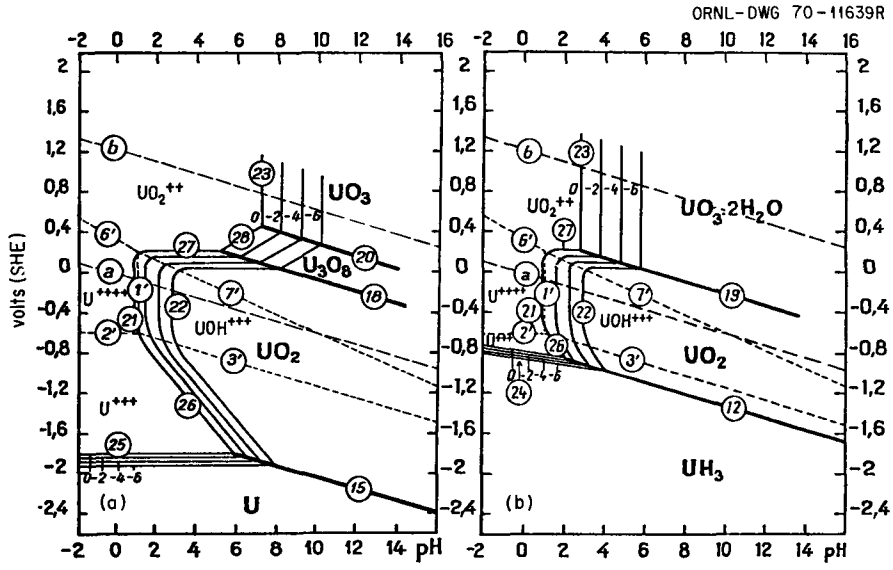

Fig. 1.1 Uranium-Water (After Pourbaix)

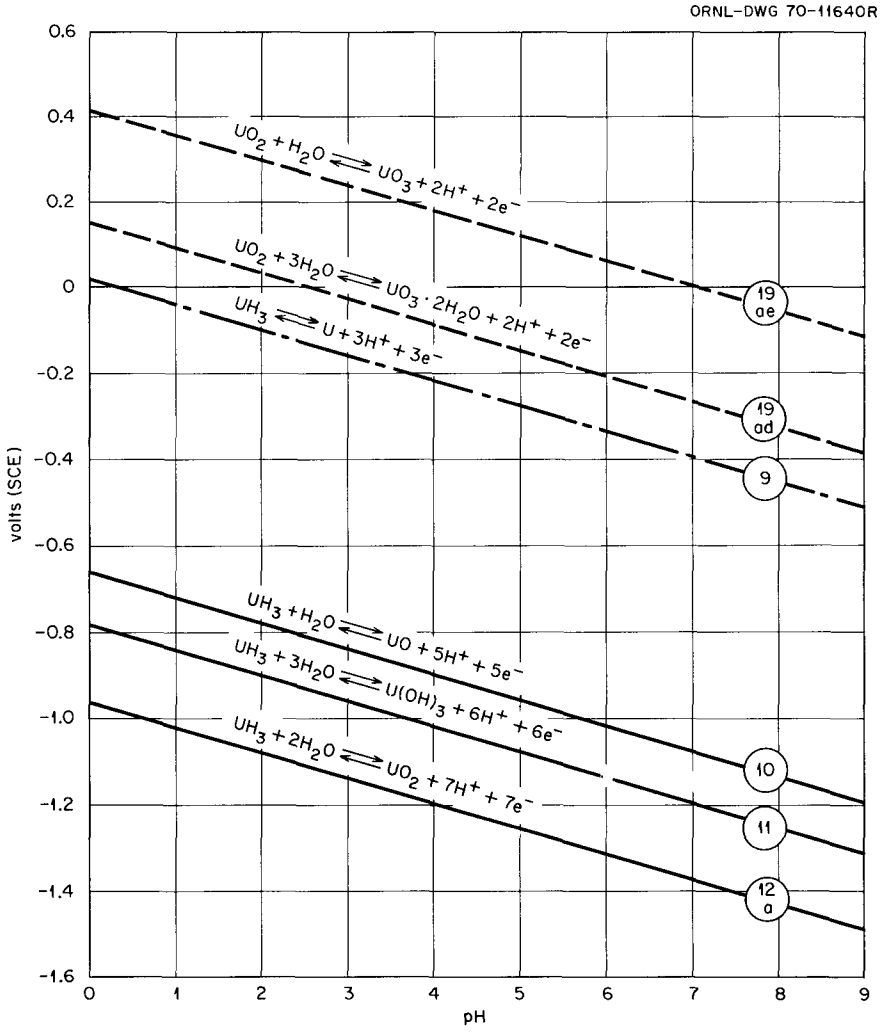

Fig. 1.2 Equilibrium Potential vs pH for Reactions Shown

Appendix 2. Summary of Available Experimental Information on Solubilities of Uranium Oxides and Comment*

1. Summary of solubility information

1.1 Anhydrous UO_3

UO_3 reacts with cold water to give $UO_3 \cdot 2H_2O$; at 70-300°C it reacts with water to form $UO_3 \cdot H_2O$. (F)

UO_3 dissolves in all mineral acids. (K - 1)

UO_3 dissolves readily in excess Na_2CO_3; it is especially soluble when $NaHCO_3$ is also in solution. (F)

$$UO_3 + Na_2CO_3 + H_2O \rightarrow Na_4UO_2(CO_3)_3 + 2NaOH \quad (1)$$

$$UO_3 + Na_2CO_3 + 2NaHCO_3 \rightarrow Na_4UO_2(CO_3)_3 + H_2O \quad (2)$$

1.2 $UO_3 \cdot 2H_2O$ and $UO_3 \cdot 1H_2O$

These compounds are very slightly soluble in water. (F) $UO_3 \cdot XH_2O$ is soluble in all mineral acids. (K - 1)

1.3 Anhydrous UO_2

1.3.1 Water

UO_2 is insoluble in water. (F)

1.3.2 Acids

a. HCl - The oxide is insoluble in concentrated hot or cold HCl. Hot fuming HCl reacts slowly. (K - 2)

---

*Letters in parentheses refer to references at back

b. H_2SO_4 - UO_2 is slowly soluble in dilute H_2SO_4. It dissolves easily in concentrated acid.(K - 1)

c. HNO_3 - Very dilute HNO_3 has no effect other than causing hydration. UO_2 is easily soluble in concentrated HNO_3 or aqua regia.(K - 1)

1.3.3 Hydrogen peroxide and alkalies

Solutions of H_2O_2 will oxidize UO_2 to $UO_4 \cdot XH_2O$.(K - 3) UO_2 dissolves in solutions of alkalies containing H_2O_2.(K - 4)

1.4 Hydrous UO_2

Freshly prepared $UO_2 \cdot 2H_2O$ is readily soluble in acids but becomes insoluble upon standing.(K - 5)

1.5 Anhydrous U_3O_8(F)

a. U_3O_8 is insoluble in water and dilute acids.

b. In concentrated acids it dissolves slowly forming a mixture of uranous and uranyl salts.

c. Concentrated HNO_3 or aqua regia readily dissolve U_3O_8.

1.6 Hydrous U_3O_8(F)

This compound dissolves readily in acids forming a mixture of uranous and uranyl salts.

It is easily oxidized in air to hydrated UO_3.

2. Reaction of UO_2 with O_2(W)

UO_2 in contact with air will absorb oxygen into interstitial positions. The bulk oxide at room temperature reaches a composition close to $UO_{2.04}$. Surface layers about 40A thick reach a composition of $UO_{2.25}$.

3. Reaction of UO_2 with oxygenated water

UO_2 is slowly oxidized to the tri-oxide by oxygenated water. (F)

4. Comments on comparisons between experimental and thermodynamic solubilities of uranium oxides.

The experimental data summarized above indicate that with the exception of anhydrous UO_2 and anhydrous U_3O_8, the solubilities of the oxides are qualitatively near those predicted from thermodynamic considerations (Appendix 1).

The apparently low solubilities of anhydrous UO_2 and U_3O_8 in solutions where they are thermodynamically soluble signifies low rates of reaction between these oxides and these solutions.*

---

*In general, it is not uncommon for anhydrous oxides (high fired oxides) to be quite unreactive toward solutions. (T)

References

F. J. M. Fulmer, "The Oxides of Uranium" ORNL, CF 51-10-133, Oct. 1951

K. J. J. Katz and E. Rabinowitch, "The Chemistry of Uranium," National Nuclear Energy Series, VIII -5, McGraw-Hill Book Co., Inc., 1951.

K - 1. op. cit., p. 327.

K - 2. op. cit., p. 322.

K - 3. op. cit., p. 316.

K - 4. op. cit., p. 326.

K - 5. op. cit., p. 281.

W. W. D. Wilkinson, "Uranium Metallurgy, Volume II: Uranium Corrosion and Alloys," Interscience Publishers, New York, 1962, p. 983.

T. A. W. Thomas, "Colloid Chemistry," McGraw-Hill Book Co., Inc., New York, 1934, p. 162.

Appendix 3. Review of Literature Information on Uranium Corrosion in Aqueous Environments

1. Corrosion of uranium in deaerated water and water vapor, 25 to 100°C.

1.1 General characteristics at temperatures of 35 to 100°C.

a. Corrosion is fairly uniform over an exposed surface and rates are approximately constant with time.[3.1]

b. Hydrogen gas is evolved at a rate corresponding approximately to that expected for the reaction,

$$U + 2H_2O \rightarrow UO_2 + 2H_2.$$

However, 2 to 9% of the reacted uranium is in the form of uranium hydride, UH_3.[3.2] The oxide has the formula[3.2] $UO_{2.06}$.

c. The reaction rate is dependent on the pressure of water vapor, but there is no difference between 100% RH* and full immersion.[3.2]

d. Rate of reaction does not depend upon pressure of H_2 up to at least 6 atm.[3.2]

e. UH_3 is present in the reaction product but does not form from gas-phase H_2.[3.2] There is no exchange between hydrogen in the gas and solid phases.

f. The amount of UH_3 is reduced at low RH.

g. The amount of UH_3 increases slightly with increasing temperature at 100% RH.

h. The open circuit potential of uranium in degassed water at 35°C is about -1.10 V(SCE).[3.3]

*Relative humidity

1.2 Corrosion rates

Orman[3.1] reported rates for HNO_3-pickled specimens in water which correspond to 11, 120, 315, and 860 mpy at 35, 65, 80 and 100°C, respectively. Others[3.4] have reported hydrogen-evolution data for water-vapor exposure at 25°C (100% RH) and 40°C (43% RH) which correspond to corrosion rates of 2.2 and 3.9 mpy, respectively.

Orman[3.4] found that the rate in water vapor at 100°C depended upon relative humidity; increasing by a factor of about five with increase of relative humidity from 10 to 100%.

2. Corrosion in oxygenated water and water-vapor

2.1 Temperatures of 50 to 100°C.

The effects of the introduction of air (or the approximately equivalent amount of oxygen) into the uranium-water vapor system at temperatures of 50 to 100°C have been summarized[3.6] as follows for RH < 90%.[3.6]

a. The rate of oxidation of the uranium is reduced approximately thirty-fold from that in the oxygen free system.

b. Evolution of H_2 is negligible.

c. There is no net consumption of H_2O during the time that oxygen remains in the gas phase.

d. The oxygen pressure falls linearly with time until all of the gas has been consumed whereupon the characteristics of the reaction become those of the deaerated systems.

When the RH exceeds 90%, the corrosion rate increases, and yellow oxide occurs together with flaking and evolution of H_2. These effects are accompanied by deep pitting.[3.6]

Experiments at 100°C in water showed that the oxygen is converted into water and does not react directly with the uranium.[3.6] The yellow oxide formed at 100°C was identified as $UO_3 \cdot 0.8\ H_2O$.[3.6,3.7]

The black oxide which also formed had the composition $UO_{2.3}$.[3.7] Uranium hydride formation is apparently very minor.[3.7] However, it has been suggested that small amounts of hydride are formed.[3.8]

2.2 Temperatures below 50°C

It is known that addition of O_2 to water vapor has the effects of markedly reducing the corrosion rate and eliminating H_2-evolution during tests of several hundred hours duration.[3.4] The indicated corrosion rate in the presence of O_2 is 1/20 that in deoxygenated systems.[3.4]

It is also known that aeration of water reduces the corrosion rate near room temperature, although it has been suggested that the corrosion increases after long exposure periods.[3.9]

3. Corrosion in water containing CO_2

With CO_2 pressures of .07 to 2 atms., the uranium corrosion and hydrogen evolution were approximately halved.[3.6] There was no change in the amount of CO_2 during the reaction, and no CO was formed.

4. Open circuit potentials in oxygenated water

Ward and Waber[3.3] found a value of 0.123V (SCE) in aerated 0.1M $KClO_4$, pH 7 at 35°C. The potentials at other partial pressures of oxygen were, 100% O_2, 0.143V; 10% O_2, 0.113V; and 3% O_2, 0.0962. Since $KClO_4$ is a more or less inert electrolyte, it is assumed that these potentials would also prevail in oxygenated water. The specimens used in the work of Ward and Waber were abraded in an inert environment. Also, they were transferred to the cell through an inert environment.

5. Crevice corrosion of uranium in aerated water

Waber[3.10] mentioned that deep pitting occurred in the crevice formed by placing a cover glass over the surface of a specimen when the assembly was exposed in aerated water. The metal near the edge of the glass was relatively unattacked. The temperature was not mentioned but was presumably room temperature.

6. Corrosion in acids

6.1 H_2SO_4

Solid uranium is only slowly attacked by deaerated, dilute H_2SO_4. The rate in deaerated 0.1 N H_2SO_4 at 100°C is about 90 mpy and less than that in boiling deaerated water by a factor of about ten.[3.11] The rate in 6 N H_2SO_4 at the boiling point is about the same as that in boiling water (about 860 mpy).[3.12]

The reaction rate in the acid can be accelerated by imposing oxidizing conditions such that the higher oxidation state of uranium, U-VI, is formed (e.g., by addition of H_2O_2 to the solution or by polarizing anodically).[3.12-3.14]

6.2 HCl

Solid uranium is dissolved by concentrated HCl. The rate and completeness of dissolution increases with increasing concentration of acid. U(IV) and U(III) are formed in varying ratios in the HCl; nearly all U(IV) in 12N, and 20 to 40% U(IV) in 6N. Variable amounts of the metal are converted into a black precipitate.[3.12]

Waber[3.10] mentioned that 1 to 2N HCl will dissolve uranium pieces 1/8 in. thick within several hours at room temperature.

6.3 HNO_3

Uranium is partially passivated by HNO_3; several months are required to dissolve 1/8 in. thick pieces in 5N HNO_3 at room temperature.[3.10]

Uranyl nitrite is formed by the dissolution.[3.12-3.14]

Dissolution rates under anodic polarization have been reported.[3.13,3.14]

6.4 HF

Solid uranium is attacked slowly by concentrated HF even at 80 to 90°C. The addition of oxidizing agents such as H_2O_2 does not accelerate the reaction appreciably.[3.12]

6.5 HBr and HI

The reactions of uranium in these acids resemble those in HCl but are slower.[3.12]

6.6 $HClO_4$

Dilute $HClO_4$ is rather inert toward reaction with uranium. However, at concentrations above 90% it reacts vigorously.[3.12] Dilute $HClO_4$ containing oxidizing agents dissolves uranium smoothly.[3.12]

7. Corrosion in alkali solutions

Solutions of alkali metal hydroxide have little effect on uranium metal. Sodium hydroxide solutions containing H_2O_2 dissolve uranium. Soluble sodium peruranates are formed.[3.12]

The corrosion rate in deaerated solutions of KOH and NaOH, pH 13.6 and 13.1, respectively, at 100°C is about the same as that at pH 7.[3.11]

8. Discussion

The experimental results on uranium corrosion in aqueous solutions reviewed above can be qualitatively explained on the basis of the electrochemical theory of corrosion as outlined below.

In deaerated water, the uranium corrodes in an active state at low potentials. The cathodic reaction is reduction of water with formation of hydrogen gas and hydroxide ions. Hydride formation by reaction of water and uranium may also be part of the cathodic reaction (Appendix 1). The anodic reaction is between water and metal and/or UH_3.

A passive film forms at the higher potentials which prevail when oxygen is present. The cathodic reaction is reduction of oxygen in this case, and hydrogen evolution does not take place. The pitting and the hydrogen evolution which were reported for oxygenated water at 50 and 100°C can be qualitatively explained on the basis of the pitting model discussed in Appendix 4 with the assumption that UO_2 is oxidized to soluble UO_3 (Appendix 1) in the oxygenated solutions at these temperatures. Experimental work at room temperature included in the text of this report showed that soluble UO_3 forms from UO_2 above the potential at which UO_2 and UO_3 are in equilibrium. This work also showed that uranium potentials in aerated solutions are near this equilibrium potential.

The corrosion in acids can be qualitatively interpreted in terms of the effects of the acids on the corrosion potentials and on the solubility and/or protective properties of the UO_2 films. For example,

the low rate in H_2SO_4 would be explained as due to low reactivity of the protective UO_2 in H_2SO_4 and to a relatively high corrosion potential (compared with that in water) brought about by the cathodic reduction of hydrogen ions. The information on corrosion in HCl implies that the protective UO_2 is disrupted by the acid and that this disruption does not involve formation of U(VI). The additional fact that anhydrous UO_2 is unreactive in HCl (Appendix 2) suggests that the disruptive action involves inclusion of chloride ions in the oxide film during corrosion.*

The effects of strong oxidizing agents such as H_2O_2 (or anodic polarization) on solubility is very likely that of promoting the formation of soluble UO_3.

Ward and Waber[3.3] interpreted their open-circuit-potential and film-appearance data in terms of the electrochemical theory. Orman and co-workers[3.6] reported the conclusion that the corrosion of uranium in aqueous solutions is not electrochemical. I do not see any sound basis for this conclusion.

---

*Uranium is not strongly complexed by chloride ions. See J. J. Katz and G. T. Seaborg, "The Chemistry of the Actinide Elements," John Wiley and Sons, New York, 1957, p. 171-194. See also, The Chemical Society, London, "Stability Constants of Metal-Ion Complexes," The Chemical Soc., Special Publication No. 17, London, 1964, p. 227-278.

References

3.1 S. Orman, "Uranium Compatibility Studies; Part 1: The Interactions of Uranium and Gas Free Water Vapour," AWRE-O-94/63, Dec. 1963.

3.2 M. McD. Baker, L. N. Less and S. Orman, "The Product and Mechanism of the U-H_2O and UH_3-H_2O Reaction," AWRE-O-45/65, July 1965; and "Uranium and Water Reactions, Part 1 - Kinetics, Products and Mechanisms," Trans. Faraday Soc., 62, 2513 (1966).

3.3 J. W. Ward and J. T. Waber, "The Electrochemical Behavior of Uranium," J. Electrochem. Soc., 109, 76, (1962).

3.4 J. J. Corcoran et. al., "The Water Vapour Corrosion of Uranium and its Prevention" AWRE-O-42/65, July 1965.

3.5 S. Orman, "The Effect of Water Vapour Pressure in an Oxygen Free Atmosphere on the Corrosion Rate of Uranium at 100°C." AWRE-O-25/64, April 1964.

3.6 M. McD. Baker, J. W. Bleloch, N. Less, and S. Orman, "The Influence of Oxygen on the Uranium-Water Reaction," AWRE-O-40/60, June 1964; and Uranium and Water Reaction, Part 2, - Effects of Oxygen and other Gases," Trans. Faraday Soc., 62, 2525 (1966).

3.7 S. Orman, "The Corrosion and Protection of Uranium." Atom, 150, April 1969, p. 93.

3.8 J. E. Draley and W. E. Reuther, "Some Unusual Effects of Hydrogen in Corrosion Reactions," J. Electrochem. Soc., 104, 329 (1957).

3.9 W. D. Wilkinson, "Uranium Metallurgy, Volume II: Uranium Corrosion and Alloys," Interscience Publishers, New York, 1962, p. 834.

3.10 J. T. Waber, "A Review of the Corrosion Behavior of Uranium," LA-2035, December 1958.

3.11 M. McD. Baker, L. N. Less, and S. Orman, "The Influence of pH On the Uranium Water Reaction," AWRE-O-44/65, December 1963.

3.12 J. J. Katz and E. Rabinowitch, "The Chemistry of Uranium," National Nuclear Energy Series, VIII-5, McGraw-Hill Book Co., Inc. 1951, p. 1968-70.

3.13 L. E. Kindlemann and N. D. Greene, "Dissolution Kinetics of Nuclear Fuels," Corrosion, 23, 29 (1967).

3.14 L. E. Kindlemann and N. D. Greene, "Mechanisms for the Acid Corrosion Behavior of Neutron-Irradiated Uranium," Corrosion, 26, 189 (1970).

Appendix 4. Review of Experimental and Theoretical Information on Pitting in Aqueous Solutions Containing Aggressive Anions

1. Introduction

Many metals which depend upon a passive layer for corrosion protection are subject to pitting attack when the solution contains certain anions; particularly chloride. Other anions e.g., bromide and iodide also cause pitting of some metals. Experimental and theoretical information on pitting in the presence of chloride is reviewed below.

Pitting which occurs in the absence of aggressive anions is discussed elsewhere in this report.

2. Definition of breakdown and pitting potentials

In general, there is a more or less well-defined potential above which pit growth takes place but below which pit growth cannot be maintained. This is called the pitting potential.[4.1] Pit initiation is also dependent on the electrode potential, and the potential at which the initiation is observed in a given experiment is called the breakdown potential. The latter potential is greater than the pitting potential in all reported work which I have seen.

The breakdown potential is usually less well defined than the pitting potential, and it has been suggested[4.2] that it is a "notional value" dependent on the time taken in experimentation. However, Wilde and Williams[4.3] have recently reported work with stainless steels and

other materials in chloride solutions which led them to conclude that there was a real difference between breakdown and pitting potentials in their systems. Similar results and conclusions were reported some years earlier by Pourbaix and Co-workers.[4.4]

Relationships between pitting and breakdown potentials are illustrated in Figs. 4.1 and 4.2 for potentiostatic and galvanostatic measurements, respectively. The illustration in Fig. 4.1 is similar to those presented by Wilde and Williams[4.3] and by Pourbaix et. al.[4.4]

3. General characteristics of pit growth under anodic polarization

a. The pitting potential appears to be independent of the size of the pit and of the current applied to the electrode.[4.1]

b. The pitting potential usually increases with increasing concentration of unaggressive anions (e.g., $SO_4^=$, $CrO_4^=$, and NO_3^-).[4.1]

c. Pits may repassivate after a certain stage of growth.[4.1]

d. The pitting potential may depend to a large extent on alloy composition and temperature.[4.1]

e. Gas evolution from pits during pit growth has been observed, and it is thought that this gas is hydrogen.[4.8] This happens while the specimen potential at an exposed surface is above the hydrogen evolution potential.[4.8]

4. General characteristics of pit initiation (breakdown potentials) under anodic polarization

The observed breakdown potential is dependent upon the rate at which the potential is raised[4.5] and also upon the time taken in experimentation.[4.2] At low rates of increase of potential the breakdown potential may depend upon the solution composition and upon the

nature of the metal or alloy, its thermal treatment, and the state of its surface.[4.4, 4.6]

Solution compositional parameters which have been found to affect this potential include the following:

a. Chloride concentration - The breakdown potential decreases with increasing concentrations of chloride.[4.4, 4.6]

b. Ratio of chloride to unaggressive anions such as sulfate - The breakdown potential increases as this ratio decreases.[4.6]

c. Composition of gas atmosphere-Wilde and Williams[4.3] in the work mentioned above found that the breakdown potentials observed with atmospheres of oxygen, hydrogen, argon and nitrogen were all different.

5. Qualitative explanations of pit initiation characteristics

Hoar[4.2, 4.5] has recently presented qualitative explanations for some of the effects of exposure parameters on pit initiation as summarized below. Earlier explanations of others were reviewed by Kolotyrkin.[4.6]

Destruction of protective oxide film by chloride ions occurs with many different metals. The mechanism by which the chloride affects an oxide is uncertain; possibly it causes formation of soluble complexes or causes peptization of the oxide. In any case, the chloride must be absorbed before it reacts, and the effects of some parameters (e.g., potential, rate of increase of potential, chloride concentration, and ratio of chloride to unaggressive anions) on pit initiation result from effects on the chloride adsorption.[4.2] In some systems, clusters of several chloride ions are thought to be required to pull out a cation from the oxide.[4.5] In others the chloride is thought to pass

slowly into the oxide.[4.5, 4.6] The effects of exposure time on pit initiation under a given set of conditions are qualitatively explained in terms of the times required for these processes to occur.[4.5]

With respect to effects of potential, it is expected that anion adsorption will depend upon the potential difference between the oxide surface and the solution; increasing positive potential will favor adsorption of ions.* It may also aid passage of chloride into and thru the oxide.

6. Qualitative explanations of pit growth characteristics[4.1]

When the oxide is penetrated and the solution is in contact with metal within the pit, the local anodic current increases immediately. Simultaneously, a large potential difference (supported by electrolyte resistance) develops between the solution at the base of the pit and that adjacent to an exposed, passive surface. The potential of the pit solution is the higher; accordingly, the potential difference between solution and metal at the base of the pit is less than that on an exposed surface. This means that the corrosion within the pit can proceed in the active potential region while the exposed surfaces remain passive. It also means that cathodic processes which require low potentials such as hydrogen-ion reduction and/or water reduction can proceed rapidly within the pit at the same time such processes remain negligible on exposed surfaces.

Reduction of electrode potential (measured at the surface) will effect a reduction of the net anodic current in the pit by further

---

*See note at back, p. 4.12.

reduction of electrode potential in the active corrosion region within the pit. When this reduction becomes sufficiently great, the IR drop thru the solution can no longer maintain pit solution at high potential, and the electrode potential within the pit jumps up into the passive region prevailing at the surface.

Simultaneously with the onset of pit growth, the solution in the pit becomes concentrated in anions from the solution. This results from the fact that hydrogen ions and/or metal ions are products of the anodic reaction, and that anions must move into the anolyte in order to maintain electrical neutrality. The restricted geometry of the pit restricts outward diffusion of electrolytes from the pit solution. The concentration of electrolytes in the pit solution will increase with increasing current, and at the same time the solution resistance will decrease with increasing concentration of electrolytes. The potential drop through the solution is then affected by two opposing factors.

Since the solution within the pit is more concentrated in chloride and hydrogen ions (if the metal ions hydrolyze) than the bulk solution, it is likely to be more corrosive than the bulk solution.

7. Quantitative theoretical evaluations of pit growth characteristics during anodic polarization - Posey[4.1]

7.1 Introduction

Posey[4.1] has reported a theoretical analysis of potentials and concentrations occurring in a pit during growth under galvanostatic anodic polarization. An HCl solution was assumed for part of the analysis, but some effects of adding an indifferent or (passivating)

anion were also considered. It was assumed that metal ions formed by corrosion within the pit were hydrolyzed but they did not restrict the diffusion path thru the pit solution.

His reference pit is shown in Fig. 4.3 which is taken from his report. The figure is largely self-explanatory. It may be noted that j is the current density at the base of the pit. The total current per pit is I, and this will be approximately equal to the total anodic current when there is one pit per specimen. A probe (Luggin Capillary) is located at some point adjacent to a passive, external surface.

Some of Posey's findings for HCl solutions at 25°C are summarized below.

7.2 Difference between potentials in solution at base and mouth of pit

Posey's analyses showed that the difference between potentials of the solutions at the base and at the mouth of the pit increased with increasing current density but approached a constant value at large j.

His expression for this limiting condition is,

$$\lim_{\text{large } j} \left[\phi(-\delta) - \phi(o)\right] = \frac{RT}{F} \ln\left(1 + \frac{4\delta}{\pi a}\right), \qquad (1)$$

where $\phi(-\delta)$ is the solution potential at the base of pit (volt).

j is current density at base of pit (amp/cm^2).

δ is depth of pit (cm).

a is radius of pit mouth (cm)

R is gas constant (1.99 Cal, deg^{-1}, mole^{-1})

T is absolute temperature (°K)

F is the Faraday constant. (2.306 x 10^4 Cal, V^{-1}, equiv^{-1})

Posey expressed the current (and other parameters) in terms of the dimensionless parameter, β,

$$\beta = j\, a/2F\, D_H\, C_o \qquad (2)$$

where F has the units (Coulb, equiv^{-1}), D_H is the diffusion coefficient for the hydrogen ion, and C_o is the concentration of HCl in the bulk solution (moles/cm^3). For the case in which $\delta/a = 2$, the value of $\phi(-\delta) - \phi(o)$ is approximately constant at .031 volts for $\beta > 3$.*

From these equations, it can be shown that, in general, the current at which the limiting potential is reached increases in direct proportion to the value of C_o and in inverse proportion to pit radius a.

7.3 Potential difference between solution at probe and at mouth of pit.

Posey found that this potential difference (highest potential at pit mouth) also increases with increasing current, but that it approaches a limiting value when the value of β is comparable to those at which the potential difference within the pit approaches a limiting value. For any likely location of the probe, the potential difference between the solution at the probe and at the pit mouth may exceed that within the pit depending upon the exact location of the probe and upon pit dimensions.

7.4 Concentration of HCl at base of pit

Posey's analyses showed that the concentration of HCl at the base of the pit ($z = -\delta$) is given by the expression

$$C\,(-\delta) = C_o + \frac{(\frac{\pi a}{4} + \delta)}{2FD_H}\, j, \qquad (3)$$

---

*My calcualtion using Posey's expressions

where C $(-\delta)$ is the concentration of HCl at the base of the pit (moles/cm^3), and the other symbols have the meanings previously stated.

Using Eqn. 2, we can write Eqn. 4,

$$\frac{C\ (-\delta)}{C_o} = 1 + \left(\frac{\pi}{4} + \frac{\delta}{a}\right)\ \beta \qquad (4)$$

and, also,

$$\frac{C\ (-\delta)}{C_o} = \frac{\left(\frac{\pi}{4} + \frac{\delta}{a}\right)\ I}{2\ FD_H\ C_o\ a} + 1 \qquad (5)$$

Eqn. 5 shows that the concentration factor with a given value for $\frac{\delta}{a}$ increases in direct proportion to I and decreases in direct proportion to C_o and a.

7.5 Illustrative values of IR drops and HCl concentrations within model pit

I have listed in Table 4.1 some values of concentrations and IR drops within the model pit which I have calculated from relationships presented by Posey.[4.1] The conditions I have selected for illustration either equal or exceed those for constant values of $[\phi\ (-\delta) - \phi\ (0)]$.

As noted in this tabulation, the limiting potential drop is reached at rather modest current densities and IR-drops. However, in practice, the IR-drops could exceed these values by large factors if the conductance-path is partially blocked by corrosion products.

In general, the concentration of HCl at the pit-base is substantially above that in the bulk solution. For example, at a = .01 cm, $-\delta$ = 0.1 cm, and current density = 5.6 milliamp/cm^2, the concentration of HCl at the pit base is .034 molar when the concentration in the bulk solution is 10μ molar.

TABLE 4.1 CONCENTRATIONS OF HCℓ AND IR DROPS WITHIN PITS DURING GALVANOSTATIC POLARIZATION; CALCULATED FROM RELATIONSHIPS PRESENTED BY POSEY,[a,b]

Pit Radius (a) (cm)	Pit Depth (-δ) (cm)	C_o (μ molar)	Net Anodic Current at Base of Pit, j (μamp/cm²)	$[\phi(-\delta)-\phi(0)]^c$ (volt)	$C(-\delta)$ (μ molar)	$C(-\delta)/C_o$
.01	.01	100	560	.031	660	6.6
.01	.01	100	56,000	.031	56,000	560
.01	.1	100	560	.066	3,400	34
.01	.1	10	56	.066	440	44
.01	.1	10	5,600	.066	34,000	3,400
.1	.1	100	56	.031	660	6.6
.1	.1	100	5,600	.031	56,000	560
.1	.1	1000	560	.031	6,600	6.6
.1	.1	1000	5,600	.031	57,000	57

For uranium, 1 μamp/cm² = .36 mpy.

a. See text.

b. The conditions used for this illustration either equal or exceed the conditions for constant $[\phi(-\delta) - \phi(0)]$.

c. Potential drop between solutions at mouth and base of pit.

7.6 Potential difference between solution and metal at base of pit.

Since a typical characteristic of pitting under anodic polarization is a constant potential (at the probe) with wide changes in current, Posey considered explanations for the failure of the potential between metal and solution at the pit base to shift into the passive region with increasing current density. Such a shift would be expected on the basis of polarization information obtained on exposed surfaces with some materials that develop passive film with increasing potentials.

Posey's postulated explanation was that the anodic reaction is dependent upon the HCl activity; as shown in Eqn. 6,

$$j = KC\ (-\delta) \exp \alpha_a F\ \Delta\phi/RT \qquad (6)$$

where K is a constant and α_a is the anodic transfer coefficient. The other symbols have been defined previously. The anodic reaction of some metals, including titanium, apparently obey a relationship of this type.[4.1] On the basis of Eqns. 6 and 3, Posey showed that $\Delta\phi$ at the base of the pit approached a low, limiting value as the value of j increases.

If the cathodic reactions at the pit-base obeys a rate expression similar in form* to that of Eqn. 6, Posey showed that $\Delta\phi$ would be expected to be independent of current density. He pointed out that when this situation occurs within a pit, the potential cannot shift into the passive regions as long as the current density j is sufficient

---

*The cathodic reaction of titanium in HCl in the active region is apparently of this form.[4.1]

to maintain the limiting potential difference between the solution at the mouth and base of the pit. The electrode potential shifts into the passive region when the current density, j, diminishes and no longer maintains the high solution potential at the pit-base. This reduction in current could result from enlargement of the pit at constant I, or by a reduction in applied current.

8. Correspondence between pitting under anodic polarization and on a freely corroding species.

Wilde and Williams[4.3] concluded that there is complete correspondence in the systems they studied between pitting susceptibility determined from electrochemical polarization data and from exposure data obtained in accelerated chemical tests. However, it is possible that other metals, e.g., uranium alloys, may behave differently.

With respect to pit growth on a freely corroding specimen, it should be noted that the cathodic current required to support the pitting potential must be supplied by cathodic reactions on the exposed surface. Pit growth may then depend to some extent on specimen size, and pitting may be impossible with specimen of very small surface area.[4.6]

Note to Section 5

It should be noted that it is difficult to generalize regarding the relationship between electrode potential and the potential difference at the oxide solution interface when passivating oxide films are present. According to Vetter,[4.7] the potential difference between the metal and solution is affected by equilibria at the metal-oxide and oxide-solution interfaces, and by potential differences across the oxide which are associated with the restricted movement of cations and/or anions ($O^{=}$ or OH^{-}). The equilibrium at the metal-oxide interface is between metal ions and/or electrons in the metal and in the oxide; that at the oxide-solution interface is

$$O^{=}_{(oxide)} + 2H^{+}_{aq} \rightleftharpoons H_2O_{aq},$$

and the potential at the oxide-solution interface is established by this equilibrium. Hoar[4.2] implies that during transient conditions when the potential is increased rapidly and the film is not at the equilibrium thickness, the potential at the oxide-solution interface is greater than the equilibrium value. He proposed that this increase accounts for the lower break-through potentials which are observed upon rapid increase of potentials. This would also be a factor leading to increased rates of film removal at localized sites following the initial removal of oxide from the surface.[4.5]

With respect to redox reactions at the oxide-solution interface (e.g., $2H_2O \rightleftharpoons 4H^{+} + O_2 + 4e^{-}$) the effective potential difference, according to Vetter,[4.7] is primarily that between the metal and solution

(the electrode potential) when the film is a good electronic conductor. When it is an electrical insulator, the redox reactions do not occur regardless of potential as long as the passivating film is intact.

The Vetter model for the potential at the solution interface is not generally accepted by present investigators. However, no other generally applicable and/or accepted model is available. The picture regarding redox reactions is thought to be reasonable.

References

4.1 Franz A. Posey, to Office of Saline Water, U. S. Department of the Interior, Washington, D. C., Water Research Program - II. Reactions and Transport Phenomena at Surfaces - Quarterly Report for the Period March 15-June 15, 1969.

4.2 T. P. Hoar, "On Corrosion -Resistant Materials," J. Electrochem. Soc., 117, 17C (1970).

4.3 B. E. Wilde and E. Williams, "On the Correspondence between Electrochemical and Chemical Accelerated Pitting Corrosion Tests," J. Electrochem. Soc., 117, 775 (1970).

4.4 M. Pourbaix, L. Klimzack-Mathieiu, Ch. Mertens, J. Meunier, Cl Valeugenhaghe, L. deMunck, L. Laureys, L. Neelemans, and M. Warzee, "Potentiostatic and Corrosimetric Investigations of the Corrosion Behavior of Alloy Steels," Corrosion Sci., 3 239 (1963).

4.5 T. P. Hoar, "Creation and Disruption of the Passive State in Metals," Protection of Metals, 3, 14 (1967).

4.6 J. A. M. Kolotyrkin, "Pitting Corrosion of Metals," Corrosion, 19, 261t (1963).

4.7 Klaus J. Vetter, "Electrochemical Kinetics; Theoretical and Experimental Aspects," English edition, Academic Press, New York, 1967, p. 754-767.

4.8 Franz A. Posey, Private Communication.

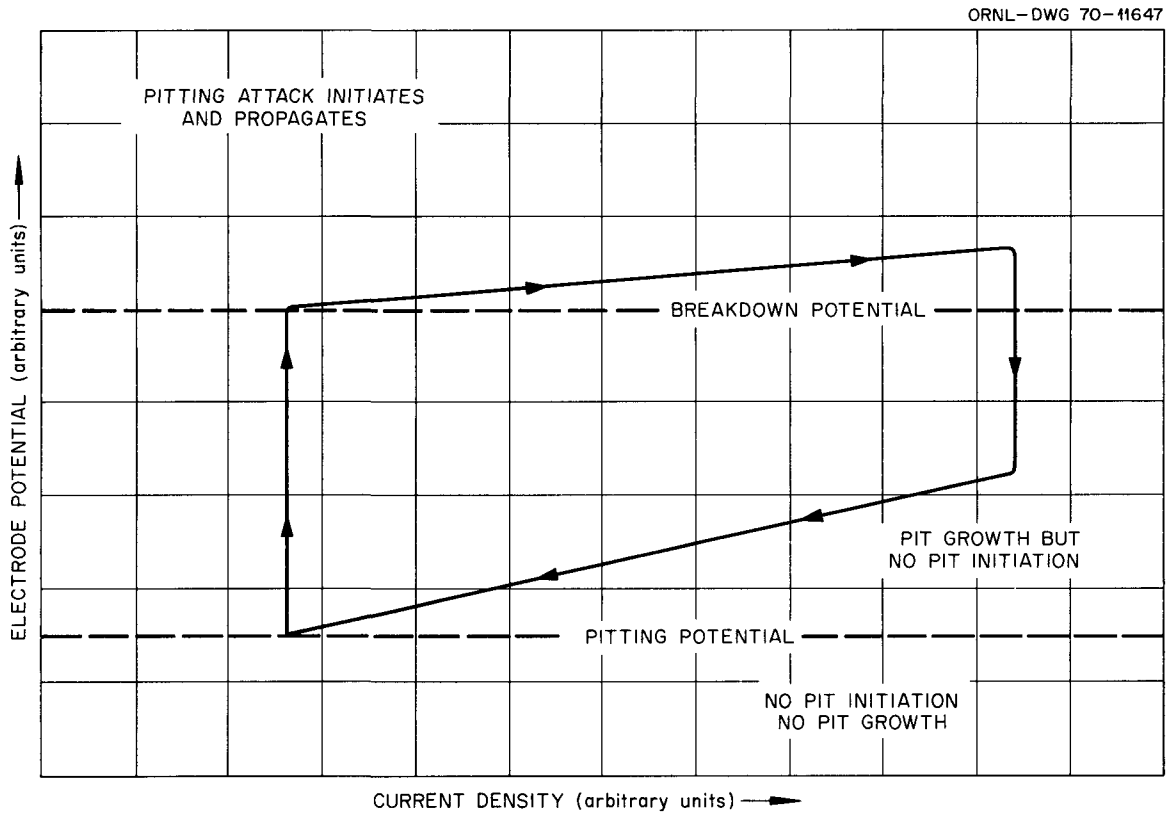

Fig. 4.1 Illustration of Breakthrough and Pitting Potentials; Potentiostatic Measurements

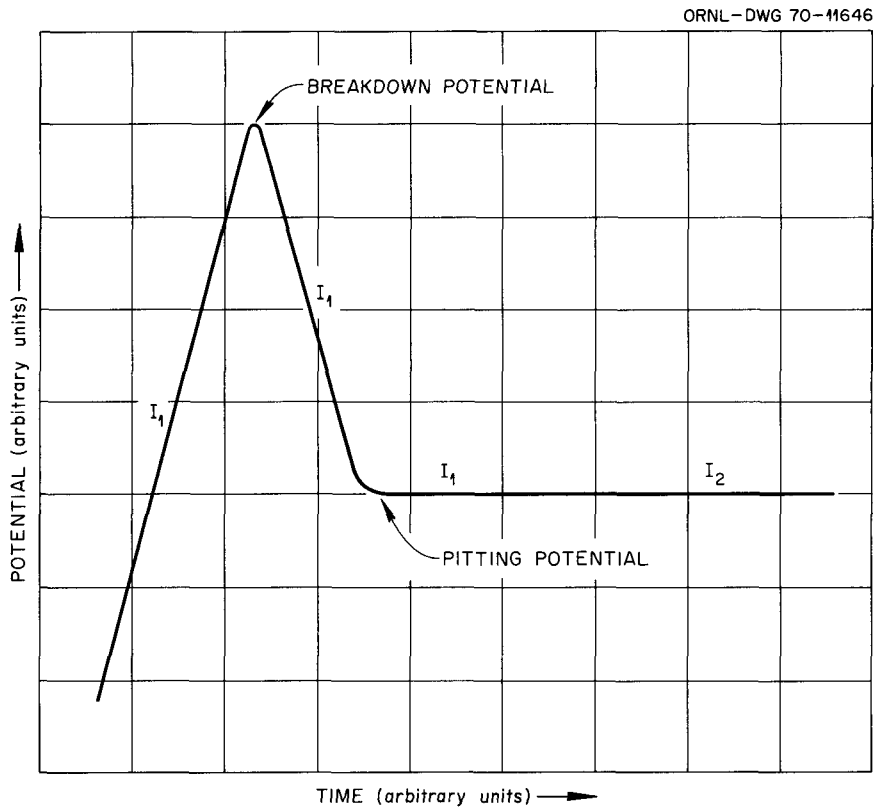

Fig. 4.2 Illustration of Breakthrough and Pitting Potentials; Galvanostatic Measurements

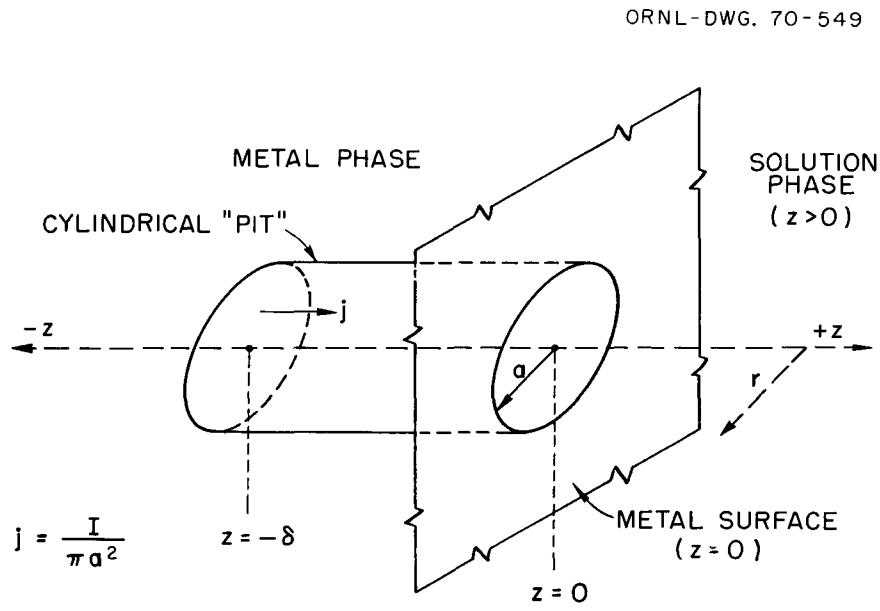

Fig. 4.3 Schematic Diagram of Simple Model for Pitting of Metals (taken from Ref. 4.1).

Appendix 5. Review of Some Theoretical and Experimental Information on the Electrochemistry of Corrosion*

1. Corrosion Reactions

Corrosion of a metal in an aqueous environment involves two electrochemical reactions, (1) an anodic reaction in which the metal is oxidized, and (2) a cathodic reaction in which some component of the solution is reduced by the electrons which are released in the anodic reaction.

The general formulation of the anodic reaction is,**

$$M \rightarrow M^{z+} + ze^- \qquad (1)$$

A more realistic formulation for ordinary aqueous corrosion is,

$$M + xH_2O \rightarrow M \cdot xH_2O^{z+} + ze^- \qquad (2)$$

The ions formed in reaction 2 may precipitate to form a stable oxide and/or hydroxide on the surface and thus stifle further corrosion,

$$M \cdot xH_2O^{z+} \rightarrow MO_{z/2} + (x - \tfrac{z}{2})H_2O + zH^+_{aq} \qquad (3)$$

A more protective oxide or hydroxide may be formed directly,

$$M + zH_2O \rightarrow M(OH)_z + zH^+_{aq} + ze^- \qquad (4)$$

or,

$$M + \tfrac{z}{2}H_2O \rightarrow MO_{z/2} + zH^+_{aq} + ze^-. \qquad (5)$$

Reactions of types 4 and 5 are favored by higher anodic potentials.[4.3]***

---

*Based in large part on information in Ref. 5.1 and 5.2.

**Part of this summary of anodic reactions is a condensation of a summary presented by Hoar, Ref. 5.3.

***With the convention employed, an increase in electrode potential, $\Delta\phi$, refers to a change in potential in the anodic (or noble) direction. A decrease is in the cathodic (or active) direction.

Another anodic reaction is one in which the cations enter the solid oxide film directly,

$$M + \frac{z}{2}\ O^{=} \rightarrow MO_{z/2} + ze^{-}. \qquad (6)$$

This type of reaction must prevail when the metal surface is covered with an oxide which is impervious to solution and in which only the anions are mobile.

For U going to U^{+4}, the above reactions become,

$$U + xH_2O \rightarrow U\cdot xH_2O^{4+} + 4e^{-}, \qquad (2A)$$

$$U\cdot xH_2O^{4+} \rightarrow UO_2 + (x - 2)H_2O + 4H^{+}_{aq} \qquad (3A)$$

$$U + 4H_2O + U(OH)_4 + 4H^{+}_{aq} + 4e^{-}, \qquad (4A)$$

$$U + 2H_2O \rightarrow UO_2 + 4H^{+}_{aq} + 4e^{-}, \qquad (5A)$$

$$U + 2O^{2-} \rightarrow UO_2 + 4e^{-}. \qquad (6A)$$

The cathodic reactions of possible importance in aerated aqueous solutions include the following,

$$O_2 + 2H_2O + 2e^{-} \rightarrow H_2O_2 + 2OH^{-}, \qquad (7)$$

$$H_2O_2 + 2e^{-} \rightarrow 2OH^{-}, \qquad (8)$$

$$2H^{+} + 2e^{-} \rightarrow H_2, \qquad (9)$$

$$2H_2O + 2e^{-} \rightarrow H_2 + 2OH^{-}, \qquad (10)$$

and, with uranium,

$$U + 3H^{+} + 3e^{-} \rightarrow UH_3 \qquad (11)$$

$$UO_2 + 7H^{+} + 7e^{-} \rightarrow UH_3 + 2H_2O \qquad (12)$$

Reaction 9 represents the reduction of protons to form H_2. The hydrogen atom is a probable intermediate.

Reaction 10 represents the direct reduction of water to form H_2. Again the hydrogen atom is a probable intermediate. Thermodynamically, there is no difference between reactions 9 and 10. However, reduction

of H^+ is usually the more favored reaction due to kinetic factors. Reduction of H_2O is usually encountered at potentials well below the equilibrium potentials for reaction 10.

Reactions 7 and 8 represent the reduction of O_2 to form OH^-. Hydrogen peroxide is an intermediate,[5.4] and its reduction may require lower potentials than needed for reduction of O_2. Accordingly, under some conditions, it is possible for H_2O_2 to accumulate in aerated solutions in which a metal is corroding. Ward and Waber[5.5] found that accumulation of H_2O_2 occurred when uranium was exposed in oxygenated 0.1M $KClO_4$ at 35°C. The potentials for O_2-reduction are normally above those for H^+-reduction.

Reaction 11 and 12 are included in the above list to serve as a reminder that UH_3 can form during corrosion of uranium, and that its formation is a cathodic reaction (See Appendix 1). Again, it should be noticed that there is no difference, thermodynamically, between reactions of U(or UO_2) with H^+ and with H_2O.

A schematic representation of the corrosion processes when an oxide film is present is shown in Fig. 5.1. In part, this follows a representation presented by Draley and Ruther.[5.6] These authors suggested that hydrogen ions may diffuse thru the oxide layer and undergo reduction at the metal-oxide interface. The hydrogen atoms formed at this location could lead to formation of hydrogen gas, and/or metal hydride at the interface. Both of these products could have adverse effects on the integrity of the oxide film. They considered it unlikely that hydrogen atoms produced at the oxide-solution interface would reach the metal-oxide interface.

2. Factors Which Affect the Rates of Anodic Reactions

The rate of the anodic (corrosion) process in aqueous solutions is dependent, basically, upon three factors: (1) the protective properties of solid films which may form on the metal surface, (2) the concentrations of any solutes which take part in the dissolution and/or in the film-building reactions, and (3) the potential differences between the metal and adjacent solution and between the surface of the film and adjacent solution. The latter quantities may differ because of the resistance of the film to passage of ions. In the general case, the film could have any composition, but the usual protective films in aqueous solutions are oxides and hydroxides. The term, protective properties, refers to the properties of: (1) permeability to ions from the solution, (2) permeability to solution, and (3) ionic and electronic conductivity of the film. With a freely corroding system, the potential is that for which the anodic and cathodic rates are equal.

In some cases, the anodic and/or cathodic reactions can be studied separately using electrical polarization methods.

The types of anodic potential-current relationship which may be encountered in polarization measurements are illustrated in Fig. 5.2. The different regions are described more fully below.

Region (1). In this region of low potential, little or no protective film is formed with some metals for one reason or another.*

---

*Possibly because the solid products of the reaction are porous and/or permeable to the solution. Also hydride formation may occur and have a detrimental effect on protective properties of the film.

The expected current-potential relationship in this region of active corrosion has the form,*

$$i_a = i_{corr} \exp\left(\frac{\alpha_a ZF}{RT}(\Delta\phi - \Delta\phi_o)\right) \qquad (13)$$

where

i_a is the anodic current,

i_{corr} is the corrosion current at open circuit,

$\Delta\phi$ is the polarized electrode potential (the difference between potentials of metal and solution),

$\Delta\phi_o$ is the electrode potential at open circuit (the corrosion potential),

Z is the charge on the metal ion,

α_a is the effective anodic transfer coefficient; values for this quantity at room temperature are usually in the range 0.5 to 2,

F is the Faraday constant,

T is the temperature,

R is the gas constant.

Region 2 and 3. With some systems, protective oxide formation begins and continues above a certain potential as indicated for regions 2 and 3 of Fig. 5.2. The formation of a protective oxide may result from the occurrence of reactions such as reactions 3 thru 6, above.

If the film is non-conductive and doesn't break down, the current may remain low as the potential is increased to very high values

---

*The general relationship between current and potential,

$$\Delta\phi = a + b \log i,$$

where a and b are constant, is called a Tafel relationship.

(several hundred volts) while protective film (barrier layer) continues to grow at a low rate. This growth is a result of the movement of anions or cations thru the film under the influence of the applied potential.

Region 4. This region indicates breakdown of film and pitting due to the presence of aggressive anions as discussed in Appendix 4.

Region 5, 6, and 7. If electrons can pass thru the oxide, redox reactions can take place at the oxide-solution interface as the potential is increased. If the oxide is a good conductor of electrons, these reactions would be expected to occur near the potentials at which they become thermodynamically possible (see note p. 4.12 of Appendix 4).

The redox reactions which might occur include oxidation of H_2O and solutes and oxidation of the protective oxide to a higher oxide. In the latter case, the higher oxide may be non-protective, or soluble, and the formation of this oxide would then result in active corrosion of the metal. This behavior is referred to as overpassivation, and the potential region is referred to as the transpassive region.

3. Theoretical and Experimental Information on Kinetics of Reduction of Hydrogen Ions and Water[5.2]

3.1 Clean Metal Surfaces

3.1.1 Theoretical Relationships for Charge-Transfer Overvoltage

The theoretical relationship for the cathodic current from reduction of ions in a single-charge-transfer redox reaction at an electrode is,

$$i_- = -k_- C_o' \exp - \left(\frac{\alpha_c F}{RT} (\Delta\phi - \zeta) \right), \qquad (14)$$

where k_- is a constant characteristic of the metal, C_o' is the concentration of the oxidized species at the interface between compact and diffuse double layers on the surface, α_c is the cathodic transfer coefficient, ζ is the zeta-potential, i.e., the potential across the diffuse double layer, and the other symbols have the usual meanings.

The value of C_o' is related to the concentration of the oxidized species in the bulk of solution, C_o, thru Eqn. 15,

$$C_o' = C_o \exp\left(\frac{-Z_o F}{RT}\zeta\right) \tag{15}$$

where Z_o is the ionic valence of the oxidized species.

Applying Eqns. 14 and 15 to reduction of H^+ and of H_2O, we have, for H^+-reduction,

$$\Delta\phi = \frac{-RT}{\alpha_c F}\ell n|i| + \frac{RT}{\alpha_c F}\ell n(H^+) - \frac{1-\alpha_c}{\alpha_c}\zeta + \text{const}, \tag{16}$$

and for H_2O-reduction,

$$\Delta\phi = -\frac{RT}{\alpha_c F}\ell n|i| + \zeta + \text{const} \tag{17}$$

If the solution contains a large excess of inert electrolyte (supporting electrolyte), the ζ-potential does not change with change in pH.* Accordingly, in this case the H_2O-reduction current at a given potential is independent of pH, and H^+-reduction current is directly proportional to (H^+) in the bulk solution.

Now if the solution is a pure acid or alkaline electrolyte, the potential does change with change in pH (Eqn. 15), and the expressions for H^+- and H_2O-reductions in these cases which are given by Vetter are the following,

---

*The ζ-potential is dependent on the value of $\Delta\phi$. However, the variation of ζ-potential with $\Delta\phi$ is small if the ζ-potential is small.

for H^+-reduction,

$$\Delta\phi = \frac{-RT}{\alpha_c F} \ell n|i| + \frac{RT}{F} \ell n\ (H^+) + \text{const}, \qquad (18)$$

or

$$|i| = \text{const}'\ (H^+)^{\alpha_c}\ \exp - \left(\frac{\alpha_c F}{RT} \Delta\phi\right) \qquad (19)$$

and for H_2O-reduction

$$\Delta\phi = \frac{-RT}{\alpha_c F} \ell n|i| - \frac{RT}{F} \ell n(H^+) + \frac{RT}{F} \ell n\ K_w + \text{const}, \qquad (20)$$

or

$$|i| = \frac{\text{const}'}{(H^+)^{\alpha_c}}\ \exp - \left(\frac{\alpha_c F}{RT} \Delta\phi\right) \qquad (21)$$

where the ionization constant of water, K_w, is included in the constant term. Eqns. 19 and 21 show that in this case the H^+-reduction current at a given potential is directly proportional to about the square root of (H^+), and the H_2O-reduction current is inversely proportional to about the square root of (H^+).

Theoretical values for α_c range between 0 and 1. Experimental values are discussed in the following sections.

It is of incidental interest to note that, according to theory, the concentration of H^+ at the interface between the compact and diffuse double layers is independent of pH in pure acid solution. The same is true for the concentration of cations in basic solution. The ζ-potential changes with pH to effect these constant concentrations. With excess of supporting electrolyte, the (H^+) at the inner double layer is directly proportional to (H^+) in the bulk solution.

It is also worth remembering that in all but the most concentrated solutions, the concentration of ions at an interface is probably small compared with the concentration of water at the interface.

3.1.2 Experimental Values for α_c and for the Order of the Reduction Reaction (Dependence of Current on pH)

Eqns. 16, 17, 18, and 20 can be expressed in terms of the overvoltage, η, as follows,*

$$\eta = \frac{-RT}{\alpha_c F} \ell n|i| - \frac{RT}{F} \ell n[H^+] - \frac{1-\alpha_c}{\alpha_c} \zeta + \text{const} \quad (16A)$$

H^+-reduction with excess of supporting electrolyte, ζ constant

$$\eta = \frac{-RT}{\alpha_c F} \ell n|i| - \frac{RT}{F} \ell n[H^+] + \zeta + \text{constant} \quad (17A)$$

H_2O-reduction with excess supporting electrolyte, ζ constant

$$\eta = -\frac{RT}{\alpha_c F} \ell n|i| + \text{const} \quad (18A)$$

H^+-reduction in pure acid, ζ dependent on pH

$$\eta = -\frac{RT}{\alpha_c F} \ell n|i| + \frac{2RT}{F} \ell n\ [OH^-] + \text{const} \quad (20A)$$

H_2O-reduction in pure base, ζ dependent on pH

The validity of Eqns. 16, 17, 18, 20 and/or Eqns. 16A, 17A, 18A, and 20A have been demonstrated with some solutions and metals. It is noteworthy that Eqn. 18A is obeyed by Pb in H_2SO_4 at concentrations of 0.1N to 8N. On the other hand, the range of acidities over which Eqn. 18A is applicable may be smaller with other metals and/or acids. For example, with Ni in HCl, the overvoltage is independent of pH only in the region 0.0003 to .003 N HCl.[5.2]

The experimental values of α_c which are quoted by Vetter[5.2] range from 0.46 to 0.53.

---

*$\eta = \Delta\phi - \Delta\phi_o = \Delta\phi - \frac{RT}{F} \ell n \frac{(H^+)}{P_{H_2}} = \Delta\phi - \frac{RT}{F} \ell n\ (H^+)$ with $P_{H_2} = 1$ atm.

3.1.3 Diffusion Limited Currents

The concentrations of reactants and products at the surface of an electrode can be affected by limitations on the rates of diffusion of these species to or from the surface. In particular it is noted here that the maximum rate at which a solute can be reduced cannot exceed the rate at which the solute diffuses to the surface. This diffusion-limited current can be estimated from the expression,

$$i_d = \frac{nFCD}{\delta} \qquad (22)$$

where

i_d = limiting diffusion current (amp/cm^2)

n = number of electrons taking part in the reduction of the species

F = Faraday Constant

C = concentration in the bulk solution of the species undergoing reduction (moles/cm^3)

D = diffusion coefficient of species (cm^2/sec)

δ = effective thickness of diffusion layer on specimen surface, (cm). This thickness will depend upon specimen shape and upon the amount of agitation of the solution. In experiments reported in the text, the estimated value of δ was about 3×10^{-3} cm.

3.2 Oxide Coated Surfaces

The effects of oxides on rates of cathodic reactions is discussed in Section 4. However, it can be noted here that the results of experimental work of Meyer[5.7, 5.9] showed that the effective values of α_c for both H^+-reduction and O_2-reduction on Zr are decreased by

formation of passive film. On the basis of Meyer's theoretical interpretations, it seems likely that passive film on the other metals would have similar effects on α_c.

4. Experimental and Theoretical Information on Kinetics of Reduction of Oxygen

4.1 Clean Metal Surfaces

Theoretical understanding of the kinetics of O_2-reduction is not as complete as that for H^+-reduction. Experimentally, the following relationships have been found for reduction of O_2 on Ag:

in acid and neutral solutions[5.2]

$$i = - k_- (O_2) \exp - \left(\frac{\alpha_c F}{RT} \Delta\phi \right) \qquad (23)$$

and in alkaline solutions[5.2]

$$i = - k_- (O_2)(H^+) \exp - \left(\frac{(1 + \alpha_c)F}{RT} \Delta\phi \right) \qquad (24)$$

At each pH, the value of α_c was 0.5. Eqn. 23 was also found with Hg in acid and neutral solutions.[5.2]

4.2 Surfaces Coated with Passive Films

Meyer[5.7] studied O_2-reduction on Zr in solutions containing 0.1M Na_2SO_4 as the supporting electrolyte. He found that the Tafel slopes for O_2-reduction increased from values of 150-160 mv/decade after a few hours exposure to values of 240-300 mv/decade after several days exposure. He also found that the Tafel slopes for reduction of H^+ were similarly increased after formation of oxide film.[5.9]

Meyer[5.7] explained these increases in slopes by assuming that the passive film imposed a second barrier for transfer of electrons from the metal to the O_2. He demonstrated that with this assumption

the effective values of α_c is,

$$\alpha_c = \frac{\alpha_f \alpha_s}{\alpha_f + \alpha_s} , \qquad (25)$$

so that the value of α_c is reduced below that for transfer of electrons at the interface, α_s. For example, if α_f and α_s are both equal to 0.5, the value of α_c is 0.25, and the expected Tafel slope is 236 mv/decade.

Others[5.10] have noted effects of oxide film on α_c and α_a and have offered different explanations which involve the electrical resistivity of the oxide.

Meyer measured the effects of O_2-pressure and pH on the kinetics of O_2-reduction on Zr in the studies mentioned above.[5.7] He found that the rate of reduction increased with O_2-pressure to the powers of 0.66 to 0.9; however changes in pH had negligible effects.

4.3 Surfaces Coated with Porous Oxide

The presence of porous oxides on an electrode would undoubtedly affect the kinetics of a reduction process on the electrode. In the simplest case, the reaction would take place only on the bare metal or on thin oxide at the bases of the pores or crevices. The effective area of the surface would then be less than the apparent area. Also, the thickness of the solution-diffusion layer might be increased depending on the film thickness.

5. Corrosion Potentials and Currents on a Freely Corroding Specimen

The corrosion potential of a freely corroding specimen is that at which the rate of the anodic and cathodic processes are equal. This potential can be measured directly. It can also be established in some cases from the results of polarization measurements as illustrated in Fig. 5.3 where the corrosion potential is that at

which the anodic and cathodic polarization curves intersect. Also, the rates of anodic and cathodic processes on the freely corroding specimen can sometimes be estimated from polarization information. For example, if the cathodic polarization data form a straight line plot as illustrated in Fig. 5.3, the cathodic rate at open circuit (which is the corrosion rate) can be estimated by extrapolating the straight line to the known open circuit potential. Also, small current polarization can be used to establish the corrosion rate.[5.8]

6. Effects of Localized Corrosion on the Local Corrosion Potential and Solution Composition.

Localized corrosion in regions of restricted access to the bulk solution* results in local changes of the corrosion potential and of the solution composition. In particular, when the anodic rate exceeds the cathodic rate within a restricted region, the electrode potential will be less than that at exposed surfaces, and also, anions from the bulk solution will be concentrated in the restricted region. Hydrogen ions and/or metal ions, which are produced in the anodic reactions, will also be concentrated within the restricted region. These effects were discussed in Appendix 4 in connection with a discussion of pitting corrosion. Additional definitions and explanations which may aid in understanding the effects of localized corrosion are presented below.

The potential of a solid metal test electrode immersed in solution is the difference between the potentials of the metal and solution

---

*For example, pitting corrosion, crevice corrosion, and stress corrosion cracking.

phases as expressed by Eqn. 26 and illustrated in Fig. 5.4,

$$\Delta\phi = \phi_m - \phi_s \tag{26}$$

The potentials represented by ϕ are the Galvani or inner potentials of the phases. The Galvani potential is the sum of the potential due to excess charge and of the surface potential due to oriented dipoles. The value of $\Delta\phi$ is measured by combining the test electrode system with a reference electrode and measuring the voltage between them. Neglecting contact potentials in the lead wire systems and also neglecting solution-junction potentials, the measured voltage, E, is the difference between $\Delta\phi$ and $\Delta\phi_R$ as expressed in Eqn. 27,

$$E = \Delta\phi - \Delta\phi_R, \tag{27}$$

where $\Delta\phi_R$ represents the arbitrarily assigned potential of the reference electrode. This is zero for the hydrogen electrode,

$$E = \Delta\phi \text{ (with hydrogen reference)}. \tag{28}$$

The set-up which is commonly used to measure the potential of a specimen-electrode when current flows thru the solution is illustrated in Fig. 5.4. The current is ionic and it may flow between the specimen and a counter electrode or between different regions on the surface of the specimen. A salt-bridge probe is placed adjacent to the specimen surface so that ϕ_s appearing in the measurement will approximate that at the specimen surface. With localized high corrosion rates, as within a pit or crevice, the probe will not generally the solution potential within the pit or crevice.

The possible situation for a pit (or crevice) is illustrated in Fig. 5.5. Assuming a net anodic current within the pit, the solution potential exceeds that at the surface by the voltage drop

between pit and surface solutions. Accordingly, the $\Delta\phi$ in the pit is given by the expression,

$$\Delta\phi = (\phi_m - \phi_s) - \delta\phi_{IR}, \qquad (29)$$

where $\phi_m - \phi_s$ represents the electrode potential measured at the exposed surface, and $\delta\phi_{IR}$ is the difference between potentials of surface- and crevice-solutions.

The relative levels of the potentials at different locations are also illustrated in Fig. 5.5.

Estimates and additional discussions of potential and solution composition changes in restricted-access-corrosion were presented in Appendix 4.

References

5.1 F. A. Posey, "Electrochemical Aspects of the Corrosion of Metals," Keynote Address for a Symposium on "Kinetics of Corrosion Processes," at 25th Annual Conference of the National Association of Corrosion Engineers, Houston, Texas, March 10-14, 1969.

5.2 Klaus J. Vetter, "Electrochemical Kinetics," English Edition, Academic Press, New York, 1967.

5.3 T. P. Hoar, "On Corrosion-Resistant Materials," J. Electrochem. Soc., 117, 17C (1970).

5.4 Klaus J. Vetter, op. cit., p. 632.

5.5 J. W. Ward and J. T. Waber, "The Electrochemical Behavior of Uranium," J. Electrochem. Soc., 109, 76, (1962).

5.6 J. E. Draley and W. E. Ruther, "Some Unusual Effects of Hydrogen in Corrosion Reactions," J. Electrochem. Soc., 104, 329 (1957).

5.7 R. E. Meyer, "The Reduction of Oxygen on Passive Zirconium," J. Electrochem. Soc., 110, 167 (1963).

5.8 M. Stern and A. L. Geary, "Electrochemical Polarization," J. Electrochem. Soc., 104, 56 (1957).

5.9 R. E. Meyer, Private Communication.

5.10 A. C. Makrides, "Electrochemistry of Surface Oxides," J. Electrochem. Soc., 113, 1158 (1966).

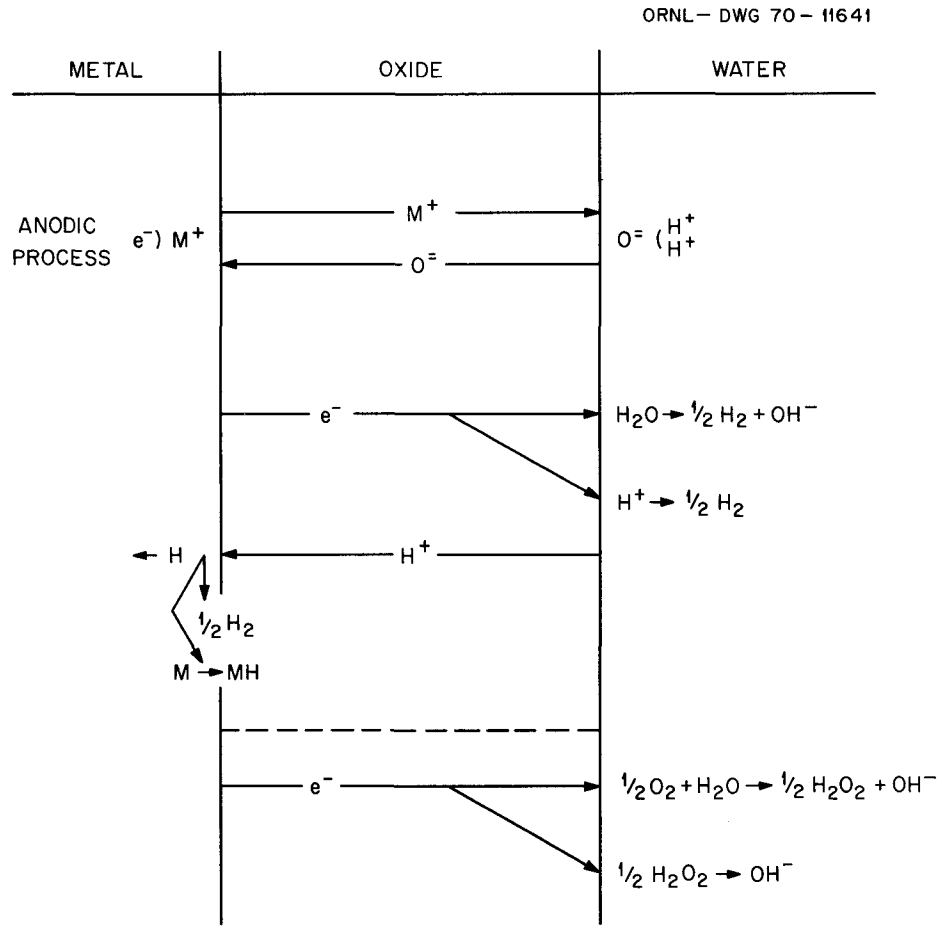

Fig. 5.1 Schematic Representation of Corrosion Processes on Oxide Coated Surfaces

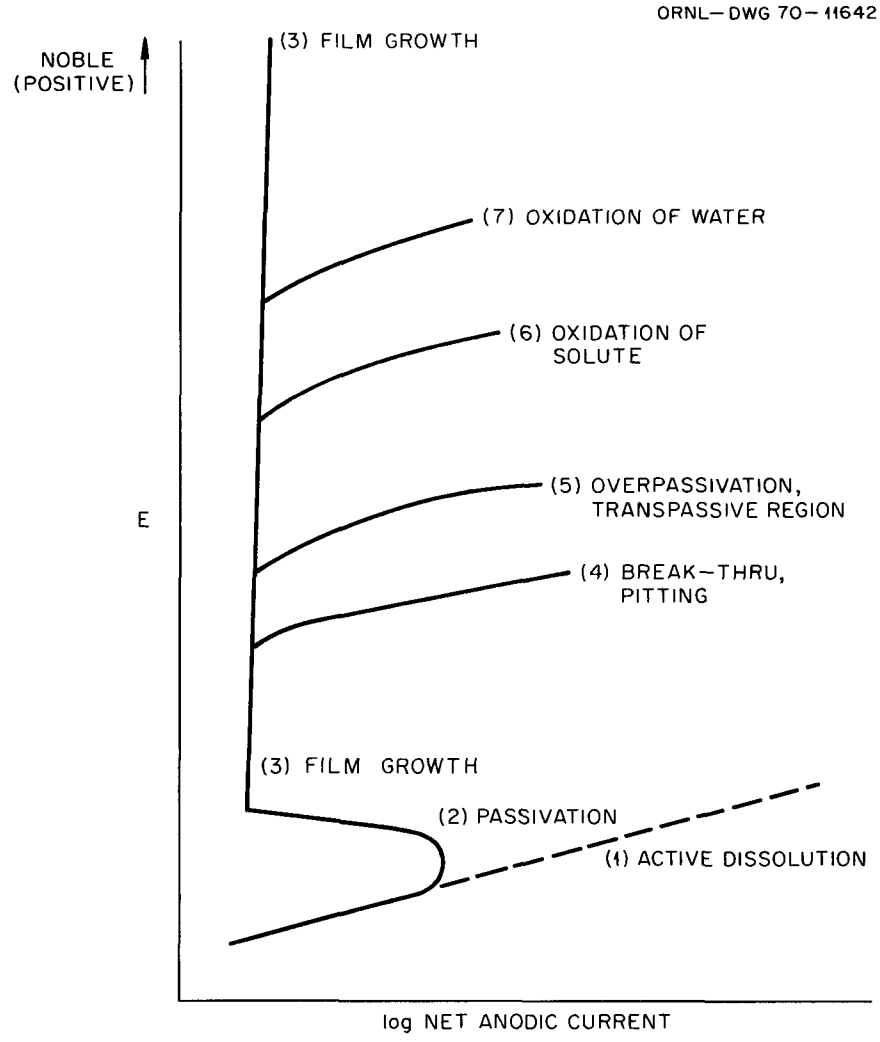

Fig. 5.2 Illustration of Types of Relationships Between Potential and Anodic Current

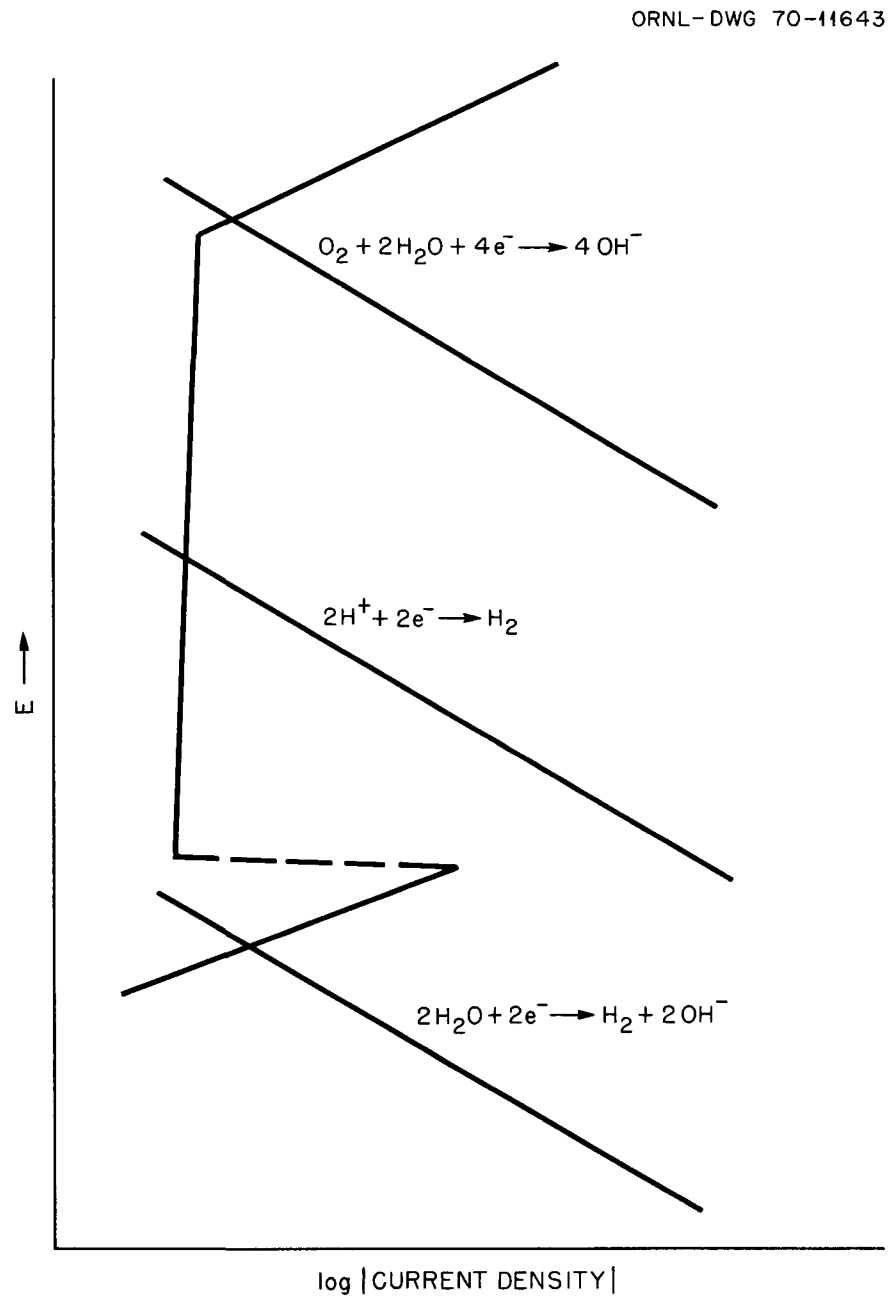

Fig. 5.3 Illustrative Plots of Cathodic and Anodic Polarization

ORNL-DWG 70-11644

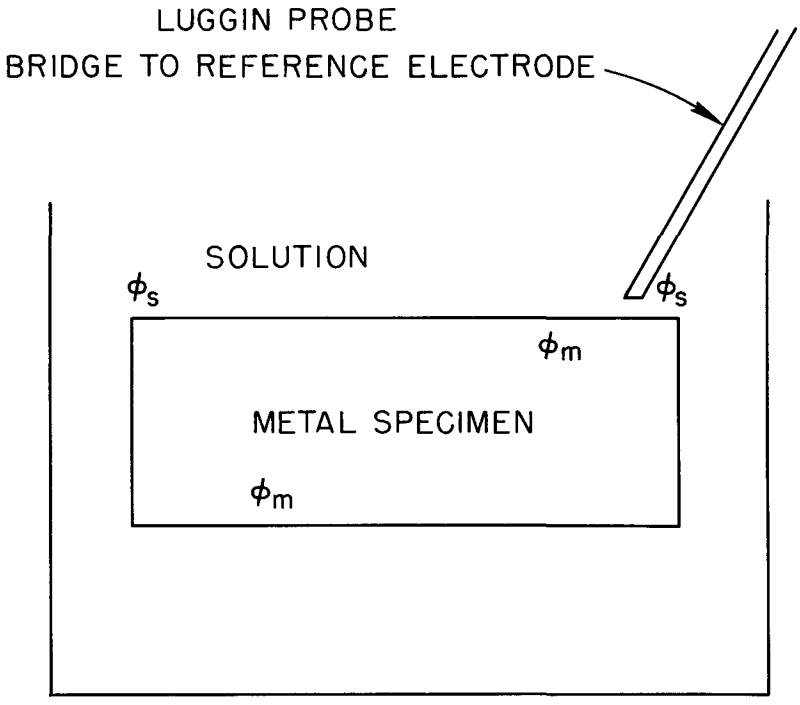

Fig. 5.4 Illustration of Set-Up Used to Measure Electrode Potential

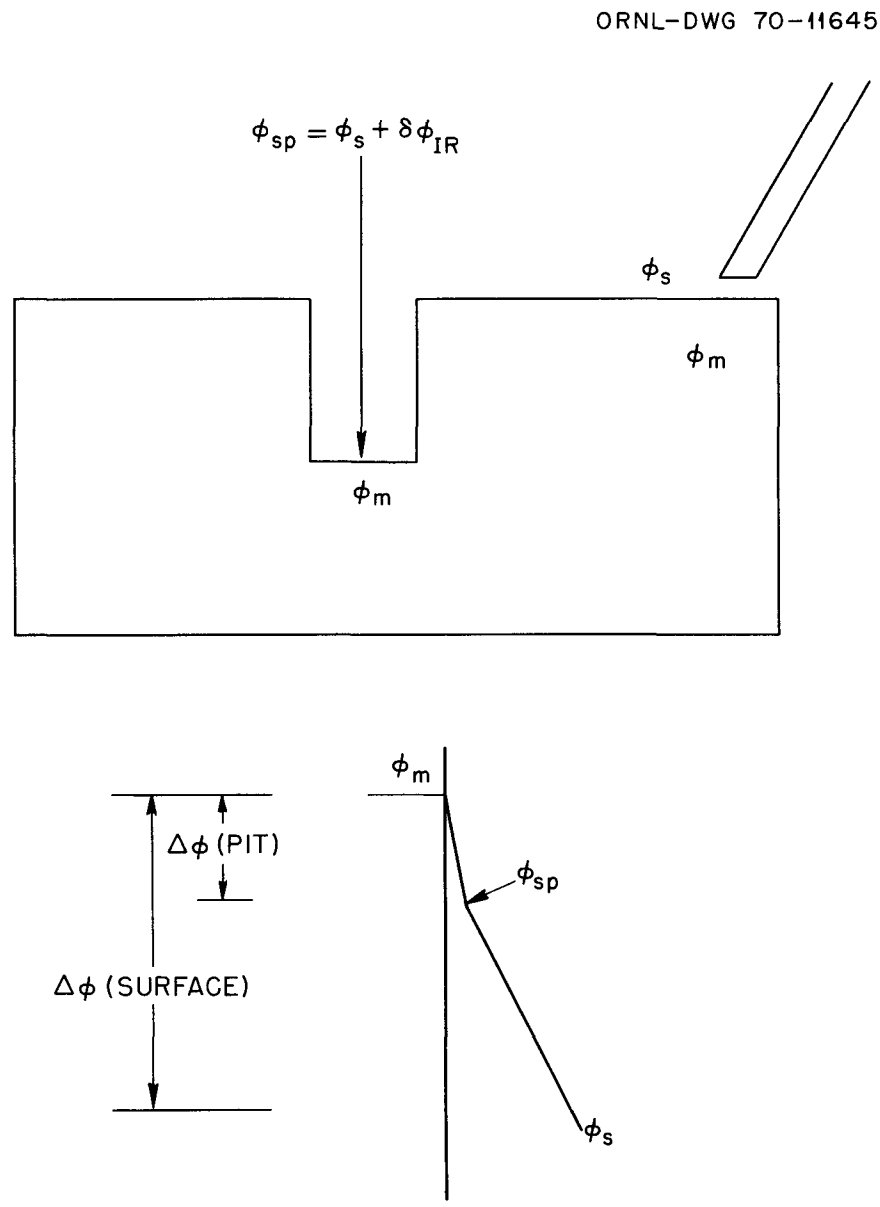

Fig. 5.5 Illustration of Effects of Restricted-Geometry Corrosion on Solution and Electrode Potentials

ORNL-4651
UC-25 — Metals, Ceramics, and Materials
UC-4 — Chemistry

INTERNAL DISTRIBUTION

1. Biology Library
2-4. Central Research Library
5. ORNL — Y-12 Technical Library Document Reference Section
6-40. Laboratory Records Department
41. Laboratory Records, ORNL R.C.
42. A. L. Bacarella
43. E. G. Bohlmann
44. J. V. Cathcart
45. J. C. Griess
46. W. R. Grimes
47. R. F. Hibbs
48-50. G. H. Jenks
51. D. L. McElroy
52. C. J. McHargue
53. R. E. Meyer
54. F. A. Posey
55. M. J. Skinner
56. R. A. Strehlow
57. D. A. Sundberg
58. D. B. Trauger
59. R. A. Vandermeer
60. A. M. Weinberg
61. H. L. Yakel
62. J. S. Bullock (Y-12)
63. J. B. Condon (Y-12)
64. W. H. Dodson (Y-12)
65. W. J. Hulsey (Y-12)
66. J. M. Schreyer (Y-12)
67. F. R. Winslow (Y-12)
68. Paul Cohen (consultant)
69. John Corbett (consultant)
70. H. H. Kellogg (consultant)
71. L. N. Zumwalt (consultant)

EXTERNAL DISTRIBUTION

72. E. Jiannetti, Dow Chemical Company, Rocky Flats Division
73. R. H. Karlson, Dow Chemical Company, Rocky Flats Division
74. J. M. Macki, Dow Chemical Company, Rocky Flats Division
75. J. R. Seed, Dow Chemical Company, Rocky Flats Division
76. L. W. Roberts, University of California, Lawrence Radiation Laboratory
77. D. R. Adolphson, Sandia Corporation, Livermore
78. M. W. Mate, Sandia Corporation, Livermore
79. B. C. Odegard, Sandia Corporation, Livermore
80. S. W. Zehr, Sandia Corporation, Livermore
81. M. J. Davis, Sandia Corporation, Albuquerque
82. N. J. Magnani, Sandia Corporation, Albuquerque
83. B. D. McLaughlin, Sandia Corporation, Albuquerque
84. R. W. Rohde, Sandia Corporation, Albuquerque
85. S. Orman, UKAEA, AWRE, Aldermaston
86. R. W. Stahle, Ohio State University
87. T. J. Sandstrom, Los Alamos Scientific Laboratory
88. J. M. Taub, Los Alamos Scientific Laboratory
89. J. A. Swartout, Union Carbide Corporation, New York 10017
90. Patent Office, AEC, ORO
91. Laboratory and University Division, AEC, ORO
92-331. Given distribution as shown in TID-4500 under Metals, Ceramics, and Materials category and to recipients under UC-4 who did not receive copies under UC-25 (25 copies — NTIS)